MITOCHONDRIAL DYNAMICS AND UNCOUPLING PROTEIN 2 IN HIPPOCAMPUS OF THE mutUNG1 MOUSE MODEL

MD MAHDI HASAN

Høgskolen i **Hedmark**

Master's Thesis in Applied & Commercial Biotechnology

Department of Natural Science & Technology, Hamar

HEDMARK UNIVERSITY COLLEGE

2013

DEDICATION

To

Dr. Linda Hildegard Bergersen
Dr. Knut Husø Lauritzen

ACKNOWLEDGEMENTS

ABSTRACT

Mitochondria are a crucial site of energy metabolism in neurons. The energy demand is higher in neurons than in most other cells, which is reflected by high consumption of oxygen in the brain. Endogenous reactive oxygen species (ROS), arising from normal oxygen metabolism, are mainly produced in mitochondria. In neurodegenerative pathology, ROS may lead to oxidative stress and mitochondrial DNA (mtDNA) damage. The transgenic mutated uracil-DNA glycosylase 1 (mutUNG1) mice express the mutUNG1 enzyme, which induces mitochondrial toxicity, caused by high numbers of apurinic/apyrimidinic-sites in mtDNA of hippocampal neurons. The uncoupling protein 2 (UCP2) has the property to allow controlled proton leakage into the mitochondrial matrix. UCP2 has the ability to protect neurons against a critically high mitochondrial membrane potential, thereby reducing ROS production. In this thesis, a previously made mutUNG1-expressing mouse model was used to study mitochondrial morphology and to quantitate the density of UCP2 (UCP2 gold particles/μm^2) in different compartments of neurons in the cornu ammonis 1 (CA1) and dentate gyrus. The structure of the mitochondria in somas was markedly different in mutUNG1-expressing mice compared to wild type littermates. The mitochondria in mutUNG1-expressing mice were aggregated, clustered, and irregularly shaped while the wild type mice had regular mitochondrial shape in the somas. The average area (nm^2) of mitochondria was increased significantly in presynaptic terminals and somas of mutUNG1-expressing mice compared to wild type mice. The average size (nm^2) of individual mitochondria was significantly higher in presynaptic terminals and myelinated axons of mutUNG1-expressing mice compared to wild type mice. Electron microscopic immunogold cytochemistry was used to quantify mitochondrial UCP2 in different neuronal compartments. In mutUNG1-expressing mice, the density of UCP2 was significantly higher compared to wild type mice in myelinated axons, presynaptic terminals, and somas. The significantly higher mitochondrial UCP2 in myelinated axons and in presynaptic terminals could help to rescue dysfunctional mitochondria in mutUNG1-expressing mice. The significantly increased density of UCP2 in the somas could result from the large numbers of damaged mitochondria, transported to the somas from different compartments of the neurons in the mutUNG1-expressing mice. The present study suggests that UCP2 is neuroprotective against neurodegeneration caused by mitochondrial dysfunction.

NORSK SAMMENDRAG

Mitokondrier er viktige organeller for energiomsetningen i nerveceller. Energibehovet er høyere i nevroner enn i de fleste andre celler, og viser seg i form av høyt forbruk av oksygen i hjernen. Endogene reaktive oksygen substanser (ROS) oppstår som et biprodukt av normal oksygenmetabolisme i mitokondriene. I nevrodegenerativ patologi kan ROS føre til oksidativt stress og skader på mitokondrielt DNA (mtDNA). Transgene muter uracil-DNA glykosylase 1 (mutUNG1) mus, som uttrykker mutUNG1-enzymet, induserer mitokondriell toksisitet forårsaket av høye antall apurine/apyrimidine-seter i mtDNA i hippocampus. "Utkoplingsproteinet" (UCP2, uncoupling protein 2) tillater kontrollert protonlekkasje til mitokondriematrix. UCP2 har evne til å beskytte nevroner mot et kritisk høyt mitokondrie-membranpotensial, og gir dermed redusert ROS-produksjon. I denne oppgaven ble en tidligere laget transgen mutUNG1-musemodell brukt til å studere mitokondriemorfologi og tetthet av UCP2 (UCP2 gull partikler/μm^2) i ulike deler av nevroner i cornu ammonis 1 (CA1) og i gyrus dentatus. Strukturen på mitokondriene i nevroncellerkroppen, soma, i mutUNG1 mus var forandret sammenlignet med i villtypekontroller. Mitokondrier fra mutUNG1 mus var aggregerte, klumpete, og irregulære i formen, mens villtypemus hadde mitokondrier med normal morfologi i soma. Gjennomsnittlig areal (nm^2) av mitokondrier var betydelig økt i både presynaptiske terminaler og i somata hos mus med mutUNG1-uttrykk sammenlignet med villtypemus. Den gjennomsnittlige individuelle mitokondriestørrelsen (nm^2) var signifikant høyere i presynaptiske terminaler og i myeliniserte aksoner hos mus med mutUNG1-uttrykk sammenlignet med villtypemus. Elektronmikroskopisk immunogull cytokjemi ble brukt til kvantifisering av UCP2 i ulike deler av nevronet. I mutUNG1-uttrykkende mus var tettheten av UCP2 signifikant høyere sammenlignet med villtypemus i myeliniserte aksoner, presynaptiske terminaler, og somata. Denne økningen av UCP2 i myeliniserte aksoner fra mutUNG1-uttrykkende mus kan gjenspeile behovet for å opprettholde aksonal energihomeostase. Den betydelige økningen av UCP2 i presynaptiske terminaler kan bidra til å redde de dysfunksjonelle mitokondriene i mutUNG1-uttrykkende mus. Den økte tettheten av UCP2 i somata kan skyldes det store antallet av skadede mitokondrier, fraktet til somata fra ulike området av nervecellen i mutUNG1-mus. Denne studien tyder på at UCP2 kan beskytte mot nevrodegenerasjon forårsaket av dysfunksjonelle mitokondrier.

TABLE OF CONTENTS

TABLE OF CONTENTS (Contd.)

TABLE OF CONTENTS (Contd.)

TABLE OF CONTENTS (Contd.)

LIST OF ABBREVIATIONS

.OH	:	Hydroxyl radical
°C	:	Degree Celsius
µl	:	Micro liter
µm	:	Micro meter
AD	:	Alzheimer's disease
ADP	:	Adenosine diphosphate
AMPA	:	α-amino-3-hydroxy-5-methyl-4-isoxazolepropionic acid
AP-site	:	Apurinic/apyrimidinic-site
ATP	:	Adenosine -5′-triphosphate
BER	:	Base excision repair
BSA	:	Bovine serum albumin
CA1	:	Cornu ammonis 1
CNS	:	Central nervous system
CaMKIIα	:	Calcium/calmodulin-dependent kinase II alpha
CoQ	:	Coenzyme Q
Cytc	:	Cytochrome complex
DNA	:	Deoxyribonucleic acid
DG	:	Dentate gyrus
Dox	:	Doxycycline
EC	:	Entorhinal cortex
ETC	:	Electron transport chain
FADH	:	Flavin adenine dinucleotide
FFA	:	Free fatty acid
H^+	:	Proton
IM	:	Inner membrane
mg/mL	:	Milligram per milliliter
MOMP	:	Mitochondrial outer membrane permeabilization
mtDNA	:	Mitochondrial DNA
mutUNG1	:	Mutated uracil-DNA glycosylase 1
NADH	:	Nicotinamide adenine dinucleotide
nm	:	Nano meter
OS	:	Oxidative stress
PD	:	Parkinson's disease
PMF	:	Proton motive force
PTP	:	Permeability transition pore
ROS	:	Reactive oxygen species
rtTA	:	Reverse Tet transactivator
SDS	:	Sodium dodecyl sulfate
SOD	:	Superoxide dismutase
TCA	:	Tricarboxylic acid
tif	:	Tagged image file
UCP	:	Uncoupling protein
UDG	:	Uracil DNA-glycosylase
UF	:	Ultra filtered

CHAPTER I

BACKGROUND

1.1 Mitochondria: structure and functions

Mitochondria are a pivotal part of the cell. They generate adenosine-5′-triphosphate (ATP) as a source of bioenergy through oxidative phosphorylation. Therefore, mitochondria are considered as the power house of cells. A typical animal cell can have 1000 to 2000 mitochondria (Alberts et al., 2002). A mitochondrion is enclosed by an outer membrane and a more complex inner membrane. The space between the inner and outer mitochondrial membranes is called the intermembrane space. The inner membrane is folded into numerous cristae, which greatly increase the surface area of the inner membrane. The proteins involved in the electron transport chain (ETC) and ATP synthesis are located within this membrane. The large internal space enclosed by the inner mitochondrial membrane is called the matrix (Figure 1.1) (Alberts et al., 2002).

The brain has a high energy demand that counts for 20% of the resting metabolism (Attwell and Laughlin, 2001). The dynamic behavior of mitochondria is an important aspect of controlling local energy demands in different compartments of neurons (Chan, 2006). Thus, defects in mitochondrial distribution can cause localized energy deficits in affected neurons, resulting in synaptic dysfunction that may progress to neurodegeneration (Lu, 2009; Selkoe, 2002). Dysfunction and disintegration of mitochondria have also been related to neurodegeneration (de Souza-Pinto et al., 2008).

The energy budget in the brain controls neuronal functions. A reduction in brain energy production is implicated with the cognitive decline associated with neurophysiopatho-logies. The production of reactive oxygen species (ROS) from the mitochondrial ETC can damage all macromolecules, including deoxyribonucleic acid (DNA) (Adam-Vizi, 2005). An irreparable oxidative DNA lesion of nuclear and mitochondrial DNA (mtDNA), can lead to mitochondrial damage (Druzhyna et al., 2008). Failure to repair oxidative DNA lesion can cause loss of its function and progression of neuropathological abnormalities (Bohr et al., 2002).
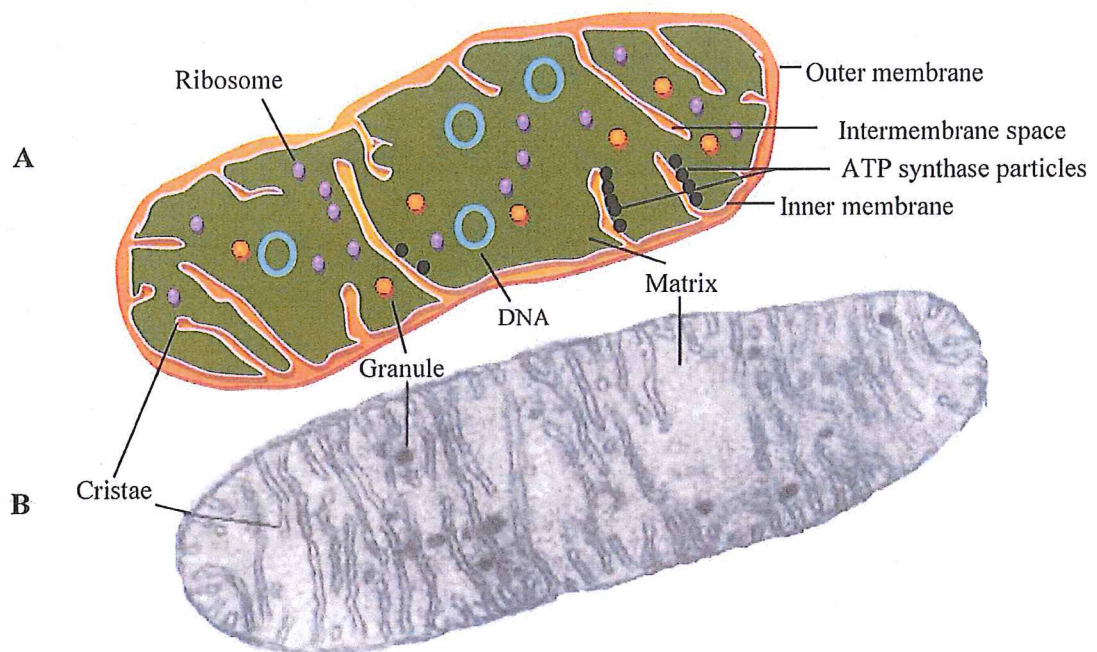
Figure 1.1: A typical mitochondrion is depicted as spherical, long, thread-like, stiff or elongated cylinder shape with a diameter of 0.5 to 1.0 micrometer (µm) and 1-2 µm in length. A mitochondrion (A: typical cartoon, B: electron micrograph) is comprised of the outer membrane, intermembrane space, inner membrane, matrix, cristae, circular DNA, ribosomes, granules, and ATP synthesis particles associated with ETC.

Mitochondria are mobile organelles. Time lapse photography shows that they are constantly moving and changing shape. The matrix is densely packed with hundreds of enzymes, including the soluble enzymes of the citric acid cycle. In addition, there are enzymes involved in the oxidation of fatty acids and amino acids. The matrix also contains mitochondrial DNA, ribosomes, and the enzymes required for the expression of mitochondrial genes. The mtDNA contains thirty-seven genes, all of which are essential for normal mitochondrial functions (Alberts et al., 2002).

The inner membrane potential of the mitochondrion determines ATP and free radical production (Kroemer and Reed, 2000; Nicholls and Ward, 2000). The production of ATP is critical for cellular energy metabolism and cell survival. Mitochondria also regulate additional physiological functions such as cellular calcium homeostasis and apoptosis (Nübel and Ricquier, 2006).

1.2 Neuron

The neuron is the functional unit of the central nervous system (CNS). It can receive, integrate, and transmit information. A typical neuron contains a soma (also called cell body), an axon, dendrites, and axon terminals (also called end bulbs or presynaptic terminals) (Figure 1.2).

The soma is the site of major metabolic activity in the neuron. The soma of a neuron consists of nucleus and other organelles (common to living cells) contained within the cell membrane including ribosomes, mitochondria, endoplasmic reticulum, lysosomes, and the Golgi complex (Figure 1.2) (Hammond, 2008).

The axon also called nerve fiber brings information away from the soma to the synaptic sites contacting other neurons. The axon is longer than the dendrites of a neuron. The axon hillock is the site of summation for incoming information and initiation of the nerve impulse. The axon terminals of a neuron are the small knobs at the end of an axon that release chemicals called neurotransmitters (Kandel, 1979). The dendrites are short branching processes extending from the soma. Dendritic spines are short outgrowths of stem dendrites receiving synaptic input (Figure 1.3).

The flow of information moves in one direction: dendrite to soma to axon to axon terminal to synapse.
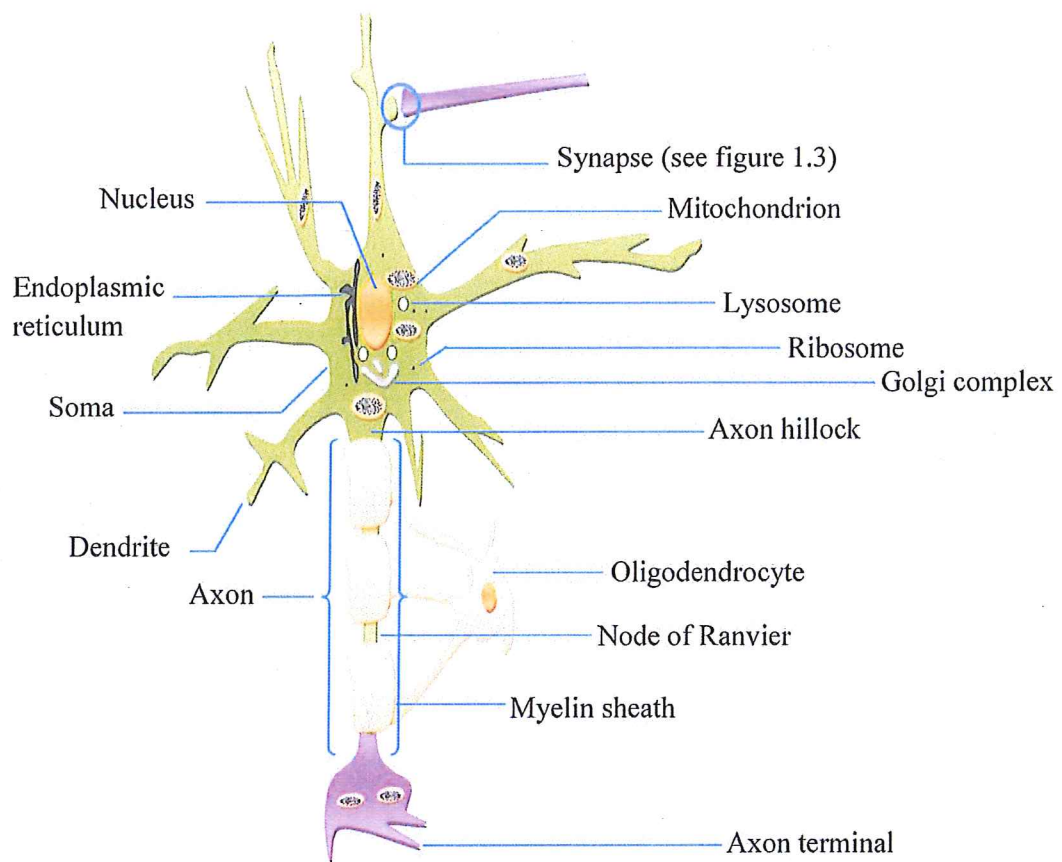
Figure 1.2: Schematic drawing of a typical neuron showing the different neuronal compartments and organelles.

The synapse is the point of connection between two neurons. Communication between neurons takes place at this junction. The synapse consists of three elements: 1) the presynaptic membrane which is formed by the axon terminal of an axon, 2) the postsynaptic membrane which is composed of a segment of a dendrite, and 3) the space between these two structures, which is called the synaptic cleft (Figure 1.3) (Kalil, 1989).
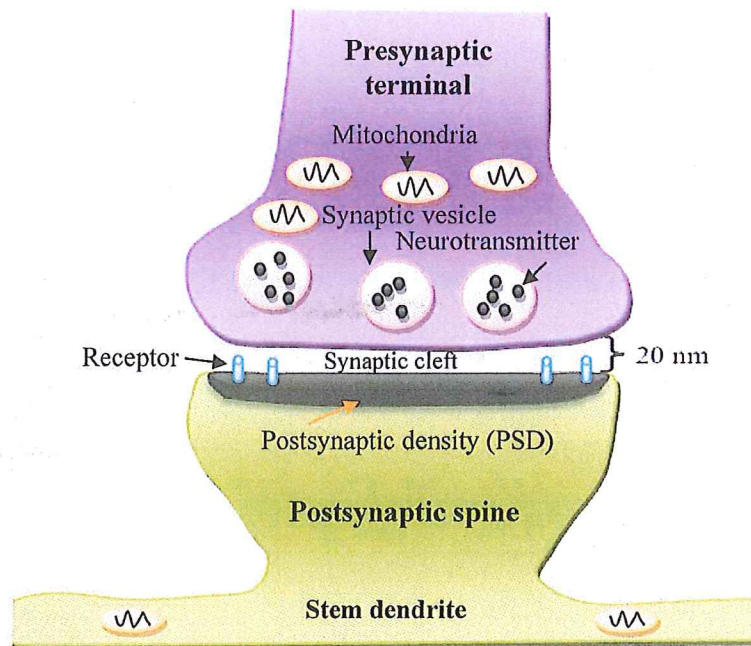
Figure 1.3: The typical structure of a synapse. The axon (Presynaptic terminal) from one nerve cell runs signaling to dendritic spine (Postsynaptic terminal) through receptors.

1.3 Role of mitochondria in neurons

Mitochondria are energy-producing factories considered to be especially important for neurons that are specialized cells of high levels of energy demands. Mitochondria are highly mobile and move into the different compartments of neurons. The produced energy plays important roles in neuronal differentiation, neurotransmitter release, neuronal growth, and dendritic modeling. Mitochondria also control the level of ROS. Therefore, any disturbance in mitochondrial functions may impair neuroplasticity and cause neuronal degeneration (Cheng et al., 2010).

1.4 Mitochondrial electron transport chain

The tricarboxylic acid (TCA) cycle is an indispensable contributor for aerobic metabolism of major nutrients (carbohydrates, fats, and proteins) into carbon dioxide and water (H_2O) in the mitochondrial matrix. The acetyl-CoA is a common product of glycolysis, fatty acid oxidation, and ketogenic amino acid catabolism. Most of the energy released during the oxidation of acetyl-CoA to carbon dioxide is retained in the reduced coenzymes nicotinamide adenine dinucleotide (NADH) and flavin adenine dinucleotide ($FADH_2$). The NADH and $FADH_2$ that are generated during TCA cycle can thus deliver electrons to mitochondrial ETC localized in the inner mitochondrial membrane (Figure 1.4).
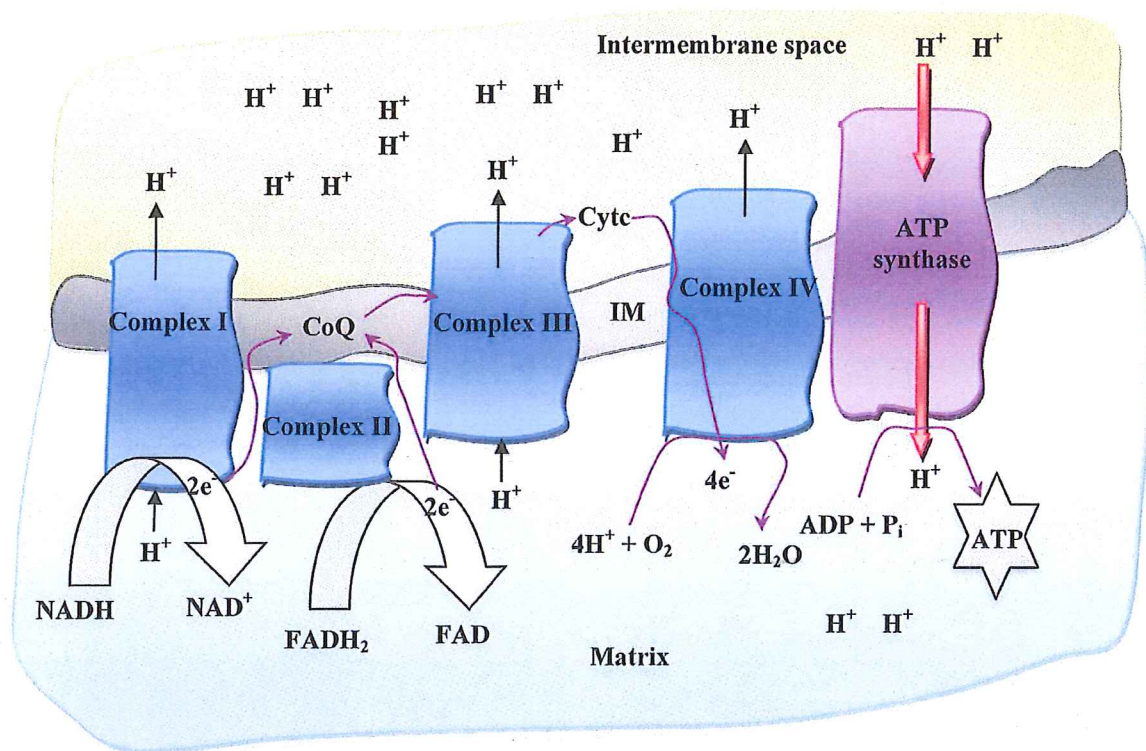
Figure 1.4: The ETC is composed of three large protein complexes (colored blue) fixed in the inner membrane and two mobile electron carriers (Coenzyme Q, CoQ and Cytochrome complex, Cytc). ETC couples electron transfer between an electron donor (such as NADH) and an electron acceptor (such as O_2). The proton (H^+) concentration is much greater in the intermembrane space than the matrix, thus generating an electrochemical H^+ gradient. The resulting electrochemical H^+ gradient is used to generate chemical energy in the form of ATP (shown in star) through ATP synthase (colored purple). IM = Inner membrane.

[Modified from Alberts et al., 2002]

During respiration, electrons are released from NADH and $FADH_2$, and they are eventually transferred to oxygen (O_2) in order to yield H_2O (Equations 1.1 & 1.2, Figure 1.4).

$$H^+ + NADH \rightarrow NAD^+ + 2H^+ + 2e^- \dots\dots\dots\dots\dots\dots\dots\dots\dots[1.1]$$

$$4H^+ + 4e^- + O_2 \rightarrow 2H_2O\dots\dots\dots\dots\dots\dots\dots\dots\dots[1.2]$$
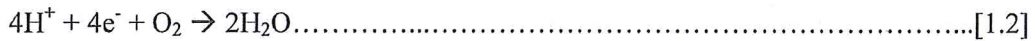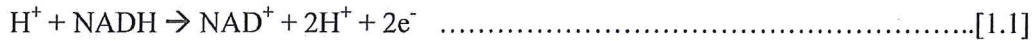
At complex I, III, and IV during electron transport, protons (H^+) from the mitochondrial matrix are transported across the inner mitochondrial membrane, resulting in a proton concentration gradient across the membrane. The movement of protons back across the inner membrane, results in a so-called proton motive force (PMF), where ATP is synthesized from adenosine diphosphate (ADP) and inorganic phosphate (P_i) by the ATP synthase, collectively this process is called oxidative phosphorylation (Figure 1.4) (Miles, 2003).

1.5 Mitochondrial dynamics and dysfunction

Mitochondria are dynamic organelles that constantly divide and fuse, thus forming interconnected networks or fragmented units within the cell (Chan, 2006; Chen and Chan, 2006; Lu, 2009). Equilibrium between fusion and fission controls the morphology of the mitochondria (Olichon et al., 2006) (Figure 1.5). Mitochondria can also be transported within the cell either by anterograde (soma to periphery) or retrograde (periphery to soma) movement (Figure 1.6). Mitochondrial dynamics and distribution are important for the physiological function of neurons. Neurons are highly specialized cells that face unique challenges, such as requiring large amounts of energy for neuronal communication (Lu, 2009). Mitochondria are distributed within neurons to provide the locally required energy (Chen and Chan, 2006), and synaptic regions of axons are well known to contain abundant mitochondria to sustain these local energy demands (Chan, 2006).
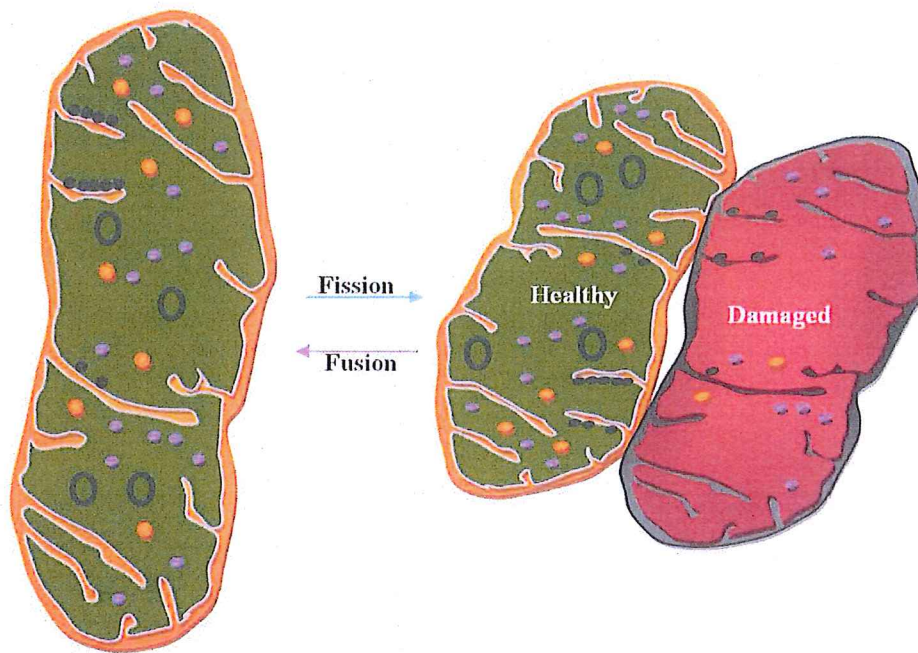
Figure 1.5: Mitochondrial fusion can rescue dysfunctional mitochondria (red) through diffusion and sharing components between organelles with functional mitochondria (green). Mitochondrial fission is the division of single mitochondria into two and facilitates quality control.

[Modified from Youle and van der Bliek, 2012]

A defect in mitochondrial function is key indicator in many neurodegenerative diseases and aging. Aggregation of mitochondria in the soma is also a common step preceding apoptosis (Lu, 2009). Mitochondria are important in determining the ability of dendrites to support synapses (Li et al., 2004).
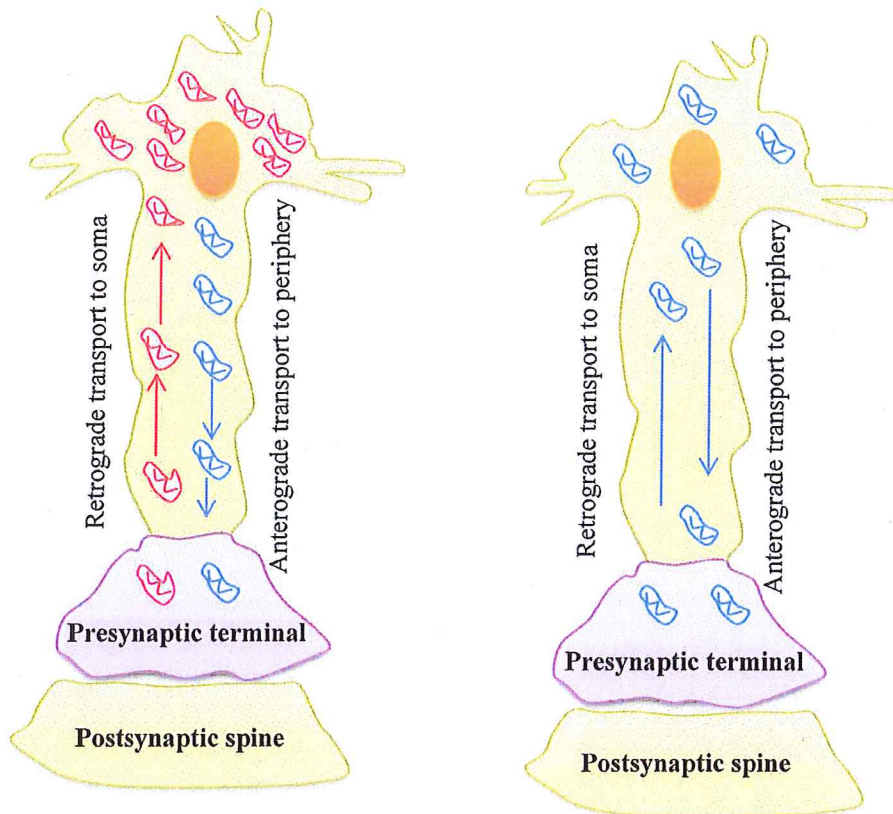
Figure 1.6: Mitochondrial dynamics showing anterograde (soma to periphery) and retrograde (periphery to soma) transport of mitochondria. An unhealthy neuron (left) is showing excessive fragmentation of mitochondria (colored red), accumulation of mitochondria in the soma, abnormal distribution, and different shapes of mitochondria in different neuronal compartments compared to the healthy neuron (right).

[Modified from Reddy and Shirendeb, 2012]

1.6 Effects of mitochondrial reactive oxygen species production

ROS are singlet electron intermediates produced during the reduction of O_2 to H_2O. Mitochondria are the major endogenous source of ROS in most cell types (Boveris et al., 1972; Boveris and Chance, 1973). When ROS are produced in excess, they lead to oxidative stress (OS) that can damage cell constituents and induce cell death. Thus, OS is associated with aging. A great number of pathologies ranging from neurological disorders to metabolic diseases are associated with ROS overproduction (Figure 1.7) (Harper et al., 2008; Piconi et al., 2003; Lemire and Appanna, 2011). However, when ROS are produced in a controlled fashion, they play very important signaling role in cell growth and differentiation (Hamanaka and Chandel, 2010). Mitochondria are well equipped with anti-oxidative defense mechanisms to detoxify ROS. The level of ROS can be decreased by re-entry of proton into the mitochondrial matrix (uncoupled respiration), thereby decreasing PMF (Mailloux and Harper, 2012).
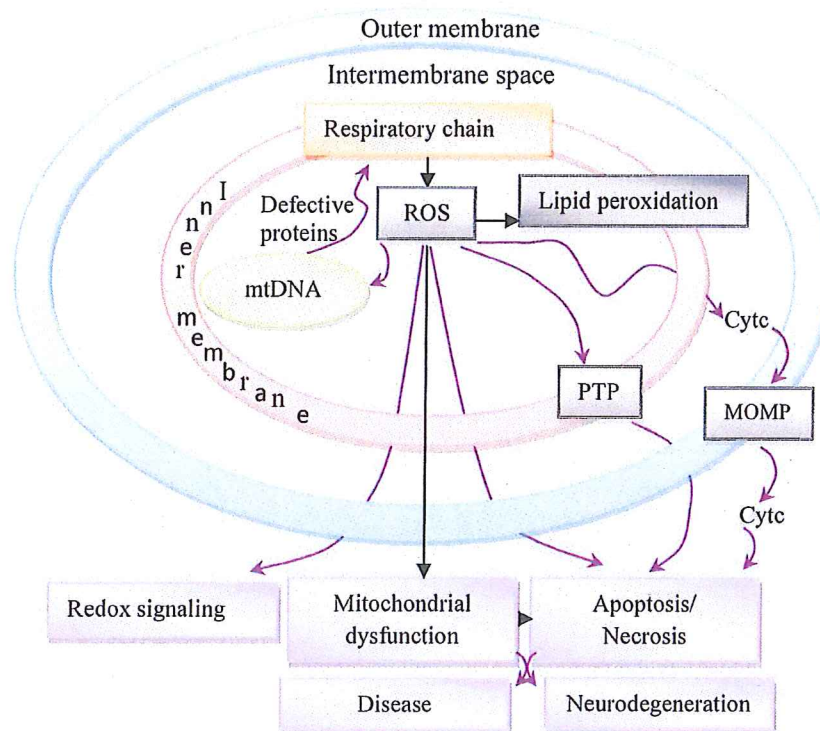
Figure 1.7: A schematic overview of mitochondrial ROS production. ROS production can lead to oxidative damage and diminish ATP production or other essential functions. Mitochondrial damage can increase the release of Cytc into cytosol by mitochondrial outer membrane permeabilization (MOMP), and induce the permeability transition pore (PTP), leading to mitochondrial dysfunction and cellular apoptosis. This abnormal cellular functioning may progress to neurodegeneration and other diseases.

[Modified from Murphy, 2009]

1.7 Mitochondrial dysfunction and neurodegenerative disease

Mitochondrial dysfunction is primarily caused by damage to the respiratory chain and is believed to be a major cause of neurological abnormalities (Figure 1.8). Though mitochondria are dependent on nuclear gene products, they also contain their own genome (16569 base pairs in human), which partly provides components for the ETC (Burger et al., 2003). Since several components of the ETC are encoded by the mtDNA, instability of the mtDNA leads to decreased mitochondrial energetic function. An accumulation of mtDNA mutations may result in dysfunctional mitochondrial respiration, which can further increase excessive ROS generation and oxidative damage. Mitochondrial OS can lead to an accumulation of damaged mitochondria, and is believed to be particularly devastating to neuronal tissue (Loeb et al., 2005). Moreover, mitochondrial dysfunction plays a critical role in neurodegeneration, due to the high energy demands of neuronal tissue (Attwell and Laughlin, 2001; de Souza-Pinto et al., 2008).
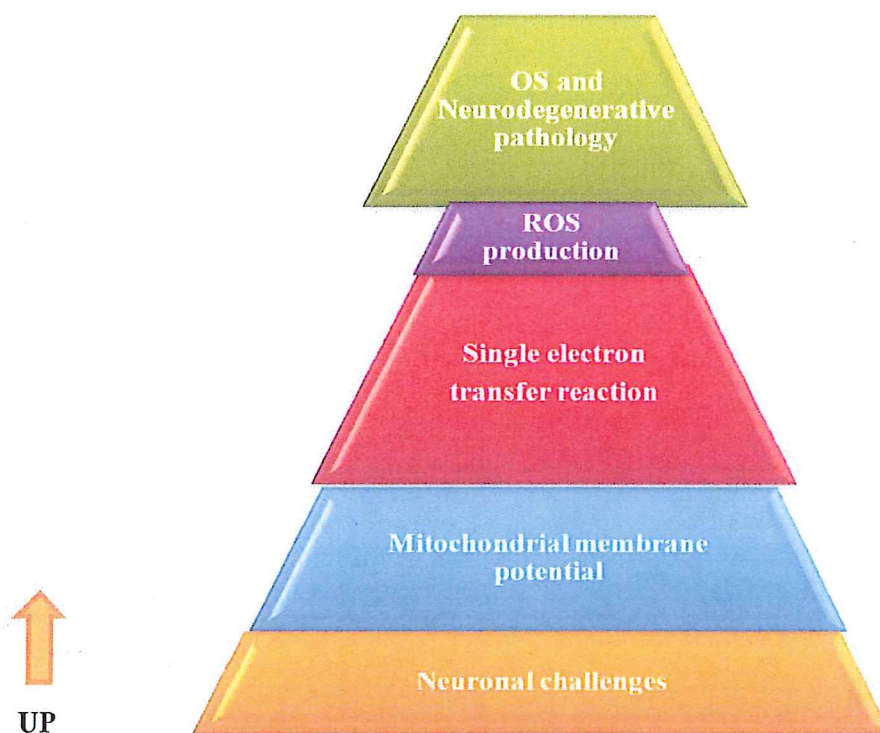
Figure 1.8: The pyramidal diagram of mitochondrial dysfunction. Dysfunctional mitochondria may lead to accelerate neuronal challenges by increasing mitochondrial membrane potential to excessive levels, which may stimulate single electron transfer reaction. Therefore, ROS production can cause to onset of neurodegenerative pathology through oxidative stress.

Loss of mitochondrial function is connected with several neuropathologies that are often associated with the old age period. These include Alzheimer's disease (AD), Parkinson's disease (PD) and Huntington's disease, all of which share the common feature of accumulation of oxidative DNA damage (de Souza-Pinto et al., 2008).

1.8 Mitochondrial DNA repair system

The mtDNA is situated inside of the inner membrane of mitochondria (Figure 1.1). Damages to the mtDNA and associated OS during the neurodegenerative processes can impair mitochondrial energy metabolism and homeostasis of neurons (Yang et al., 2008). The frequency of oxidative damage of mtDNA is ten to twenty times greater than that of nuclear DNA (Richter et al., 1988). Therefore, mitochondria need to have efficient DNA repair mechanisms to maintain an error-free mitochondrial genome and to prevent dysfunction of the organelles (Larsen et al., 2005; Wallace, 1994).

Base excision repair (BER) is a multistep pathway that corrects DNA damage often arising from cellular ROS metabolism (Lindahl and Wood, 1999). BER has been found and characterized in both the nucleus and mitochondria (Anderson and Friedberg, 1980; de Souza-Pinto et al., 2008). The initial step of BER is recognition and removal of a base-lesion by a specific DNA glycosylase, creating an apurinic/apyrimidinic-site (AP-site) (Kubota et al., 1996). The continued BER of DNA can occur either through a short patch (1 nucleotide) or a long patch (2-10 nucleotides) repair pathway. The completion of the BER pathway is accomplished by the coordinated action of series of additional enzymes which carry out strand incision, gap-filling, and ligation (Robertson et al., 2009). The capacity of the BER system exhibits tissue-specific variations and even though the brain is one of the tissues with the lowest BER-capacity with the highest oxidative loads (Karahalil et al., 2002). Mitochondrial BER-glycosylase activity is decreased in all regions of the brain in mice during aging (Imam et al., 2006).

Uracil-DNA glycosylase (UDG/UNG) removes unnatural uracil from DNA by cleaving the N-glycosylic bond and thereby initiating the BER pathway (Anderson and Friedberg, 1980). There exists both a nuclear form (called UNG2) and a mitochondrial form of UNG (called UNG1) (Nilsen et al., 1997; Sousa et al., 2007).

1.9 mutUNG1 mouse model

The mutUNG1 mouse model was previously generated to investigate the impact of mtDNA damage in forebrain neurons (Lauritzen et al., 2010). This model is based on a mutation in the catalytic site of UNG1 (mutated UNG1 or mutUNG1), resulting in an amino acid substitution where tyrosine in position 147 is replaced with alanine, with the ability to remove thymine in addition to uracil from mtDNA (Kavli et al., 1996).

The mouse model utilizes the Tet-on system for spatial and temporal control of transgene expression. This system contains two genetic elements: a transactivator and a Tet-promoter that responds to the transactivator. In the Tet-on system, the reverse transcriptional activator (rtTA) initiates transcription of target gene in the presence of antibiotic Doxycycline (Dox) (Gossen et al., 1995). By using the α-calcium/calmodulin-dependent kinase II alpha (CaMKIIα) promoter to control the expression of the transactivator, the activity of the Tet-on system (and thereby the expression of the transgene mutUNG1) is limited to forebrain neurons of brain regions like the hippocampus (Sola et al., 1999; Mayford et al., 1996). An improved second generation reverse Tet transactivator (rtTA2) has been used in this model, which has improved affinity for Dox and reduced background activity (Urlinger et al., 2000). Tet-on mice expressing rtTA2 under the control of the CaMKIIα promoter shows high, tight, and specific expression in their forebrain neurons (Mansuy et al., 1998).

The Tet-promoter used in this model is a bi-directional promoter, which in addition to controlling the expression of mutUNG1, enables expression of the reporter protein Luciferase (Lauritzen et al., 2010). The presence of Dox enables the transactivator to bind to the responsive Tet-promoter, thereby enabling expression of mutUNG1 accompanied by a Luciferase (Lauritzen et al., 2010; Gossen and Bujard, 1992; Gossen et al., 1995) (Figure 1.9). The mutUNG1 expression is thereby spatially regulated by the forebrain specific CaMKIIα promoter and temporally by the addition of Dox (Lauritzen et al., 2010).
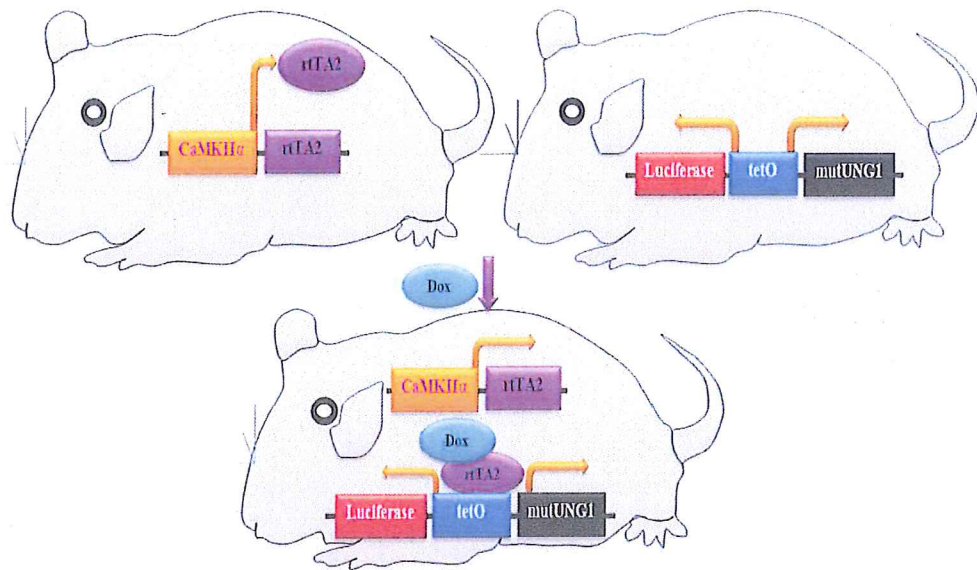
Figure 1.9: Transgenic mouse model for inducible mutUNG1 expression. The presence of Doxycycline (Dox) enables the transactivator (rtTA2) to bind to the Tet-promoter (tetO). The bi-directional doxycycline-responsive promoter induces both mutUNG1 and Luciferase, the former leading to mtDNA damage and mitochondrial dysfunction.

[Modified from Knut H. Lauritzen]

In this experiment, mutUNG1-expressing mice were used as a model to test the effects of dysfunctional mitochondria in neurodegenerative disease (Lauritzen et al., 2010).

1.10 mutUNG1 and mitochondrial dysfunction

Neuronal cells in the hippocampus show severe, progressive neurodegeneration and apoptosis from impaired BER capacity (Lauritzen et al., 2010). However, hippocampal neurons are highly sensitive to elevated levels of AP-sites in mtDNA (Lauritzen et al., 2011).

AP-sites are a threat to cellular viability and genomic integrity (Dianov et al., 2003; Pinz et al., 1995). They are highly cytotoxic and lead to DNA damage (Pages et al., 2008). This type of damage is especially deleterious to mammalian mtDNA, since mitochondria do not have translesion synthesis repair mechanisms (Zhang et al., 2006; Ropp and Copeland, 1996). AP-sites can be introduced spontaneously by base loss, and are critical intermediates of the base excision repair pathway (Hoeijmakers, 2001; Lindahl, 1993).

The increase of AP-sites causes phenotypical abnormalities in mutUNG1-expressing mice. They show a loss of neuronal tissue, atrophy, and signs of increased apoptosis in the hippocampus. There is also an accumulation of mitochondria in the soma of hippocampal neuronal cells. This is believed to be caused by the high levels of AP-sites in mtDNA, which in turn leads to mitochondrial dysfunction followed by a breakdown of mitochondrial dynamics (Lauritzen et al., 2010). Similar situations with accumulation of mitochondria in the soma of hippocampal neuronal cells are observed in neurodegenerative pathologies like AD (Chen and Chan, 2009).

There are also abnormalities on the synaptic level in mutUNG1-expressing mice. They show a decrease of α-amino-3-hydroxy-5-methyl-4-isoxazolepropionic acid receptor (AMPA) subunit density in the hilus of the dentate gyrus (DG) region, but this is not seen in the stratum radiatum of the cornu ammonis 1 (CA1) region in the hippocampus. However, there is a decrease in the average length of post synaptic densities (PSDs) in the stratum radiatum but increased the average length of PSDs in the hilus of the DG of mutUNG1-expressing mice compared to wild type littermates (Lauritzen et al., 2011).

There is a loss of the mtDNA copy number in the hippocampus of mutUNG1-expressing mice, and a reduction of mtDNA expression compared to wild type controls (Lauritzen et al., 2011). This is reflected on the protein level, where immunohisto-chemical studies show that the levels of mitochondrial encoded complexes (Complex I, III, and IV) in ETC are affected by mutUNG1 expression. Complex II which is exclusively nuclear encoded remains unaffected (Lauritzen et al., 2011). Astrocytes are essential in the CNS and reactive astrogliosis may contribute in CNS disorders by impairing normal astrocyte function (Sofroniew and Vinters, 2010). The process of astrogliosis can modify tissue morphology and causes overlapping of astrocytes, which can lead to scar formation. Reactive astrogliosis can also cause OS (Sofroniew, 2009). Signs of astrogliosis with increased number and severe infiltration of astrocytes have been observed in the hippocampus of mutUNG1-expressing mice during the induction period (Lauritzen et al., 2011).

A gradual elevation of antioxidant proteins superoxide dismutase has also been noticed during the induction period of mutUNG1-expressing mice. This induction of the endogenous antioxidant system indicates increased level of ROS from mitochondrial dysfunction in mutUNG1-expressing mice, since the mitochondrial version of superoxide dismutase (SOD2) is expressed early and highly expressed (Lauritzen et al., 2011).

The mutUNG1-expressing mice show defects associated with behavioral alterations. In the Morris water maze test, mutUNG1-expressing mice show poorer learning ability with memory deficit compared to wild type littermates. Other behavioral tests display increased locomotor activity and lack of anxietylike responses in induced mutUNG1 mice (Lauritzen et al., 2010).

1.11 Uncoupling protein 2

Uncoupling proteins (UCPs) are transmembrane proteins, which act as protonphores, and belong to a large family of the mitochondrial solute carrier 25 (SLC25s) proteins. There are five known UCP homologues present in various types of mammalian and plant tissues. Of these, UCP1, UCP2, and UCP3 are closely related, while UCP4 and UCP5 are more divergent (Ricquier and Bouillaud, 2000).

The UCP2 was discovered in 1997 (Fleury et al., 1997). UCP2 belongs to the family of mitochondrial solute carrier 25, member 8. It is ubiquitously expressed in the spleen, lung, intestine, brain, muscle, heart, kidney, pancreatic islets, and immune cells (lymphocytes, macrophages, adipocytes, and thymus) (Ricquier and Bouillaud, 2000, Pecqueur et al., 2001; Rousset et al., 2006).

In the mouse brain, UCP2 has been found to be an abundant in the hippocampus, ventral septal region, hypothalamus, hindbrain (medulla), cerebellum (Richard et al., 1999), dorsal endopiriform nucleus, piriform cortex, and other tissues (Clavel et al., 2003).

UCP2 is located in the inner membrane of the mitochondria (Figure 1.10) and is encoded by nuclear DNA. UCP2 is composed of 309 amino acids and molecular weight of 37 kDa. This transmembrane protein mediates a regulated discharge of proton gradient generated by the mitochondrial respiratory chain (Ledesma et al., 2002).
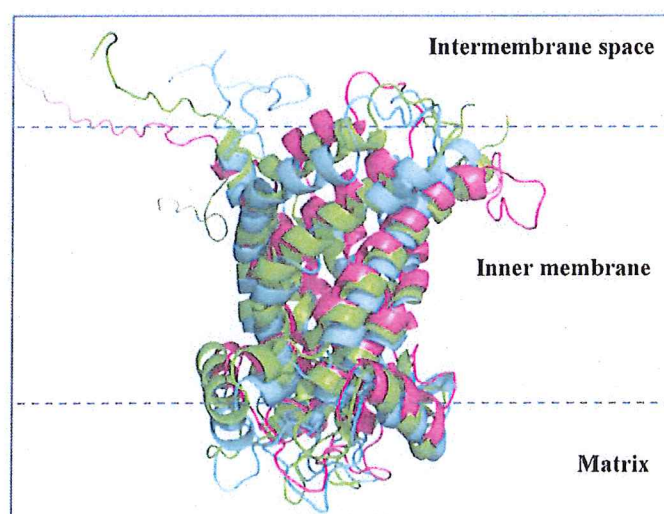
Figure 1.10: The 3D crystal structure of UCP2. UCP2 is localized in the mitochondrial inner membrane.

[Source: Pebay-Peyroula et al., 2003]

The proton transport capacity of UCP2 is stimulated by free fatty acids (FFA) (Figure 1.11). UCP2 has triggered an important question about controlled oxidative phosphorylation uncoupling and the physiological function of this process. UCP2 can influence mitochondrial membrane potential and mitochondrial ROS production. It is also thought to be involved in apoptotic signaling pathways and has been suggested as important in the regulation of energy utilization, mitochondrial bioenergetics, cell proliferation, synaptogenesis, and cardio- and neuroprotection in the adult brain (Valouskova and Modriansky, 2008; Simon-Areces et al., 2012).
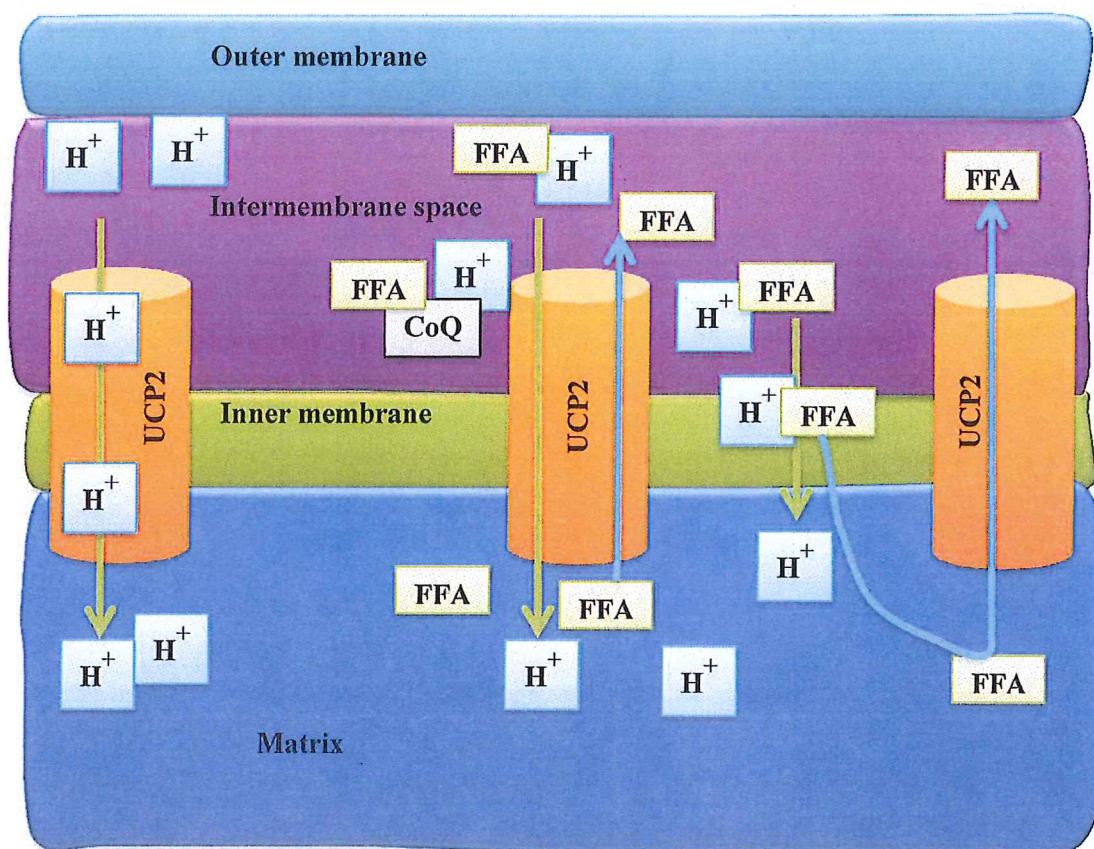
Figure 1.11: UCP2 mediated uncoupling. UCP2 transport H^+ directly or with the help of free fatty acid (FFA), to the matrix from the intermembrane space. FFA donates H^+ directly to the UCP2, which translocate the H^+ to the matrix. The donation is activated by direct interaction between the FFA and UCP2 or CoQ and FFA.

[Modified from Klingenberg and Huang, 1999; Echtay et al., 2001]

1.12 Relationship between UCP2 and mitochondrial ROS

Mitochondrial uncoupling mediated by UCP2 allows controlled H^+ re-entry into the mitochondrial matrix, thereby reducing the membrane potential and producing heat (Andrews et al., 2005) (Figure 1.12). An excessive mitochondrial membrane potential causes a disproportionately large amount of ROS production (Korshunov et al., 1997), which is counteracted by increasing the level of UCP2 by reducing the activity of ETC or increasing the biogenesis of mitochondria without compromising ATP production (Pecqueur et al., 2001). Thus, UCP2 plays a positive physiological role in neuroprotection (Diano et al., 2003; Bechmann et al., 2002) and aging (Conti et al., 2006; Fridell et al., 2005).
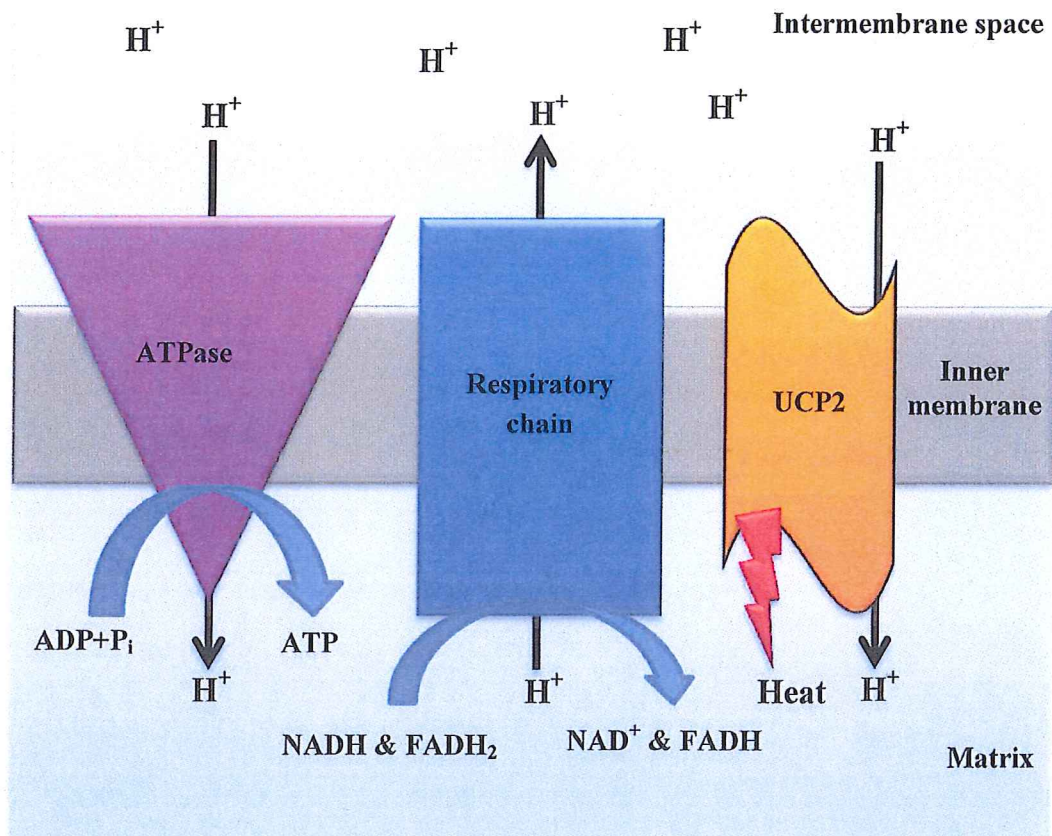
Figure 1.12: Effect of uncoupling respiration in inner mitochondrial membrane by UCP2. UCP2 may control the thermal homoeostasis by producing heat in mitochondrial matrix.

[Modified from Andrews et al., 2005]
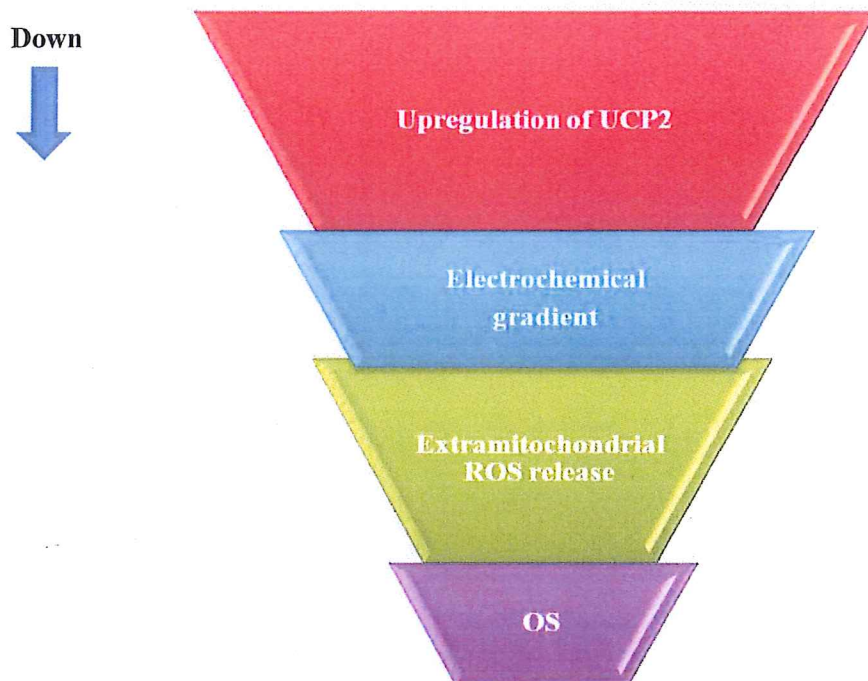
Figure 1.13: The functional model of UCP2. The upregulation of UCP2 dissipates the proton electrochemical gradient across the mitochondrial inner membrane and thereby lowers the level of ROS production. Thus, UCP2 balances OS in nerve cells.

Mitochondrial dysfunction and ROS production are believed to be involved in the aging process. Overexpressing UCP2 in adult neurons has resulted in increased uncoupled respiration, decreased ROS production, decreased oxidative damage (Figure 1.13), and extended lifespan of mice (Andrews and Horvath, 2009) and adult flies without compromising fertility or physical activity (Fridell et al., 2005). These results support the "uncoupling-to-survive" hypothesis (Brand, 2000). This hypothesis states that uncoupling leads to greater oxygen consumption and reduces the PMF by reducing the mitochondrial membrane potential, which subsequently reduces ROS generation (Mattiasson and Sullivan, 2006).

1.13 Hippocampal anatomy

The hippocampus is a part of the temporal lobe in the limbic system (Figure 1.14 A). It is particularly important for forming new memories, emotions, senses (such as smell and sound), navigation, and spatial orientation. The hippocampus is a sea horse-shaped paired structure and there is a hippocampus located in each brain hemisphere (Figure 1.14 B). A hippocampus consists of two interlocking laminae of gray matter i.e., the cornu ammonis (CA) and dentate gyrus (DG). The DG contains the fascia dentata and the hilus, while the CA region is differentiated into the CA1, CA2, and CA3 subfields (Figure 1.14 C) (Andersen et al., 2007).

A

[Modified from Dorr et al., 2007]

B
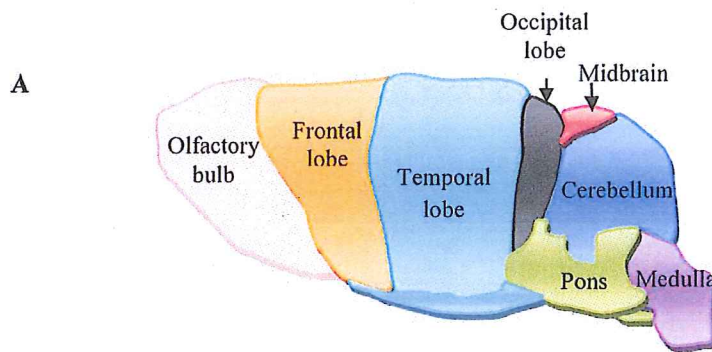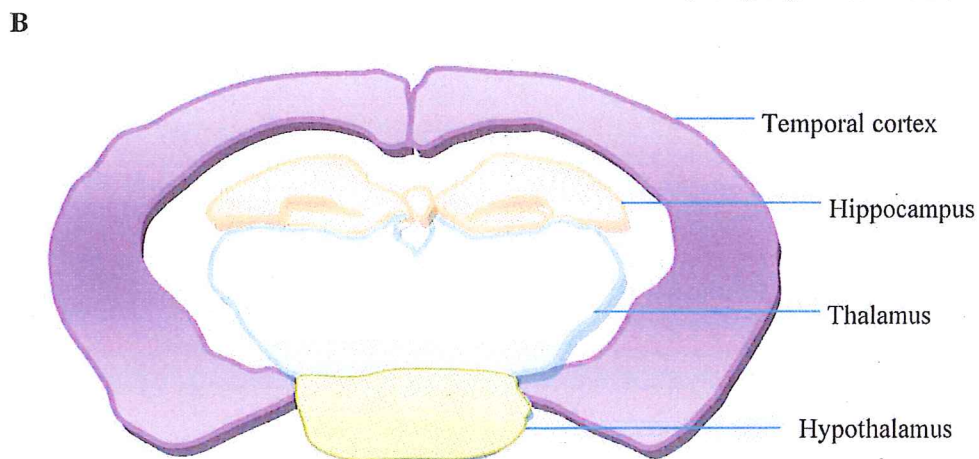
[Modified from Dorr et al., 2007]
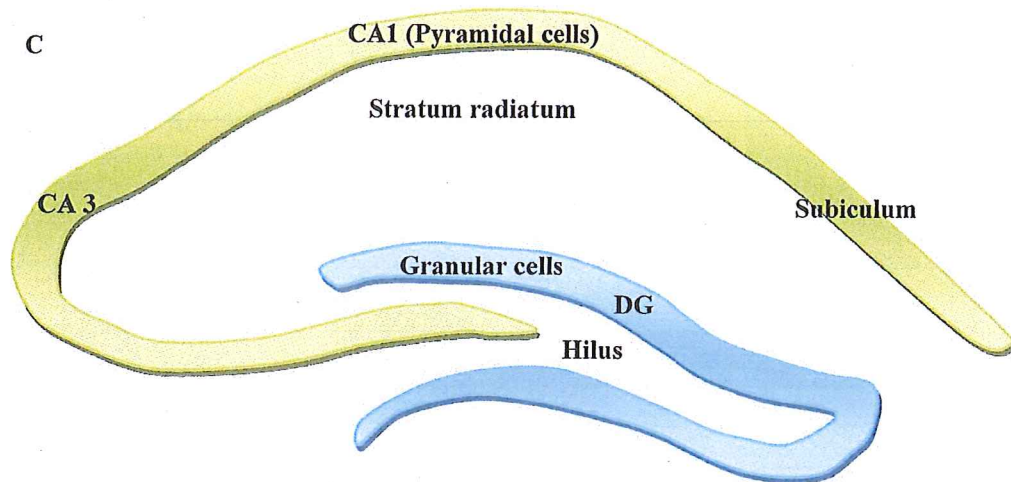
Figure 1.14: Anatomy of hippocampus. The brain with temporal lobe (A) contains hippocampus (B), which consists of the interlocked CA and DG (C).

[Modified from Neves et al., 2008]

2.14 Cornu ammonis 1 and dentate gyrus

CA1 is the first subfield of the hippocampal circuit that yields a significant output pathway, going to the entorhinal cortex (EC) layer V. It also sends significant output forward to the subiculum (Figure 1.15). Like CA3, it receives input from the superficial EC along the perforant pathway. Unlike CA3, it contains very few recurrent connections.

CA1 contains about 250000 pyramidal cells in mice (Amaral et al., 1990). The areas after the CA1 are called the subiculum, presubiculum, and parasubiculum (Andersen et al., 2007). The neurons in CA1 subfield are associated with the formation and recalling of memory (Welberg, 2011).
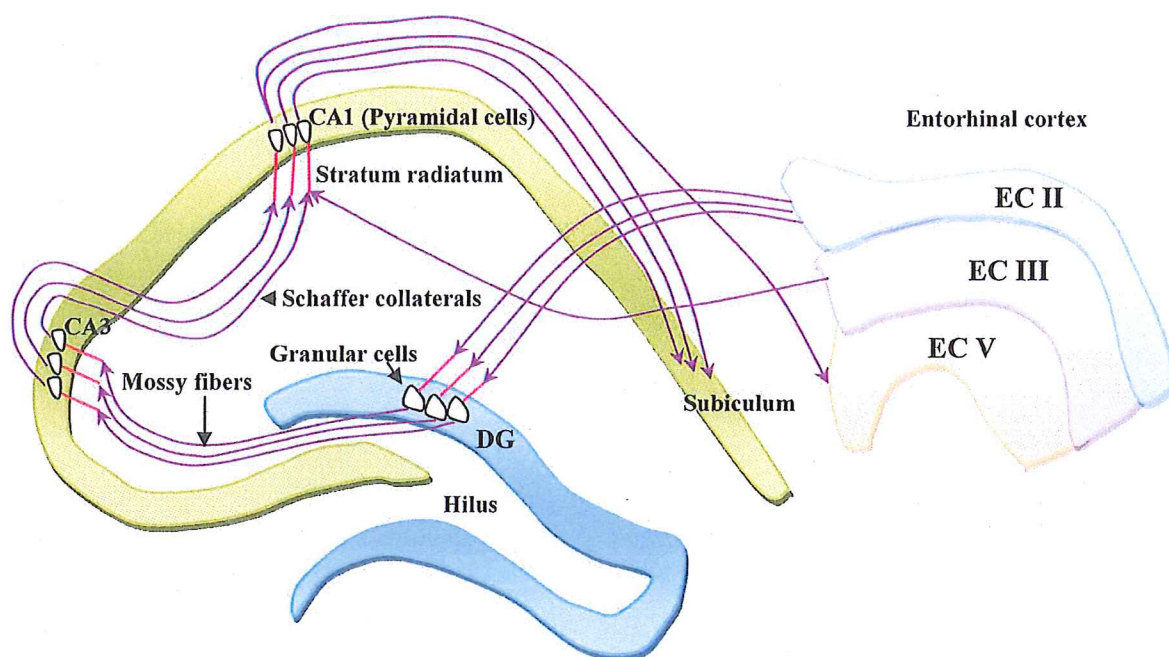
Figure 1.15: CA1 and DG neural circuits. The external input comes from the adjacent EC to the DG. Granule cells of the DG send their axons (called mossy fibers) to CA3. The pyramidal cells of CA3 send their axons to CA1. There is a distinct pathway from layer 3 of EC directly to CA1. The CA3 region combines the input, and sends extensive connections to CA1 through a set of fibers called the Schaffer collaterals. The pyramidal cells of CA1 send their axons to the subiculum.

[Modified from Neves et al., 2008]

The DG is actually a separate structure, and is tightly packed with small layer of granule cells. The DG region in the hippocampus is one of the two brain regions where new neurons are generated throughout life (Eriksson et al., 1998). The DG is comprised of three layers: the molecular layer, the granular layer, and the hilus which is also referred to as the polymorphic layer. The main neurons of the DG are the granule cells, which have most of the typical features of small neurons (Andersen et al., 2007).

The number of granule cells is estimated to be 445280 per hemisphere in adult mice (Ihunwo and Schliebs, 2010). Hippocampus-dependent learning and memory are related to neurogenesis in the DG (Gao et al., 2007; Li et al., 2008). This is a pivotal part of the hippocampus in which a substantial amount of damage can impair spatial learning (Conrad and Roy, 1995). In the present model, mutUNG1 is expressed selectively in forebrain neurons, including the hippocampus, which has been studied thoroughly (Lauritzen et al., 2010).

1.15 CA1 subfield associated neurodegeneration

The CA1 subfield is susceptible to different documented neurodegenerative pathologies. Age-related neuropathologies such as AD are caused by losing functional synapses in the CA1 and DG regions, which alter synaptic connectivity in several ways (Rosenzweig and Barnes, 2003). In AD patients, the mitochondria in CA1 pyramidal neurons are accumulated in the soma (Wang et al., 2009a). Beta-amyloid-induced neurodegeneration in the rats' hippocampal neurons of the CA1 subfield shows neuronal apoptosis (Miguel-Hidalgo and Cacabelos, 1998). The CA1 subfields are also found to be vulnerable to epilepsy (Ramirez-Munguia et al., 2003). The pathology of hypoxic-ischemic encephalopathy is connected with the hippocampal pyramidal cells of CA1 (Plenger et al., 1996).

1.16 Dentate gyrus subfield associated neurodegeneration

A genetic model of neurodegeneration shows that the dorsal DG region is more susceptible to neurodegeneration than ventral DG region (Fuster-Matanzo et al., 2011). The DG region is vulnerable to the neurotoxic effects of ethanol and shows neurodegeneration in rats' hippocampi (Crews and Nixon, 2009). A gradual age-related loss of neurons is found in the DG of mice (Han et al., 2006) and in aged albino rats (Hashem et al., 2010). In addition, PD, Huntington's disease, and AD can be caused due to specific alterations of neurons in the DG (Simuni and Sethi, 2008). A variety of neuro-developmental disabilities such as epilepsy, schizophrenia, and autism show a direct correlation with damage of DG granular cells (Molnar and Nadler, 1999; Stevens, 1992). The specific loss of DG granular cells is related to long-term adrenalectomy in the hippocampi of adult rats (Spanswick et al., 2011).

1.17 Role of UCP2 in neurodegeneration

UCP2 reveals an intimate relation in the aging process (Dikov et al., 2010) and is found to be increased in the spinal cord and brain of aging rats (Mizuno et al., 2000). UCP2 is significantly expressed in the brain, including seizure-sensitive regions (Richard et al., 2001; Horvath et al., 1999). UCP2 has an important neuroprotective role in ischemia (Mattiasson et al., 2003) and overexpression of UCP2 has been documented to protect thalamic neurons following global ischemia in mice and rats (Olsson et al., 2008). The increment of UCP2 expression has been found after cerebral ischemia to protect against neuronal cell death in the hippocampus (Chen et al., 2010). UCP2 has a role in nigral dopamine cell metabolism for prevention and treatment of PD (Andrews et al., 2008).

The activation of UCP2 synthesis after hippocampal injury demonstrates the neuroprotective effects of this protein (Lebed and Arkhipov, 2010). Acute traumatic brain injury also causes elevation of UCP2 (Bechman et al., 2002). UCP2 overexpression is susceptible to triggering a massive mitochondrial uncoupling in the muscles of amyotrophic lateral sclerosis patients (Dupuis et al., 2003). The increased level of UCP2 has also been reported in the study of epilepsy (Diano et al., 2003).

UCP2 has a role in maintaining hippocampal neuronal number, size, dendritic growth, and synaptogenesis in mice (Simon-Areces et al., 2012). UCP2 plays a major role in neurogenic hypertension associated chronic OS (Chan et al., 2009). Therefore, the brain may initiate neuroprotection by increasing the amount of UCP2 under different neurodegenerative conditions (Figure 1.16).
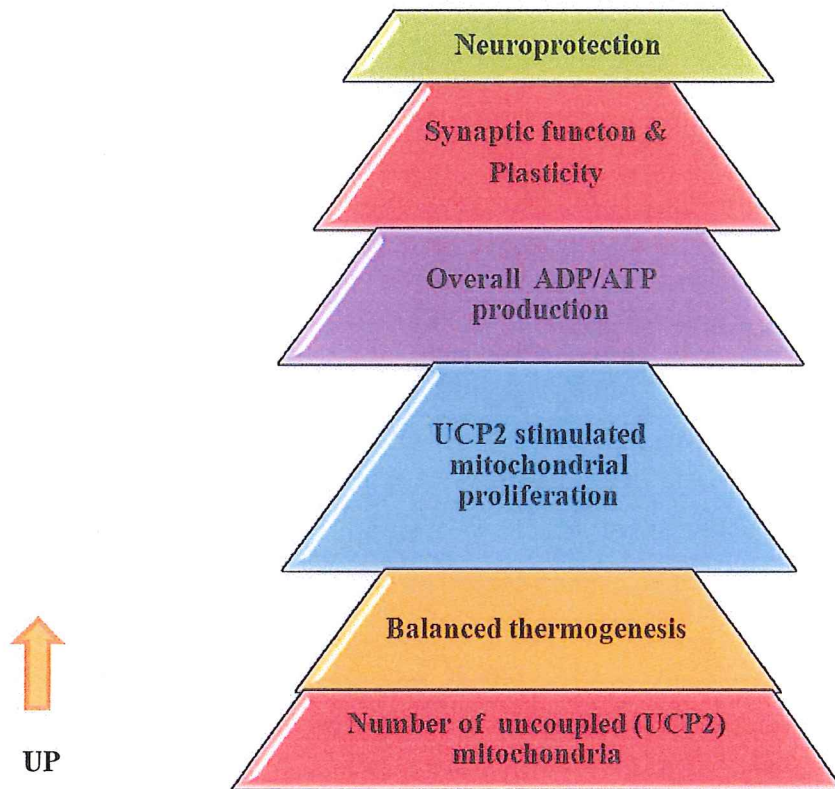
Figure 1.16: Schematic drawing of the neuroprotective mechanism of UCP2 in neurodegeneration. The increase number of UCP2 may balance thermogenesis, and increase ATP production by stimulating mitochondrial proliferation. The energy homeostasis then may contribute to synaptic plasticity and neuroprotection.

1.18 Study objectives

In the present thesis, I have used a previously made mouse model, expressing the mutated base repair enzyme mutUNG1, which causes progressive mitochondrial damage. The model was designed to mimic mitochondrial changes in neurodegenerative disease.

The experiments are focused on two research objectives:

- **Do mutUNG1-expressing mice show changed mitochondrial morphology in the neurons of CA1 and dentate gyrus compared with wild type mice?**

- **Is the level of UCP2 altered in different compartments of neurons in hippocampal CA1 and dentate gyrus subfields of mutUNG1-expressing mice compared with wild type mice?**

CHAPTER II

MATERIALS AND METHODS

This study was carried out from 01 June 2012 to 31 December, 2012 in the institute of Basic Medical Sciences (IMB) (Brain and Muscle Energy group), University of Oslo, to study the mitochondrial morphology and quantitative distribution of the mitochondrial UCP2 in different neuronal compartments of CA1 pyramidal cells in stratum radiatum and granular cells in DG and hilus regions of mutUNG1-expressing mice compared to wild type mice.

2.1 Experimental animals

❖ Three wild type (ID: 5968-1, 5969-1, and 5970-1) and three transgenic mutUNG1-expressing mice (ID: 5964-1, 5965-1, and 5966-1).

2.2 Determination of total protein concentration from wild type mice hippocampi

2.2.1 Equipments for determining total protein concentration

❖ Predissected wild type mice hippocampus
❖ Glass pestle
❖ Incubator (Sanyo, MIR-262, Ser. No. 10707098, Japan)
❖ Electric shaker (Model G 2, New Brunswick Scientific co. Inc., USA)
❖ Spectrophotometer (SPECTROstar Omega, Ser. No. 415-0505, BMG Labtech, D-77656 Offenburg, Germany)

2.2.2 Reagents for determining total protein concentration

❖ BCA Reagent A (Uptima, product no. UP95424A, France)
❖ BCA Reagent B (Uptima, product no. UP95425B, France)

BCA Reagent A contains bicinchoninic acid and sodium carbonate.

BCA Reagent A contains cupric (II) sulfate.

2.2.3 Reagents setup for determining total protein concentration

❖ **1% sodium dodecyl sulfate (SDS) homogenization buffer solution:** The solution was made by mixing 2.3 g disodium hydrogen phosphate (Na_2HPO_4), 0.46 g monosodium phosphate (NaH_2PO_4), 2 g SDS, and 2 tablets of protease inhibitor (SIGMAFAST™, S8820) in 200 mL UFwater.

❖ **Mixed BCA reagent:** 24.5 mL BCA reagent A mixed with 500 µL BCA reagent B

2.3 Gel electrophoresis and Western blotting

2.3.1 Equipments for gel electrophoresis

❖ Criterion™ Precast Gel (4-12%) (BIO-RED, catalog 345-0015)

❖ Gel electrophoresis cassette

❖ Power supply system (PowerPac™, BIO-RED)

2.3.3 Reagents set up for gel electrophoresis

❖ **Laemmli sample buffer:** Stock solution Laemmli sample buffer (2X) was made by mixing glycerol (20%, 20 mL), Tris hydrochloric acid (HCl) (0.125 M, pH 6.8, 12.5 mL of stock 1M Tris HCl), SDS (4%, 4.0 g), 0.004% bromophenol blue (a few grains), 10% β-mercaptoethanol (10 mL) and UFwater (up to 100 mL). The solution was adjusted a pH of approximately 6.8. The β-mercaptoethanol was used to reduce intra-and intermolecular disulfide bonds of the proteins to allow proper separation not by shape but by size. The SDS detergent binds to all the proteins positive charges which occur at a regular interval, thus giving each protein the same overall negative charge so that proteins will separate based on size and not by charge. The SDS also denatures the proteins. Bromophenol blue serves as an indicator dye. Glycerol in the Laemmli buffer increases the density of the sample so that it will fall to the bottom of the well, minimizing loss of protein sample in the buffer.

❖ **Running buffer (10X):** Solution was made by adding Tris Base (30.3 g), glycine (144 g), SDS (10 g), and UFwater (up to 1000 mL).

2.3.4 Equipments for Western blotting

- ❖ Plastic cassette
- ❖ Fiber pad
- ❖ Paper pad
- ❖ Gel
- ❖ Nitrocellulose membrane
- ❖ Roller
- ❖ Paper pad
- ❖ Fiber pad
- ❖ Magnetic stirrer
- ❖ Image Reader LAS-3000

2.3.5 Reagents setup for Western blotting

- ❖ **Blotting buffer (1X):** Solution was made by adding Tris Base (25 mM, 15.1 g), glycine (192 mM, 75 g), isopropanol (10%, 500 mL), and UFwater (up to 5000 mL).

- ❖ **Tris buffer saline Tween (TBST):** Solution was made by adding Tris HCl (10 mM, 7.9 g), NaCl (150 mM, 43.8 g), Tween 20 (0.05%, 2.5 mL), and UFwater (up to 5000 mL).

- ❖ **Blocking solution:** 2 g bovine serum albumin (BSA) in 200 mL TBST.

- ❖ **Primary antibody:** Goat anti-UCP2 IgG primary antibody was mixed with blocking solution. (6, 10, 12 and 15 μL of UCP2 primary antibody were brought to volumes of 6 mL, 10 mL, 12 mL, and 15 mL respectively with blocking solution to make 1:6000, 1:10000, 1:12000, and 1:15000 dilution.

- ❖ **Secondary antibody:** Rabbit anti-goat IgG conjugated with Horseradish Peroxidase (HRP, Catalog Number R-21459). 15, 20, and 30 μL of secondary antibody were brought to volumes of 15 mL, 20 mL, and 30 mL respectively with blocking solution to make 1:15000, 1:20000, and 1:30000 dilution.

- ❖ **Enhanced chemiluminescent substrate:** SuperSignal® West Dura Extended Duration substrate A (2 mL) was mixed with B (2 mL) (Thermo scientific, Lot. LL152462). SuperSignal® West Dura Substrate is a luminol-based enhanced chemiluminescence (ECL) HRP substrate with every stable light output for femtogram-level detection with digital imager.

2.4 Electron microscopy

2.4.1 Equipments for electron microscopy

- ❖ Peristaltic pump (Watson-Marlow U/D 323, Watson-Marlow Bredel)
- ❖ Adhesive pen (Electron Microscopy Science)
- ❖ Cryofixation unit (Reichert KF80, Reichert-Jung, Austria)
- ❖ Cryosubstitution unit (Reichert)
- ❖ Ultramicrotome (Reichert Ultracut S-2.GA-E-12/92, Leica Microsystems, Germany)
- ❖ Diamond knife for ultrathin sectioning (Diatome 45, Diatome, USA)
- ❖ Nickel mesh grids (300 mesh) (Electron Microscopic Sciences, cat. no. G300-Ni)
- ❖ Tweezers (Dumont tweezers, Electron Microscopic Sciences, cat. no. 72800-D)
- ❖ Electron microscope (Tecnai™ electron microscope, FEI Company, USA)
- ❖ Glass beaker
- ❖ Glass plate

2.4.2 Reagents for electron microscopy

- ❖ Pentobarbital
- ❖ Dextran 70 (Mw 70000, Sigma-Aldrich, cat. no. 31390)
- ❖ 0.1 M sodium phosphate buffer (PB)
- ❖ 0.5 % uranyl acetate
- ❖ Lowicry HM20 (Polysciences)
- ❖ Glycerol (10-20-30%) (Sigma-Aldrich, cat. no. G5516)
- ❖ Na_2HPO_4 and NaH_2PO_4
- ❖ Propane
- ❖ Liquid nitrogen
- ❖ Anhydrous methanol
- ❖ Sodium ethanol

2.4.3 Reagents for post-embedding

- ❖ 2% (wt/vol) hydrogen peroxide (H_2O_2) (Sigma-Aldrich, cat. no. 95302)
- ❖ Na_2HPO_4 and NaH_2PO_4 (Sigma-Aldrich, cat. nos. 71496 and 71642)
- ❖ Sodium borohydride (Sigma-Aldrich, cat. no. 452882)
- ❖ Glycine (Sigma-Aldrich, cat. no. 50050)
- ❖ Triton X-100 (Sigma-Aldrich, cat. no. 234729)
- ❖ Trizma (Sigma-Aldrich, cat. nos. T3253 and T1503)
- ❖ Polyethylene glycol (PEG, Sigma-Aldrich, cat. no. P2263)
- ❖ Human serum albumin (HAS, Sigma-Aldrich, cat. no. A1653)
- ❖ Lead citrate (Electron Microscopic Sciences, cat. no. 17800)
- ❖ Uranyl acetate (Sigma-Aldrich, cat. no. 73943)
- ❖ Parafilm (Pechiney Plastic Packing)
- ❖ Goat anti-UCP2 IgG primary antibody (Sigma-Aldrich, SAB2501087, Lot-7716C2G2P2).
- ❖ Rabbit anti-goat IgG secondary antibody coupled with 15 nm gold particle (British-biochemical.co.uk, Batch-6010) (Figure 2.1).
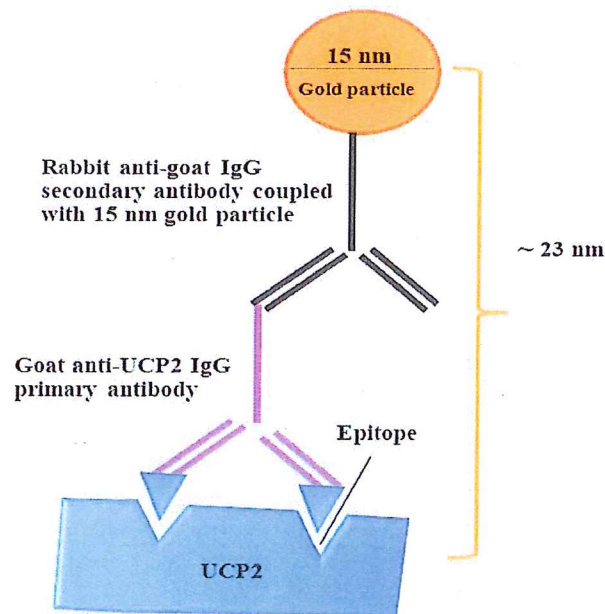
Figure 2.1: The distance from the center of a gold particle (diameter 15 nm) and the UCP2 epitope is about ~23 nm, which has an effect to lateral resolution to specify signal (Bergersen et al., 2008; Ottersen, 1989).

2.4.4 Reagents setup for post-embedding

- ❖ **0.1 M sodium phosphate buffer (PB):** 11.5 g Na_2HPO_4 and 2.3 g NaH_2PO_4 was dissolved in 1000 mL UFwater and adjusted pH to 7.4.

- ❖ **2% (vol/vol) H_2O_2:** 40 mL 2% H_2O_2 was mixed with 560 mL 0.1 M PB.

- ❖ **Tris-buffered saline Triton (TBST):** 0.758 g of 0.05 M Trizma, 3 g NaCl and 1 mL Triton X-100 were mixed and brought the volume to 1000 mL UFwater. Triton is a detergent that can contribute to enhancement of the immunogold signal.

- ❖ **0.1% sodium borohydride and 500 mM glycine solution:** 0.01 g sodium borohydride and 0.0375 g glycine were dissolved in 10 mL TBST.

- ❖ **Blocking solution:** 0.1 g HSA was mixed with 5 mL TBST

- ❖ **Primary antibody solution:** 0.8 µL UCP2 primary antibody solution was mixed with 499.2 µL TBST with 2% HAS to make 1:500 dilution.

- ❖ **TBST with 2% HSA and PEG solution:** 0.2 g HAS was added in 0.005 g PEG mixed 10 mL TBST solution.

- ❖ **Secondary antibody solution:** 20 µL secondary antibody solution was mixed with 380 µL TBST in 2% HAS with PEG solution to make 1:20 dilution.

- ❖ **Contrast-enhancing agents:** 1% (wt/vol) solution of uranyl acetate (1 g in 100 mL UFwater) and 0.3% (wt/vol) lead citrate (0.3 g in 100 mL UFwater) solution were made separately. Uranyl and lead are used as contrast-enhancing agents.

2.5 Bicinchoninic acid protein assay

The bicinchoninic acid (BCA) protein assay is based on BCA for the colorimetric detection and quantification of total protein. This method combines the well-known reduction of cupric ion (Cu^{+2}) to cuprous ion (Cu^+) by protein in an alkaline medium (the biuret reaction) with highly sensitive and selective colorimetric detection of the Cu^+ cation using a unique reagent containing BCA. The purple-coloured reaction product of this assay is formed by the chelation of two molecule of BCA with one Cu^+ cation (The BCA-Protein reactions). This water-soluble complex shows a strong absorbance at 562 nm that is linear with increasing protein concentrations over a broad working range of 20 μg/mL to 2000 μg/mL.

The BCA-Protein reactions:

Protein (peptide bonds) + Cu^{+2} $\longrightarrow$ tetradentate-Cu^+ complex (light blue coloured)

Cu^+ + 2 bicinchoninic acid (BCA) $\longrightarrow$ BCA-Cu^+ complex (purple coloured, read at absorbance 562)
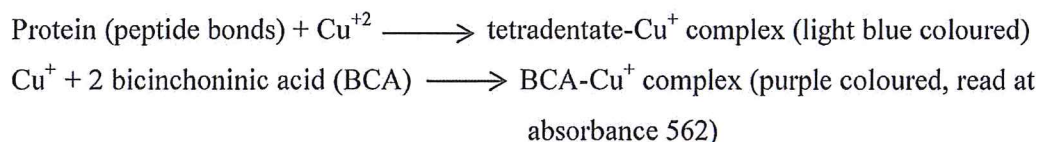
2.5.1 Determination of total protein concentration

The predissected mice brain hippocampi were weighed (52.2 mg), and immediately added to the previously made 1% SDS homogenization buffer solution (10X, 0.525 mL). The hippocampus sample was homogenated and transferred to an eppendorf tube and sonicated (60 seconds) for disruption of the cell membrane.

The standard curve analysis was used to measure the total protein concentration from the hippocampal tissue homogenate. The serial dilutions were made with bovine serum albumin (BSA, 2 mg/mL) and 1% SDS buffer solution to maintain the respective concentration of the stock solution (Table 2.1)

The well-mixed solution of BSA (2 mg/mL) and 1% SDS buffer with respective concentrations (Table 2.1) were pipetted (1 mL) accordingly in the first column of 96-well plate. The mixed solution (BSA and buffer) in well column 1 was then pipetted in triplicates accordingly (10 μL) with mixed BCA reagent (200 μL). Then 1% SDS homogenization buffer solution (180 μL) and hippocampus homogenate (20 μL) were pipetted in well column 6 in triplicates (Figure 2.2).

The mixed solution (1% SDS homogenization buffer solution and hippocampus homogenate) from well column 6 was pipetted (10 µL) with mixed BCA reagents of A and B (200 µL) in column well 7 (Figure 2.2).

Table 2.1: The pipetted volume of BSA (2 mg/mL) and buffer to prepare the stock solution in different concentrations (0-2000 µg/mL). Std= Standard

Well number	Stock solution	BSA (2mg/mL)	Buffer	Concentration (µg/mL)
A	Std 1	60 µL stock	-	2000
B	Std 2	60 µL stock	60 µL	1000
C	Std 3	84 µL stock	140 µL	750
D	Std 4	20 µL stock	60 µL	500
E	Std 5	20 µL stock	140 µL	250
F	Std 6	40 µL Std 5	60 µL	100
G	Std 7	20 µL Std 5	80 µL	20
H	Std 8	-	60 µL	0

The 96-well plate was then covered with thin plastic foil prior to shaking (15 minutes) on an electric shaker. The plate was then incubated (37°C for 30 minutes) before taking absorbance at 562 nm by Spectrophotometer.
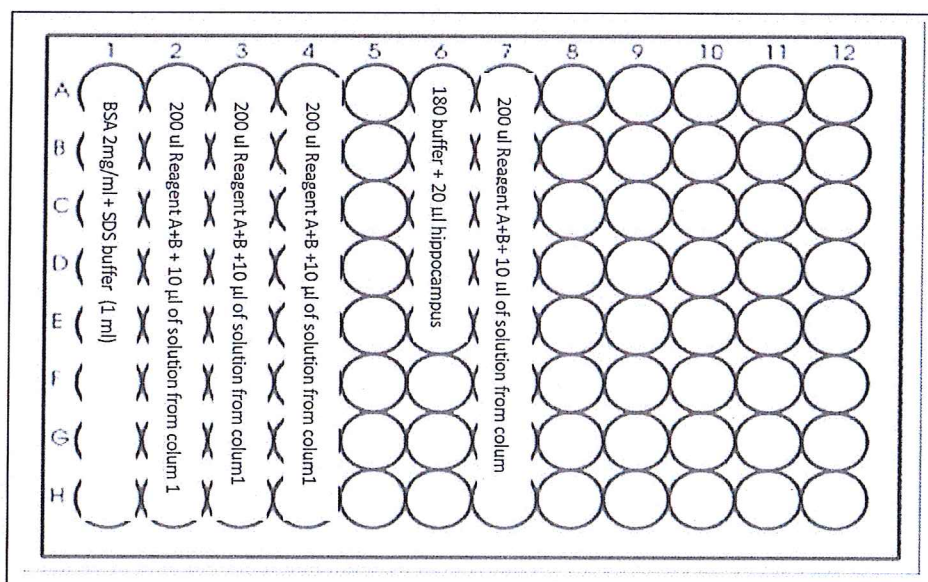
Figure 2.2: The absorbance reading (562 nm) was measured using the following pipetted scheme for making a standard curve.

The absorbance readings were measured and used to calculate the concentration of total protein in the mice hippocampi using the standard curve method (Y=a+bx, Y= known absorbance, a= slope, b= y-intercept and x= unknown concentration) (Appendix 1).

2.6 Western blotting

Western blotting was carried out to check the binding specificity of the UCP2 primary antibody.

2.6.1 Preparation of sample

The calculated concentration (9.07 g/mL) from the standard curve analysis was then diluted (2 mg/mL) by adding 1% SDS buffer solution (707.48 µL SDS buffer + 200 µL original hippocampal homogenate) in an eppendorf tube. The pipetted solutions were mixed properly and then incubated (96°C for 10 minutes) prior to dilute (1 mg/mL) with the Laemmli sample buffer (Calculation in appendix 2).

2.6.2 Gel electrophoresis of proteins

Gel electrophoresis was carried out to separate polypeptides in hippocampal homogenate by size. Precast Gel (4-20% Criterion™ Precast gel) was taken out from packaging and the white tape at bottom was removed. The gel cassette was placed in one of the slots in the Criterion™ tank. Approximately 50 mL of running buffer was poured and filled up to the upper buffer chamber. The well comb was then removed gently by pulling upward. The protein standard ladder (5 µL) and prepared hippocampus samples were loaded in different volumes (5, 15, and 20 µL) using a micropipette with gel-loading tips. Once the samples were loaded, approximately 400 mL of running buffer was added to the lower chamber of the cell (up to the FILL line). The lid was snapped onto the chamber and the lid was plugged into the power source. The electrophoresis was run for about an hour (200V, 3.0 A, 300W). The electrophoresis gel was separated from the gel cassette and the tank was rinsed with UFwater.

2.6.3 Electrophoretic transfer of proteins

In electrophoretic transfer, an electric field was used to elute proteins from electrophoresis gel and transferred to nitrocellulose membrane. In this transfer process, a nitrocellulose membrane and protein-containing gel were placed together, with two fiber pads and filter papers between two electrodes (Figure 2.3). A small roller tool was used to remove air bubbles between the gel and the nitrocellulose membrane. The sandwich was placed in the blotting tank. A cold element and magnetic bar were placed in the tank. The tank was filled with blotting buffer and placed onto an electric magnetic stirrer. The lid was snapped onto the tank and a constant voltage supply was applied (50 volts, 2 hours, 1.0 A, 200W). The proteins in the gel were then transferred to the nitrocellulose membrane in the blotting chamber.

When the run was finished, the sandwich was opened and the paper pads were removed carefully to get the nitrocellulose membrane. The transferred protein in the nitrocellulose membrane was air dried on Kleenex-paper.
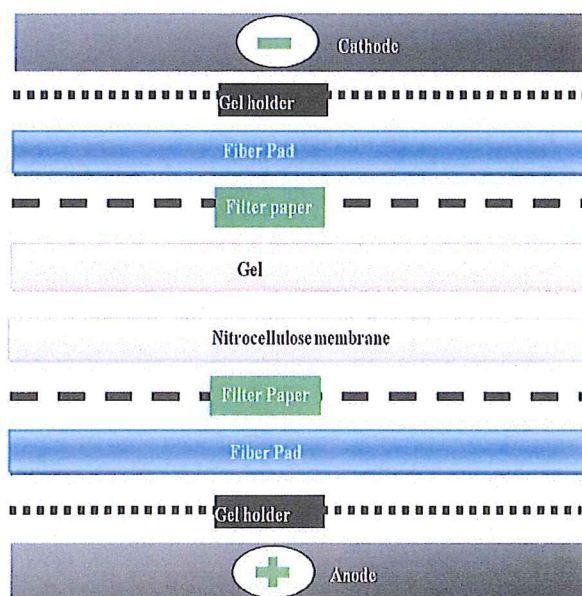
Figure 2.3: The orientation of gel sandwich. Gel holder was used to holds the sandwich.

2.6.4 Immunoblotting

Immunoblotting was used to visualize the UCP2 primary antibody specificity. The nitrocellulose membranes were incubated with different concentrations of primary and secondary antibodies. The protein-free spaces on the membrane were blocked by incubating the nitrocellulose membrane with blocking solution (1% BSA in TBST) for an hour on an electric shaker. The nitrocellulose membrane was then rinsed in TBST. The primary antibody (goat anti-UCP2 IgG) was diluted in different concentrations (1:6000, 1: 10000, 1:12000, and 1: 15000) with the blocking solution (1% BSA in TBST). The nitrocellulose membrane was incubated with the UCP2 primary antibody (overnight) on an electric shaker and then rinsed (3x10 minutes) in blocking solution. The secondary antibody (rabbit anti-goat IgG conjugated with HRP) in the diluted blocking solution (1:15000, 1:20000, and 1:30000) was used for incubating (1 hour) the nitrocellulose membrane on an electric shaker prior to rinse quickly (3x10 minutes) in blocking solution.

2.6.5 Detection and visualization of proteins

The blotted proteins were detected using chemiluminescence detection technique by secondary antibody conjugated HRP enzyme and ECL substrate reaction. In this technique, when ECL substrate was added (5 minutes, 2 mL A: 2 mL B), a chemiluminescence product was formed and the light signal was visualized with a digital imaging system (Image Reader LAS-3000).

2.7 Immunogold electron microscopy

Immunogold electron microscopy was used (Bergersen et al., 2008) in order to quantify the density of UCP2 in different compartments of the neurons (myelinated axons, presynaptic terminals, dendrites, and somas) in the CA1 pyramidal cells, stratum radiatum, DG granular cells, and hilus regions.

2.7.1 Hippocampal tissue preparation

The following procedures were carried out to prepare ultrathin tissue sections from wild type and mutUNG1-expressing mice hippocampi.

2.7.2 Perfusion fixation

The experimental mice were anesthetized using pentobarbital (0.3 mL per 100 g), in accordance with animal welfare laws. The mice were perfused transcardially with the fixative (4% formaldehyde and 0.1% glutaraldehyde in 0.1 M sodium phosphate buffer (PB)) through a peristaltic pump for 10 minutes after a brief flush (for a few seconds) of 2% dextran 70 in PB. The fixed mice were put in plastic bags and left overnight at 4°C.

2.7.3 Dissection and cryoprotection

The brains were dissected out and sliced in 500 μm thickness. CA1 and DG region were cut into small specimens (typically 0.5 mm×0.5 mm×1 mm). The specimens were cryoprotected by immersing in graded concentrations of glycerol (10%, 20% and 30% (vol/vol)) in PB (30 minutes at room temperature (~20 °C) and overnight in 30% at 4°C).

The tissue samples were then plunged into liquid propane cooled to minus 190°C (-190°C) in liquid nitrogen. The specimens were dehydrated and treated with 0.5 % uranyl acetate (1.5% uranyl acetate dissolved in anhydrous methanol, overnight at -90°C) to increase the contrast of the tissue. A gradual increment of temperature (5°C, per hour) was continued from -90°C to -45°C. The tissue was rinsed with anhydrous methanol three times and incubated in Lowicryl HM20:Methanol 1:1, 2:1, to pure Lowicryl HM20 (2 hours each) and finally in pure Lowicryl overnight. The tissue was polymerized by ultraviolet radiation (360 nm) for 24 hours at -45°C, and the temperature was then gradually increased by 5°C to a final temperature of 0°C (48 hours).

The ultrathin sections were cut on an ultramicrotome using a diamond knife (90 nm thick). Ultrathin sections with a bright gold color were chosen and mounted on nickel mesh grids (routinely 300 mesh) using an adhesive pen. The ultrathin sections were then left for drying at room temperature (~20 °C, about 12 hours).

2.7.4 Post-embedding and immunogold labelling

The hippocampal ultrathin sections on the grids were etched with 2% H_2O_2 in PB (40 µL H_2O_2 and 560 µL PB) droplets (50 µL) for 15 minutes. Then the tissue grids were rinsed gently in PB (3 times×15 seconds) in a 10 mL glass beaker. In order to neutralize free aldehyde groups in the fixed tissue, sections were treated with a solution of TBST with 50 mM glycine and 0.1% sodium borohydride ($NaBH_4$) droplets for 10 minutes and then washed in TBST (3 times×15 seconds). Nonspecific antibody binding sites were blocked using 2% (wt/vol) HSA in TBST solution for 10 minutes and followed by the same step once again.

The ultrathin sections on grids were then incubated with the goat anti-UCP2 primary antibody (UCP2, 1:500) overnight at 4°C. They were then washed in TBST (3 times×15 seconds) prior to being dipped in TBST droplets (10 minutes) and followed by the same step once again. Then the grids were dipped in a TBST with 2% (wt/vol) HSA droplets (0.1 g HSA with 5 mL TBST) for 10 minutes. Then they were dipped in 2% HSA with PEG in TBST droplets (10 minutes) to avoid gold particle aggregation.

Then the ultrathin sections on grids were incubated with the rabbit anti-goat IgG secondary antibody (1:20, coupled with 15 nm colloidal gold particle in TBST with 2% HSA and PEG) for 2 hours. Finally, they were rinsed with TBST (3 times×15 seconds) followed by dipping into TBST and then rinsed in UFwater (3 times×15 seconds).

2.7.5 Contrasting

The ultrathin sections were counterstained with 1% uranyl acetate (10 minutes) and 0.3% lead citrate (2 minutes). 1% uranyl acetate and 0.3% lead citrate were pipetted in two labeled eppendorf tubes and spun down for 5 minutes at 1000 rpm. The ultrathin sections were left for drying (20 minutes) before dipping in 1% uranyl acetate. Then, the tissue grids were rinsed with UFwater (3 times×15 seconds) followed by drying at room temperature (20 minutes) prior to being dipped into lead citrate droplets for 90 seconds. Finally the sections were rinsed with UFwater (3 times×15 seconds), placed in the grid box and dried overnight at room temperature.

2.7.6 Image acquisition

The prepared tissue sections were observed in an electron microscope. All images were taken at primary magnifications of twenty-six thousand five hundred times (×26500). They were taken from four different neural compartments (myelinated axons, presynaptic terminals, dendrites, and somas) in both CA1 and DG regions (CA1 stratum radiatum and DG hilus) (Figure 2.4).
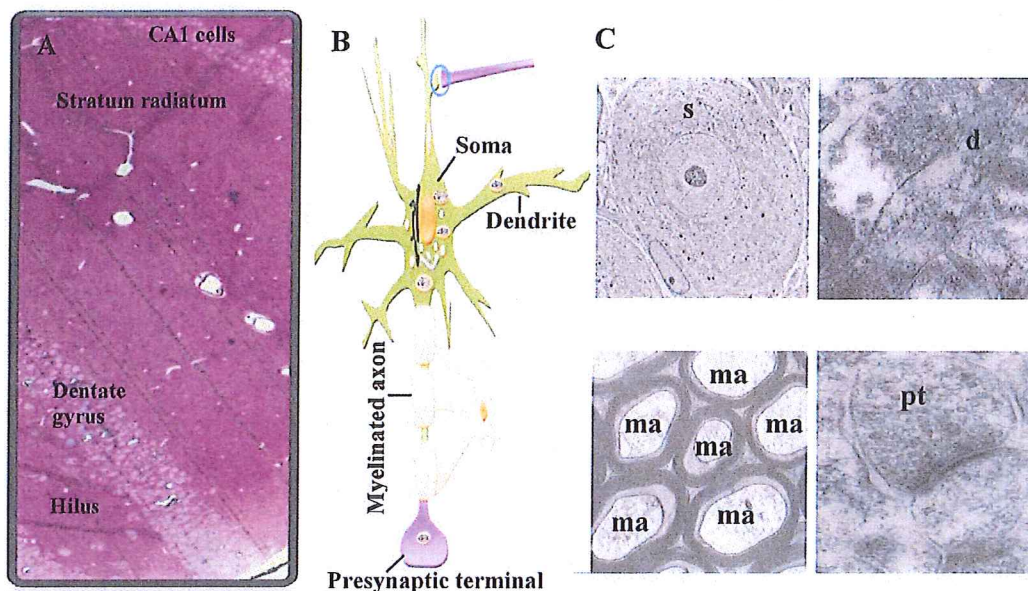
Figure 2.4: The localization of mitochondrial UCP2 was observed in four different compartments. A) The light microscopic view of CA1 pyramidal cells, stratum radiatum, DG granular cells, and hilus of hippocampus. B) A typical cartoon and C) electron micrographs of four different compartments (ma=myelinated axon, pt=presynaptic terminal, d=dendrite, and s=soma).

2.8 Immunogold quantitative analysis

The density of UCP2 in the four different neural compartments (myelinated axons, axon terminals, dendrites, and somas) of the hippocampus was analyzed after taking images along the CA1 stratum radiatum and DG hilus regions.

The electron micrographs were opened with the software ImageJ version 1.46r (http://imagej.nih.gov/ij/) and the scale (500 nm) was set. The "ParticleDensity" plugin (http://www.neuro.ki.se/broman/maxl/software.html), was used to count each gold particle within the defined neural compartment. Then the electron micrograph profiles were saved as "tif" and "tif.pd" formats in another file, named "Analyzed data". The saved electron micrograph profiles were then read by a "Point Density" plugin for ImageJ (http://www.neuro.ki.se/broman/maxl/software.html) to get an output profile summary.

The total number of counted immunogold particles was divided by the sum of total area (nm^2) in a particular compartment followed by multiplying with 1000000 to get the density of UCP2 gold particles (UCP2 GP/μm^2) in particular neural compartment (Equation 2.1).

Density (UCP2 GP/μm^2) = (Total number of UCP2 GP/Total area, nm^2) × 1000000..........[2.1]

2.9 Statistics

The mean UCP2 density (UCP2 GP/μm^2) of each compartment (myelinated axons, dendrites, presynaptic terminals, and somas) was analyzed on three grids per mouse and three mice per genotype (3×3).

UCP2 density for each compartment was calculated from twenty electron micrographs (EMs). The data contained total 77-78, 83-96, 74-84, and 265-364 numbers of EM profiles for myelinated axons, dendrites, presynaptic terminals, and somas respectively (Table 2.2) from both wild type and mutUNG1-expressing mice. Each compartment was analyzed with standard error of the mean (SEM) from three wild type and three mutUNG1-expressing mice (n = 3, n representing the number of animals) in each group.

The detailed analysis of UCP2 in cellular compartments was done in one wild type and one mutUNG1-expressing mouse (Figure 3.9 and appendix 16) from 10-21 EM profiles of 10 EMs (n = 10-21).

The quantitative differences of UCP2 between wild type and mutUNG1-expressing mice in the different neuronal compartments were assessed with the two-tailed Student's t-test where $p < 0.05$ is defined as significant. The level of significance is symbolized with * (p-value ≤ 0.05), ** (p-value ≤ 0.01), and *** (p-value ≤ 0.001) (Appendix 13, 16, and 19). The statistical analyses as well as presentation of graphs were performed using Microsoft Excel 2010 and the results presented as mean ± SEM.

Table 2.2: The total numbers of EM profiles for each compartment (myelinated axons, dendrites, presynaptic terminals, and somas) obtained from twenty electron micrographs (for each compartment)

Analyzed compartment	mutUNG 1 EM profile	mutUNG 2 EM profile	mutUNG 3 EM profile	Total EM profile
Myelinated axons	30	22	25	77
Dendrites	31	27	25	83
Presynaptic terminals	28	26	30	84
Somas	199	100	145	364

Analyzed compartment	WT1 EM profile	WT2 EM profile	WT3 EM profile	Total EM profile
Myelinated axons	30	22	26	78
Dendrites	32	28	36	96
Presynaptic terminals	23	26	25	74
Somas	78	94	93	265

2.10 Precautions

- ❖ Cylinder flask was used to measure the desired volume of solution.
- ❖ Weighing balance was used very carefully to get desired weight of analytes.
- ❖ Hand gloves were used throughout the working hours in the laboratory.
- ❖ Images from CA1 (stratum radiatum) and DG (hilus) were taken randomly and selectively.
- ❖ Electron microscope was used carefully in accordance with instructor advice.

CHAPTER III

RESULTS

3.1 Western blotting

Western blotting was carried out to demonstrate the binding specificity of the UCP2 primary antibody (goat anti-UCP2 IgG) in hippocampi extract. The paratope of UCP2 primary antibody showed the binding specificity to its epitope. There was one strongly stained band close to the molecular mass (37 kDa) of UCP2 on the Western blot, showing acceptable binding specificity of the UCP2 primary antibody (Figure 3.1). Based on this, the primary antibody was chosen for immunogold incubation followed by electron microscopy.
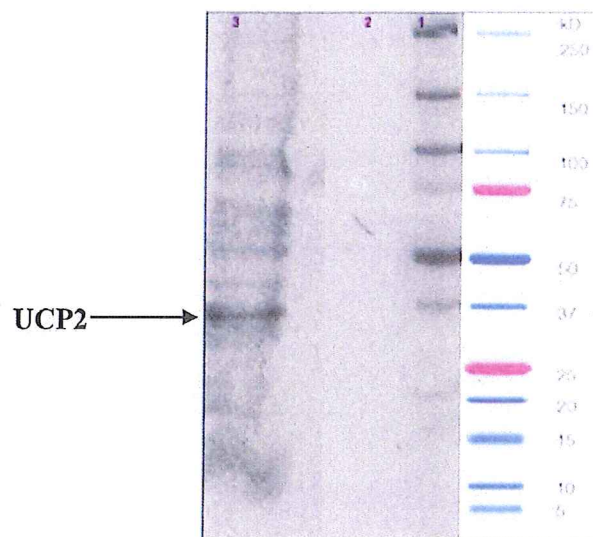
Figure 3.1: Western blot of UCP2 protein in total hippocampal protein extract (1 mg/ml, 20 µl): Lane 1 shows the Precision Plus Protein™ Dual Color Standards (5 µl) connecting with different molecular weights (on right). Lane 2 shows the negative control (20 µl), confirmed that the secondary antibody gave no staining. Lane 3: The strongest band has the appropriate molecular mass of UCP2 (37 kDa) Arrow indicates the UCP2 band.

3.2 Mitochondrial morphology in somas of CA1 pyramidal and dentate gyrus granular cells

The mutUNG1-expressing mice showed a wide variety of mitochondrial shapes in the somas. There were different shapes like, aggregated (Figure 3.2 B), clustered, and irregular shaped mitochondria in mutUNG1-expressing mice (Figure 3.2 C). Clusters or aggregates of mitochondria may represent fusion and/or fragmentation. However, wild type mice had regular structure of mitochondria in somas (Figure 3.2 A).
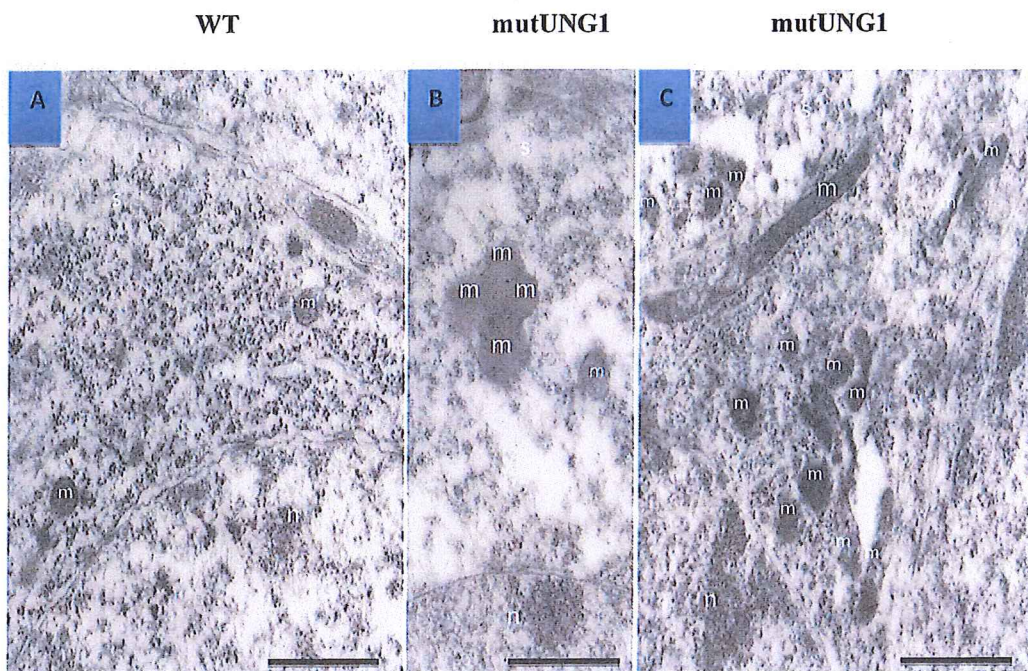
Figure 3.2: Mitochondrial dynamic tendencies were visualized in somas. (A) Typically shaped mitochondria were seen in the somas of wild type mice. Abnormal mitochondrial morphology was found in mutUNG1-expressing mice, where mitochondria could fuse together (B) or were fragmented (C). Magnification: 26500 X, 500 nm scale bar.

The average mitochondrial area (nm^2) in presynaptic terminals and somas showed a significant difference between wild type and mutUNG1-expressing mice (Figure 3.3 and appendix 11-13). However, there was no significant difference of mitochondrial area (nm^2) in myelinated axons and dendrites of wild type and mutUNG1-expressing mice.
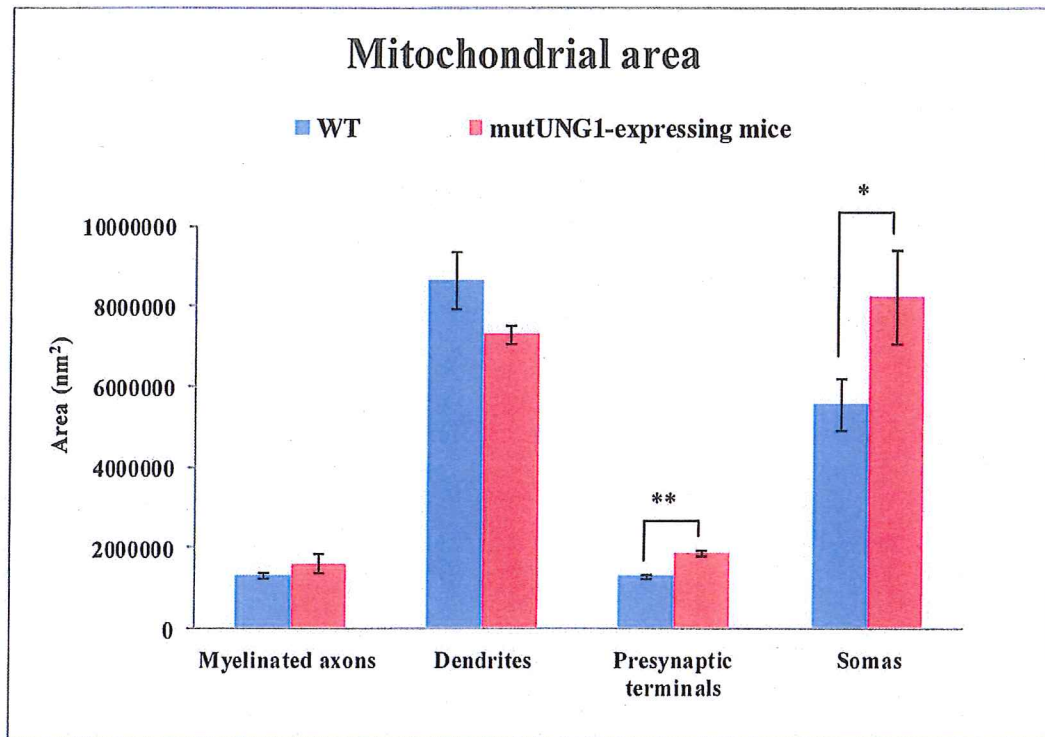
Figure 3.3: The average mitochondrial area (nm^2) of four different neuronal compartments (myelinated axons, dendrites, presynaptic terminals, and somas) was measured in CA1 pyramidal and DG granular cells from the three wild type (WT) and three mutUNG1-expressing mice (Appendix 11-12). The data are based on 20 electron micrographs (EMs) containing 77-78, 83-96, 74-84, and 265-364 EM profiles (also representing the number of mitochondria) for myelinated axons, dendrites, presynaptic terminals, and somas respectively from three wild type and three mutUNG1-expressing mice (n = 3) (Table 2.2). The mean differences of mitochondrial area (nm^2) between wild type and mutUNG1-expressing mice were analyzed with mean ± SEM. The level of significance is symbolized with * (p-value = 0.05) and ** (p-value = 0.002) (Appendix 13).

The average size of the individual mitochondria varied in different neuronal compartments. The size of the individual mitochondria was significantly higher in presynaptic terminals and myelinated axons of mutUNG1-expressing mice compared to wild type mice. However, smaller sized mitochondria were found in somas whereas dendrites showed larger sized mitochondria in both wild type and mutUNG1-expressing mice (Figure 3.4).
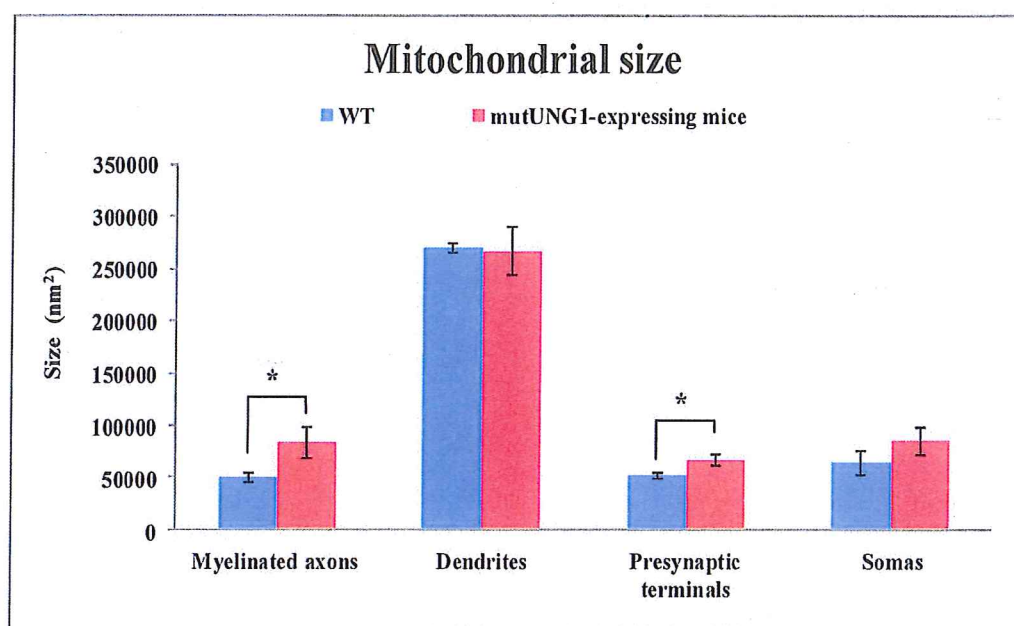
Figure 3.4: The average individual mitochondrial size (nm^2) was measured for four different neuronal compartments (myelinated axons, dendrites, presynaptic terminals, and somas) in CA1 pyramidal and DG granular cells. There was a significant mitochondrial size difference in presynaptic terminals (P = 0.03) and myelinated axons (p = 0.05) between wild type and mutUNG1-expressing mice. The data are based on 20 electron micrographs (EMs) containing 25-26, 28-32, 24-28, and 88-121 average EM profiles (also representing the average number of mitochondria) for myelinated axons, dendrites, presynaptic terminals, and somas respectively from three wild type and three mutUNG1-expressing mice (n = 3) (Appendix 20-21). The mean differences of mitochondrial size (nm^2) between wild type and mutUNG1-expressing mice were analyzed with mean ± SEM (Appendix 14-15). The level of significance is symbolized with * (p-value = 0.05) (Appendix 16).

3.3 Post-embedding immunogold electron microscopy

Through immunogold labeling UCP2 was found to be present in mitochondria of CA1 pyramidal, stratum radiatum, DG granular cells, and hilus in both WT and mutUNG1-expressing mice.

3.3.1 Immunogold quantification of mitochondrial UCP2 in myelinated axons of CA1 pyramidal and dentate gyrus granular cells

The density of mitochondrial UCP2 was two times higher in myelinated axons of CA1 pyramidal and granular cells of DG in mutUNG1-expressing mice (Figure 3.5 B and appendix 17) compared to wild types mice (Figure 3.5 A and appendix 18). The statistical analysis showed a significant difference of the UCP2 level between mutUNG1-expressing and wild type mice (Figure 3.5 C and appendix 19).
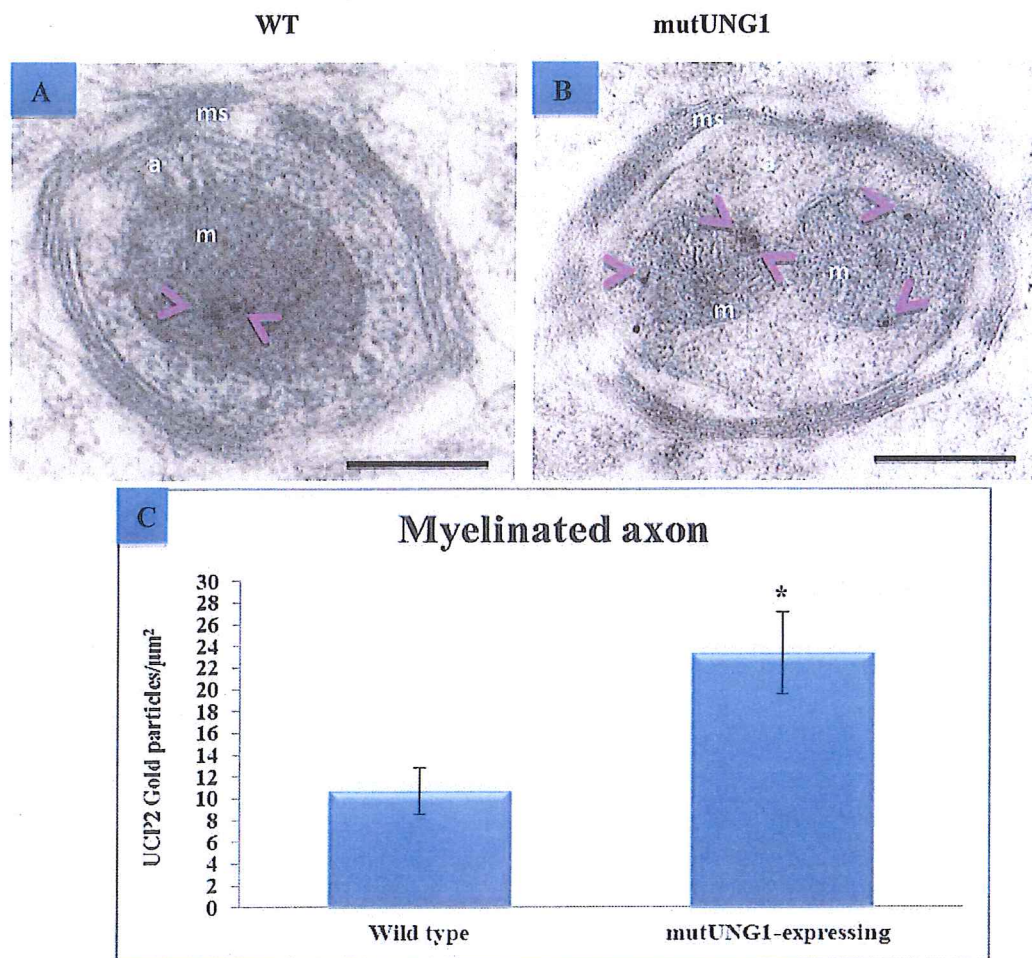
Figure 3.5: Electron micrographs (EMs) show the immunoreactivity of mitochondrial UCP2 in myelinated axon of A) wild type and B) mutUNG1-expressing mice. C) Quantification of UCP2 density (UCP2 GP/μm^2) at myelinated axons in CA1 pyramidal and DG granular cells. There was a statistically significant difference between wild type and mutUNG1-expressing mice (P = 0.02). The data are based on 20 EMs containing 77-78 EM profiles (also representing the total number of mitochondria) for myelinated axons from three wild type and three mutUNG1-expressing mice (n = 3) (Table 2.2). The mean differences of mitochondrial UCP2 density between wild type and mutUNG1- expressing mice were analyzed with mean ± SEM. The level of significance is symbolized with * (p-value < 0.05) (Appendix 19). The arrowheads (purple) indicate UCP2, represented by gold particles in mitochondrial myelinated axon. a = myelinated axon, m= mitochondrion, and ms= myelin sheath. Magnification: 26500 X, 500 nm scale bar.

3.3.2 Immunogold quantification of mitochondrial UCP2 in dendrites of CA1 pyramidal and dentate gyrus granular cells

UCP2 immunoreactivity was found in dendritic mitochondria. Mitochondria were mostly found in groups in dendrites of mutUNG1-expressing mice (Figure 3.6 B). The average density of UCP2 was higher in mutUNG1-expressing (Figure 3.6 B & C and appendix 17) compared to wild type mice (Figure 3.6 A & C and appendix 18), but the difference was not statistically significant (Figure 3.6 C and appendix 19).
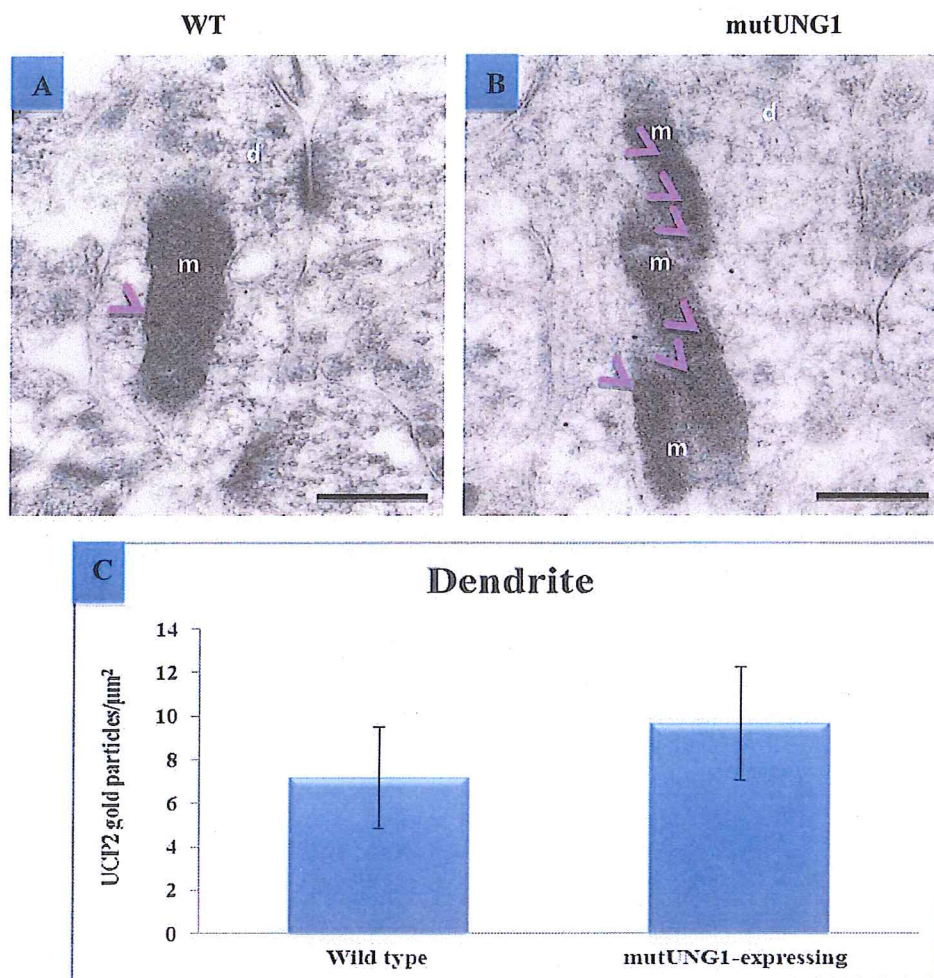
Figure 3.6: Electron micrographs (EMs) show the immunoreactivity of mitochondrial UCP2 in dendrites of A) wild type and B) mutUNG1-expressing mice. C) Quantification of UCP2 density (UCP2 GP/μm^2) at dendrites in CA1 pyramidal and DG granular cells. There was no statistically significant difference between wild type and mutUNG1-expressing mice (P=0.51) (Appendix 19). The data are based on 20 EMs containing 83-96 EM profiles (also representing the total number of mitochondria) for dendrites from three wild type and three mutUNG1-expressing mice (n = 3) (Table 2.2). The mean differences of mitochondrial UCP2 density between wild type and mutUNG1-expressing mice were analyzed with mean ± SEM. The arrowheads (purple) indicate UCP2, represented by gold particles in dendritic mitochondria. m= mitochondrion, and d= dendrite. Magnification: 26500 X, 500nm scale bar.

3.3.3 Immunogold quantification of mitochondrial UCP2 in presynaptic terminals of CA1 pyramidal and dentate gyrus granular cells

The mutUNG1-expressing mice (Figure 3.7 B & C) showed significantly higher labeling of UCP2 than wild type mice (Figure 3.7 A & C) in presynaptic terminals of CA1 pyramidal and DG granular cells (Appendix 17-19). The presence of mitochondria was hardly observed in dendritic spins of synapses (Figure 3.7 B).
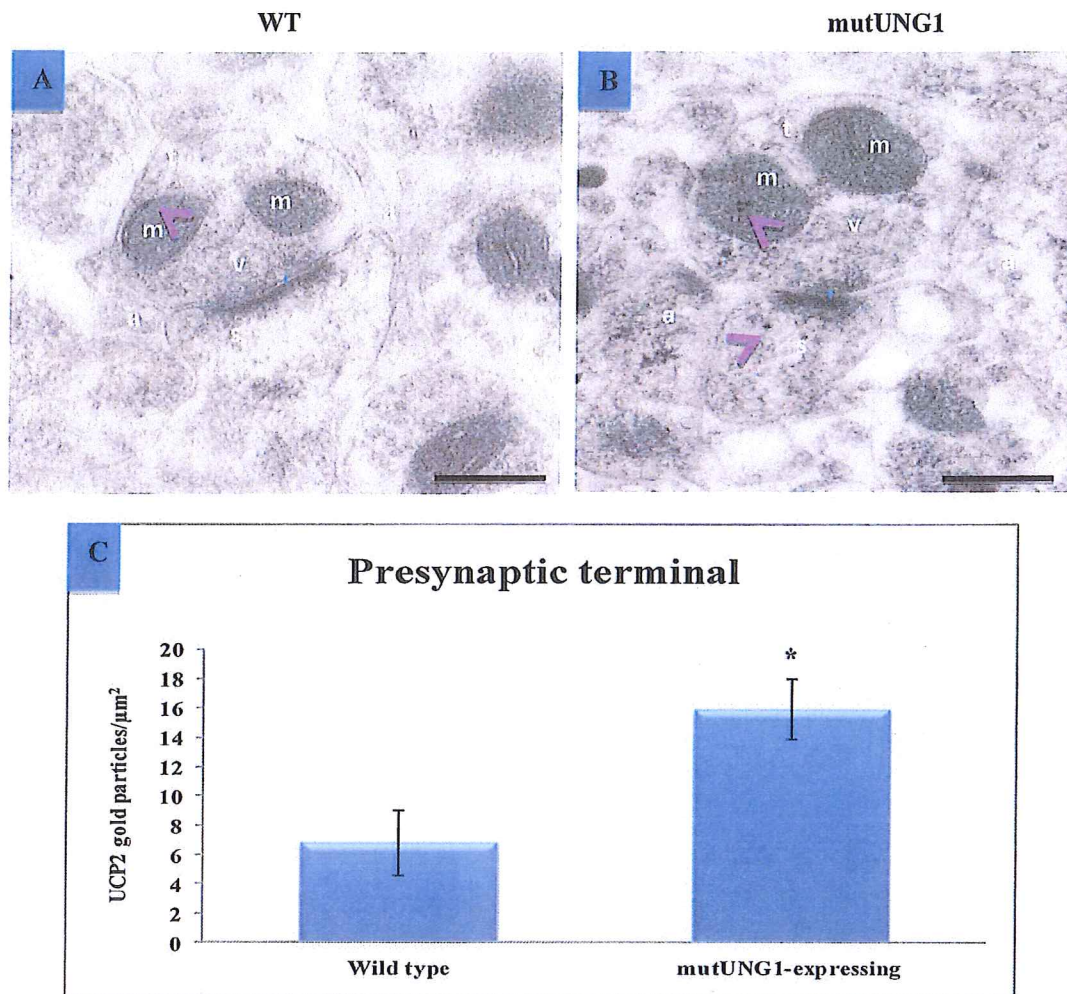
Figure 3.7: Electron micrographs (EMs) show the immunoreactivity of mitochondrial UCP2 in presynaptic terminals of A) wild type and B) mutUNG1-expressing mice. C) Quantification of UCP2 density (UCP2 GP/μm^2) at presynaptic terminals in CA1 pyramidal and DG granular cells. There was statistically significant difference between wild type and mutUNG1-expressing mice (P = 0.04). The data are based on 20 EMs containing 74-84 EM profiles (also representing the total number of mitochondria) for presynaptic terminals from three wild type and three mutUNG1-expressing mice (n = 3) (Table 2.2). The mean differences of mitochondrial UCP2 density between wild type and mutUNG1-expressing mice were analyzed with mean ± SEM. The level of significance is symbolized with * (p-value < 0.05) (Appendix 19). The arrowheads (purple) indicate UCP2, represented by gold particles in presynaptic terminals. m= mitochondria, t= presynaptic terminal, s= dendritic spine, a= astrocyte, v= synaptic vesicle. The horizontal blue line shows the synaptic cleft. Magnification: 26500 X, 500nm scale bar.

3.3.4 Immunogold quantification of mitochondrial UCP2 in somas of CA1 pyramidal and dentate gyrus granular cells

Compared to wild type, mutUNG1-expressing mice showed a significantly higher density of UCP2 in somas (Figure 3.8 A, B & C and appendix 17-19) of CA1 pyramidal and DG granular cells. The shapes of mitochondria were markedly distinguished between wild type and mutUNG1-expressing mice (Figure 3.8 A & B).
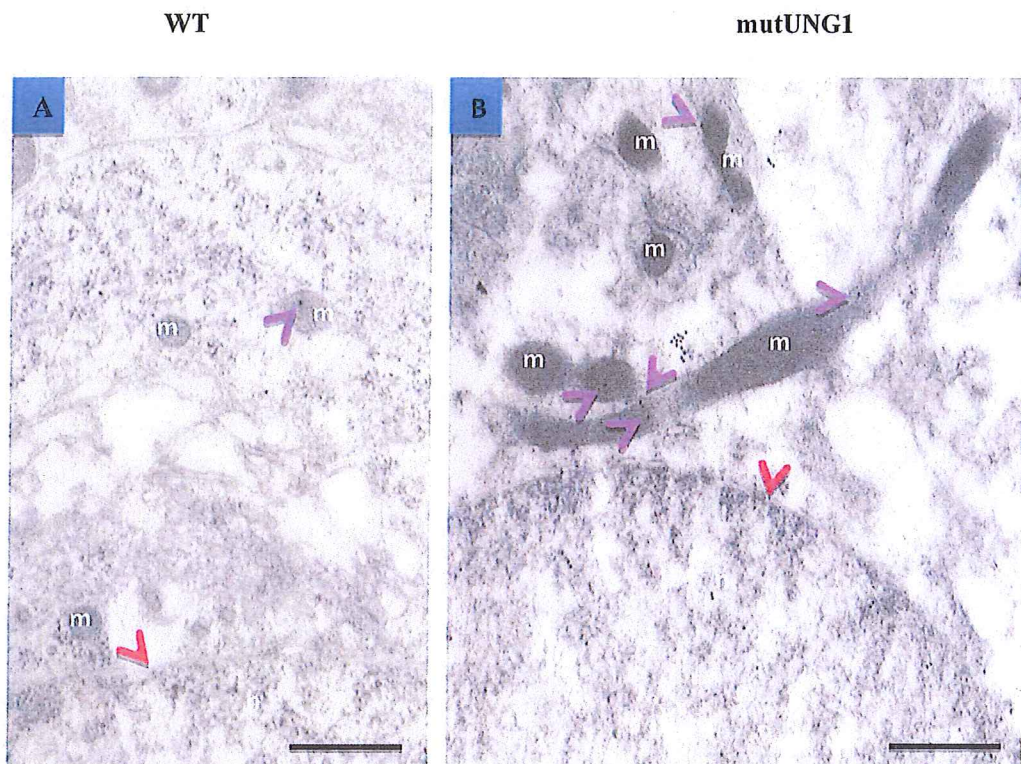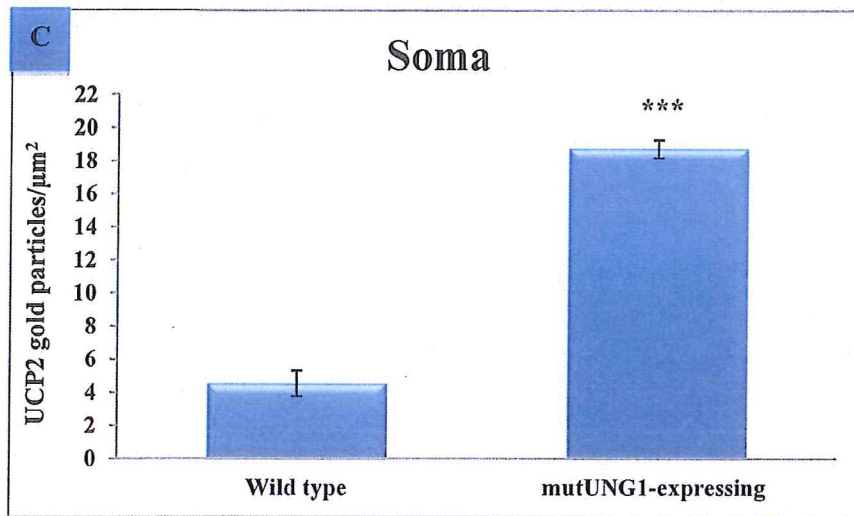
WT   mutUNG1

Figure 3.8: Electron micrographs (EMs) show the immunoreactivity of mitochondrial UCP2 in soma of A) wild type and B) mutUNG1-expressing mice. C) Quantification of UCP2 density (UCP2 GP/μm^2) at somas in CA1 pyramidal and DG granular cells. There was a statistically significant difference between wild type and mutUNG1-expressing mice (P = 0.0001). The data are based on 20 EMs containing 265-364 EM profiles (also representing the total number of mitochondria) for somas from three wild type and three mutUNG1-expressing mice (n = 3) (Table 2.2). The mean differences of mitochondrial UCP2 density between wild type and mutUNG1-expressing mice were analyzed with mean ± SEM. The level of significance is symbolized with *** (p-value < 0.0001) (Appendix 19).The arrowheads (purple) indicate UCP2 represented by gold particles in soma. m= mitochondria, and n=nucleus. The red arrowhead shows the nuclear membrane. Magnification: 26500 X, 500nm scale bar.

3.3.5 Immunogold quantification of mitochondrial UCP2 in different neuronal compartments of CA1 pyramidal cells (stratum radiatum) and DG granular cells (hilus region)

The average density of UCP2 was quantified in detail in one wild type and one mutUNG1-expressing mouse. The level of UCP2 was significantly higher in presynaptic terminals and myelinated axons of mutUNG1-expressing mice compared to wild type mice. There was significantly increase of UCP2 in neuronal cells somas, granular cells increasing more than pyramidal cells. Dendrites showed an insignificant difference of UCP2 level between mutUNG1 and wild type mice (Figure 3.9).
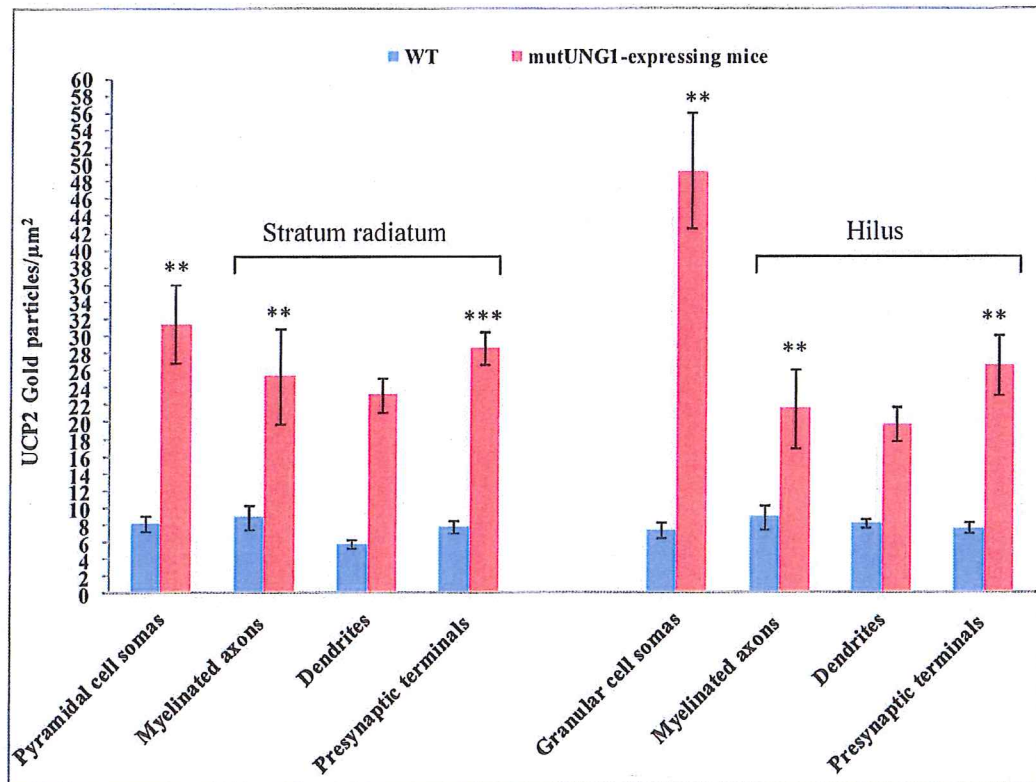
Figure 3.9: Quantification of mitochondrial UCP2 density (UCP2 GP/μm^2) in CA1 pyramidal, DG granular cell somas, myelinated axons, dendrites, and presynaptic terminals. The data are based on 10 EMs (Containing 10-21 EM profiles), analyzed for each compartment (n = 10-21, number of EM profiles) from one wild type and one mutUNG1-expressing mouse. The mean differences of mitochondrial UCP2 density between wild type and mutUNG1-expressing mice were analyzed with mean ± SEM. The level of significance is symbolized with ** (p-value ≤ 0.01) and *** (p-value ≤ 0.001) (Appendix 22).

CHAPTER IV

DISCUSSION

4.1 Western blot

The Western blot showed a binding specificity of the UCP2 primary antibody with UCP2 in protein extract from wild type mouse hippocampi. The dilutions of primary and secondary antibody were optimized with different concentrations as well as different volumes of loading sample to find the optimal conditions for the UCP2 antibody. The major band was at the molecular mass of UCP2 (37 kDa) and considered to be suited for immunogold electron microscopy. The additional weakly stained bands may represent aggregates or breakdown products of UCP2 and/or background binding to tissue proteins (Figure 3.1).

4.2 CA1 and dentate gyrus

The hippocampus is considered to be an ideal part of the brain for studying selective neuronal vulnerability to OS due to its having densely packed layers of neurons (Wang and Michaelis, 2010). However, the CA1 region reacts to OS differently from other regions like CA2, CA3, and DG. Most importantly, the pyramidal neurons in the CA1 region are more susceptible to massive neural death from OS (Wilde et al., 1997; Vornov et al., 1998; Sarnowska, 2002; Wang et al., 2005). The relatively low capacity of BER in basal conditions and the apparent failure to repair oxidative damage after oxygen and glucose deprivation might contribute to the high vulnerability of the CA1 of hippocampus to ischemic injury (Rolseth et al., 2008).

The DG region is vulnerable to neurotoxins such as alcohol intoxication, and shows neurodegeneration in the rat (Crews and Nixon, 2009). The neuronal loss in the DG is found to be related with the ages of the rats (Hashem et al., 2010) and mice (Han et al., 2006).

There are different neuropathologies preferentially connected with the CA1 and DG subfields. AD (Rosenzweig and Barnes, 2003), epilepsy (Ramirez-Munguia et al., 2003), experimental autoimmune encephalomyelitis (Ziehn et al., 2010), multiple sclerosis (Sicotte et al., 2008), hypoxic-ischemic encephalopathy (Nau and Bruck, 2002), and PD (Galvin et al., 1999) are associated neuropathologies within both the CA1 and DG (Simuni and Sethi, 2008) subfields.

Therefore, this study was focused on exploring the mitochondrial morphology and quantity of UCP2 in different neuronal compartments of the CA1 and DG using the mutUNG1-expressing mouse model (Lauritzen et al., 2010).

4.3 Mitochondrial morphology in somas of CA1 pyramidal and dentate gyrus granular cells

Mitochondria are considered to be of central importance for the complex processes of neurotransmission, neuronal plasticity, and energy homeostasis of neurons (Kann and Kovacs, 2007). Moving mitochondria are reported to be smaller in size and to travel with occasional brief pauses (Misgeld et al., 2007). The complex shape of neurons requires specialized mechanisms to allocate a sufficient numbers of mitochondria to different compartments of the neuron for balancing energy demands. Mitochondria travel along microtubules using axonal transport motor proteins to reach their functional places. The balanced delivery of mitochondria helps to serve multiple functions inside the neurons, including energy provision, prevention of apoptosis, synaptic transmission and plasticity (Chan, 2006; Li et al., 2004).

The disruption of mitochondria and their transport has been documented in a wide variety of neurological diseases (Beal, 2005). The aged mitochondria are thought to follow retrograde transport. However, the anterograde transport is important for energy demands in peripheral parts of the neuron (Figure 1.6) (Saxton and Hollenbeck, 2012). The fission and fusion processes that occur in the soma determine whether mitochondria stay as single organelle (Li et al., 2004). Mitochondrial fission and fusion in the soma produce discrete mitochondria that are suitable for long distance transport (Saxton and Hollenbeck, 2012). Most of the necessary mitochondrial proteins are encoded by nuclear genes in the soma (Lee and Hollenbeck, 2003).

The mitochondrial membrane potential drives ATP production, which determines the direction of mitochondrial transport. However, the mitochondrial membrane potential differs in time and space in response to different neuronal challenges (Overly et al., 1996). Mitochondria with low membrane potential move preferentially toward the soma, which implies that old or damaged mitochondria require maintenance (Miller and Sheetz, 2004) by fission or fusion processes. Mitochondrial fission generates healthy mitochondria by facilitating quality control that run along axons toward presynaptic terminals. On the other hand, old and dysfunctional mitochondria are repaired either by fusion with healthy mitochondria or degraded through mitophagy (Chang and Reynold, 2006). Parkinson protein 2 (PARK2, mutated gene) induces mitochondrial degradation in the soma in PD (Cai et al., 2012) and Huntington's disease (Reddy and Shirenbed, 2012) while healthy mitochondria are transported distally to assist synaptic function. Abnormal mitochondrial dynamics are evident in neurodegenerative diseases including AD (Wang et al., 2009a), PD, and Huntington disease (Exner et al., 2007; Deng et al., 2008; Mortiboys et al., 2008; Poole et al., 2008; Yang et al., 2008; Park et al., 2009; Wang et al., 2009).

The present study indicates a breakdown of mitochondrial dynamics in the soma of mutUNG1-expressing mice. The mutUNG1 induced mtDNA damage in the form of AP-sites, creating mtDNA toxicity leading to OS, which caused mitochondrial dysfunction (Lauritzen et al., 2010). Therefore, the disturbed mitochondria in mutUNG1-expressing mice have less ATP producing capacity, which could lead to transport and aggregation of mitochondria in the somas (Miller and Sheetz, 2004). CA1 and DG neuronal functions could possibly be rescued by retrograde axonal transport of mitochondria from CA3 neurons. In mutUNG1-expressing mice, however, mitochondrial aggregation was found in the somas (Figure 3.2 B & C), which could represent an attempt to save healthy mitochondria from old and dysfunctional mitochondria through fusion and fission mechanisms in the somas.

Moreover, some smaller mitochondria form clusters in the soma (Figure 3.2 C) in mutUNG1-expressing mice, which could either follow anterograde transport after fission or fuse together for rescuing healthy mitochondria. The average area of mitochondria was increased in somas and presynaptic terminals in mutUNG1-expressing mice, which could likely be caused by the presence of more mitochondria in mutUNG1-expressing mice compared to wild type littermates. The increased mitochondrial area (Figure 3.3) and the smaller size of mitochondria (Figure 3.4) in somas of mutUNG1-expressing mice could also result from fusion and fission respectively (Chan, 2006; Alberts et al., 2002).

The present study revealed irregular shapes of mitochondria in mutUNG1-expressing mice and this could be caused by both mitochondrial fusion and fission processes that might happen in a simultaneous fashion. In wild type mice, most of the mitochondria were symmetric, small, and round shaped while in mutUNG1-expressing mice the mitochondria were more heterogeneously shaped in the somas. Thereby, the present study suggested a breakdown of mitochondrial dynamics in the somas of mutUNG1-expressing mice, and thus supported the notion that the mutUNG1-expressing mice model could be suitable for studies of neurodegenerative diseases.

4.4 The mutUNG1-expressing mouse model and mitochondrial uncoupling protein 2

The mutUNG1-expressing mouse model was tested as a model for progressive neurodegeneration in the hippocampus, relating to mitochondrial dysfunction. The high level of AP-sites in hippocampal mtDNA has been found to progress mtDNA cytotoxicity that lead to neurodegeneration and apoptosis (Lauritzen et al., 2010). There are some other neurodegenerative diseases and aging associated experiments also show that mtDNA mutations can be responsible for mitochondrial respiratory chain dysfunction (Nicholls, 2008; Reeve et al., 2008). Moreover, mtDNA damage and mitochondrial OS are accepted to be harmful for neurons (Loeb et al., 2005). The mtDNA damage has been documented to be devastating to mitochondrial energy homeostasis and can increase the levels of ROS.

The increased level of ROS can cause neuronal suicide (Nicholls, 2008; Loeb et al., 2005). Thus, an increasing level of AP-sites in mtDNA can accelerate brain aging and neurodegeneration (Lauritzen et al., 2010).

The present study showed a higher quantity of UCP2 in hippocampus in the mutUNG1-expressing mice, which corroborates the current understanding of the role of UCP2 in neurodegeneration and neuroprotection (Figure 3.5 to 3.9). The present study is consistent with the other neurodegenerative models that support UCP2 as a neuroprotective against neuropathologies, related with the CA1 and DG subfields (Richard et al., 2001, Simuni and Sethi, 2008).

The elevated level of UCP2, leading to increased oxygen consumption can control the level of ROS produced in the brain (Rolfe et al., 1994). UCP2 has the ability to attenuate ROS produced in different regions in brain, and can be viewed as a neuroprotector (Negre-Salvayre et al., 1997). The role of UCP2 in diminishing ROS is reported in studies of brain injury in experimental transgenic mice (Bechmann et al., 2002). Thus, UCP2 may guard against neuronal degeneration (Richard et al., 1999; Richard et al., 2001).

UCP2 has a role in maintaining synaptic temperature homeostasis (Horvath et al., 1999). The presence of UCP2 in the hypothalamus was reported in maintaining hypothalamic temperature (Diano et al., 2000). In the presynaptic terminal, the increased level of UCP2 in mutUNG1-expressing mice (Figure 3.7 B & C) might reflect a role of thermal energy in facilitating the differences of neurotransmitters to their receptors.

mutUNG1 expression induces neuropathological phenotypes (Lauritzen et al., 2010). However, in the present study, increasing amounts of UCP2 in different neuronal compartments (myelinated axons, presynaptic terminals, dendrites, and somas) (Figure 3.5 to 3.9) in the mutUNG1-expressing mice could be a part of compensatory mechanism for improving neural resilience.

UCP2 has been documented as a novel neuroprotector in mice models of PD (Andrews et al., 2005a; Conti et al., 2005), epilepsy (Diano et al., 2003), and stroke (Mattiasson et al., 2003). An overexpression of UCP2 in the CA1 and DG regions has been shown of the global ischemia in mice (Olsson et al., 2008). Administration of neuroexcitotoxic and epileptogenic (e.g. kainic acid) chemicals in mice has been shown to lead to increased levels of UCP2 in the CA1 subfield of the hippocampus, which suggests a neuroprotective role of UCP2 against excitotoxic challenges (Clavel et al., 2003).

4.5 Mitochondrial uncoupling protein 2 in myelinated axons in CA1 pyramidal and dentate gyrus granular cells

The presence of mitochondria in axons is essential to generate ATP and thereby control synaptic and action potentials (Kwong et al., 2006). One-third of mitochondria in axons are mobile and the rest stay stagnant (Cai and Sheng, 2009). Mitochondrial health is pivotal for keeping functional neural circuits. Therefore, axonal mitochondria are an important key to regulate the bioenergetic metabolism and control ROS production (Court and Coleman, 2012).

In the present experiments, the level of mitochondrial UCP2 was found significantly higher in myelinated axons of mutUNG1-expressing mice compared to wild type mice (Figure 3.5 A, B, & C and 3.9), which supports a relation between UCP2 and healthy axonal energy homeostasis.

4.6 Mitochondrial uncoupling protein 2 in dendrites in CA1 pyramidal and dentate gyrus granular cells

Mitochondria in dendrites provide sufficient ATP supply for synaptic function and neuronal plasticity. The loss of mitochondria from dendrites may lead to change in dendritic bioenergetics and alter the synaptic activity (Li et al., 2004). Dendrites play an important role in transporting mitochondria to both the periphery and the soma (Sheng and Cai, 2012). Most of the mitochondria in dendrites appear to be stationary (Chen et al., 2007). But, in the cultured hippocampal neurons, the number of motile mitochondria has been found to be higher in dendrites than in axons (Overly et al., 1996; Chen et al., 2007).

The results from the present study showed an insignificant difference of UCP2 present in dendrites between mutUNG1-expressing (Figure 3.6 B & C and 3.9) and wild type mice (Figure 3.6 A & C and 3.9). This result could be explained by the lower energy budget in dendrites (Creutzfeldt, 1975; Nicholson, 1979; Morris and Hollenbeck, 1993). Therefore, mitochondria might not produce increased quantities of UCP2 against dendritic challenges.

4.7 Mitochondrial uncoupling protein 2 in presynaptic terminals of CA1 pyramidal and dentate gyrus granular cells

Mitochondria are commonly located in presynaptic terminals (Shepherd and Harris, 1998; Rowland et al., 2000). The localization of mitochondria in synapses (Chang et al., 2006; Kang et al., 2008; Li et al., 2004) is mandatory for proper neuronal function and development (Guo et al., 2005; Kang et al., 2008; Tang and Zucker, 1997). Mitochondrial dysfunction in the presynaptic terminals in Drosophila has been shown to cause disturbed synaptic transmission (Stowers et al., 2002; Guo et al., 2005; Verstreken et al., 2005). The abnormal transport of mitochondria results in impaired neuronal functions and accelerates human neurological disorders and neurodegenerative diseases (Hirokawa and Takemura, 2004; Chan, 2006; Stokin and Goldstein, 2006).

High energy is required for neurotransmission (Kang et al., 2008; Talbot et al., 2003; Levy et al., 2003; Laughlin et al., 1998). UCP2 in presynaptic terminals could speed up synaptic transmission by enhancing synaptic vesicle formation and neurotransmitter release and reuptake through heat produced presynaptically (Horvath et al., 1999).

In the present study, the increase of UCP2 in presynaptic terminals, could contribute to a role of UCP2 in modulating neurotransmission through temperature homeostasis (Horvath et al., 1999). UCP2 in hippocampus has been implied in disrupted synaptogenesis of UCP2 knockout mice (Simon-Areces et al., 2012). The significant increase of UCP2 in presynaptic terminals of mutUNG1-expressing mice could also represent an attempt to rescue dysfunctional mitochondria from mtDNA damage (Lauritzen et al., 2010) (Figure 3.7 B & C and 3.9).

4.8 Mitochondrial uncoupling protein 2 in somas of CA1 pyramidal and dentate gyrus granular cells

The soma of a neuron contains all organelles such as nucleus, mitochondria, smooth and rough endoplasmic reticulum, Golgi complex, and degradation machinery, like lysosomes, and proteasomes. All protein constituents are synthesized in the soma and are subsequently transported to their sites of functions (Kaplan et al., 2009) to optimize the local energy and metabolic demands (Hollenbeck, 1996). The proteins in the soma are important for the growth and function of neurons including axon regeneration (Hanz et al., 2003; Verma et al., 2005), synapse formation (Schacher and Wu, 2002), axon viability (Hu et al., 2003), neuronal survival, and synaptic plasticity (Martin et al., 1997; Casadio et al., 1999; Beaumont et al., 2001; Liu et al., 2003; Si et al., 2003).

In the present study, the abnormal morphologies of mitochondria (Figure 2.3 B & C) might relate to the higher quantity of UCP2 in somas of mutUNG1-expressing mice compared to wild type littermates (Figure 3.8 A, B & C and 3.9). This could however, indicate that aged and dysfunctional mitochondria could get neuroprotection from UCP2 in somas in order to preserve supply of healthy mitochondria to the distal parts of neurons. The significant higher levels of UCP2 in the granular cell soma compared to the pyramidal cell soma in mutUNG1-expressing mice (Figure 3.9) indicate that more ROS was produced in mitochondria of granular cell.

4.9 Further research possibilities

The current study indicates that the mutUNG1-expressing mouse model can be used to identify the level of neuroprotector (UCP2) and mitochondrial dynamics in neuropathological conditions. However, the understanding of the expression of UCP2 and additional UCPs of UCP2 (UCP3, UCP4, and UCP5), both mRNA and protein level in different brain regions in the mutUNG1-expressing mouse model may help in identifying therapeutic approaches against neuropathological abnormalities. Importantly, UCPs may be used as novel neuronal biomarkers that may be useful for drug discovery against neurodegenerative diseases. Mitochondrial bioenergetic studies are necessary to determine the physiological condition of mitochondria in different neuropathologies. Therefore, future experiments are required to establish the role of UCPs in mitochondrial energy deprivation and neurodegenerative disease.

CONCLUSION

In conclusion, the research objectives were answered as follows:

The mutUNG1 mice, compared to wild type mice, showed mitochondria of abnormal morphology, i.e., irregular shapes, and clusters or aggregates in the neurons of CA1 and dentate gyrus.

The level of UCP2 in different parts of neurons in CA1 and in the dentate gyrus was increased in mutUNG1-expressing mice compared to wild type mice. Statistically significant differences were observed for myelinated axons, presynaptic terminals, and somas.

These results suggest that raising UCP2 levels may serve to counteract neurodegenerative diseases. The increased level of UCP2 in neuropathophysiologies may serve as a starting point for the innovation of therapy in neurodegenerative diseases.

REFERENCES

Adam-Vizi, V. (2005). Production of reactive oxygen species in brain mitochondria: contribution by electron transport chain and non-electron transport chain sources. *Antioxid Redox Signal, 7,* 1140-1149.

Alberts, B., Johnson, A., Lewis, J., Raff, M., Roberts, K., & Walter, P. (2002). Molecular Biology of the Cell (4th edition). *GS Garland Science Taylor & Francis group,* 808-821.

Amaral, D. G., Ishizuka, N., & Claiborne, B. (1990). Neurons, numbers and the hippocampal network. *Prog Brain Res, 83,* 1-11.

Andersen, P., Morris, R., Amaral, D., Bliss, T., & O'Keefe, J. (2007). The hippocampus book. *Oxford University Press.* ISBN 978-0-19-510027-3.

Anderson, C. T., & Friedberg, E. C. (1980). The presence of nuclear and mitochondrial uracil-DNA glycosylase in extracts of human KB cells. *Nucleic Acids Res, 8,* 875-888.

Andrews, Z. B., & Horvath, T. L. (2009). Uncoupling protein-2 regulates lifespan in mice. *Am J. Physiol Endocrinol Metab, 296,* 621-627.

Andrews, Z. B., Diano, S., & Horvath, T. L. (2005). Mitochondrial uncoupling proteins in the CNS: in support of function and survival. *Nat.Rev.Neurosci, 6,* 829-840.

Andrews, Z. B., Horvath, B., Barnstable, C. J., Elsworth, J., Yang, L., Beal, M. F., Roth, R. H., Matthews, R. T., & Horvath, T. L. (2005a). Uncoupling protein-2 is critical for nigral dopamine cell survival in a mouse model of Parkinson's disease. *J. Neurosci, 25*(1), 184-191.

Andrews, Z. B., Liu, Z. W., Walllingford, N., Erion, D. M., Borok, E., Friedman, J. M., Tschop, M. H., Shanabrough, M., Cline, G., Shulman, G. I., Coppola, A., Gao, X. B., Horvath, T. L., & Diano, S. (2008). UCP2 mediates ghrelin's action on NPY/AgRP neurons by lowering free radicals. *Nature, 454,* 846-851.

Attwell, D., & Laughlin, S. B. (2001). An energy budget for signaling in the grey matter of the brain. *J. Cereb Blood Flow Metab, 21,* 1133-1145.

Beal, M. F. (2005). Mitochondria Take Center Stage in Aging and Neurodegeneration. *Ann Neurol, 58,* 495-505.

Beaumont, V., Zhong, N., Fletcher, R., Froemke, R. C., & Zucker, R. S. (2001). Phosphorylation and local presynaptic protein synthesis in calcium- and calcineurin-dependent induction of crayfish long-term facilitation. *Neuron, 32,* 489-501.

Bechmann, I., Diano, S., Warden, C. H., Bartfai, T., Nitsch, R., & Horvath, T. L. (2002). Brain mitochondrial uncoupling protein 2 (UCP2): a protective stress signal in neuronal injury. *Biochem Pharmacol, 64*, 363-367.

Bergersen, L. H., Storm-Mathisen, J., & Gundersen, V. (2008). Immunogold quantification of amino acids and proteins in complex subcellular compartments. *Nat Protoc, 3*(1), 144-152.

Bohr, V. A., Stevnsner, T., & de Souza-Pinto, N. C. (2002). Mitochondrial DNA repair of oxidative damage in mammalian cells. *Gene, 286*, 127-134.

Boveris, A., & Chance, B. (1973). The mitochondrial generation of hydrogen peroxide. General properties and effect of hyperbaric oxygen. *Biochem. J, 134*, 707-716.

Boveris, A., Oshino, N., & Chance, B. (1972). The cellular production of hydrogen peroxide. *Biochem. J, 128*(3), 617-630.

Brand, M. D. (2000). Uncoupling to survive? The role of mitochondrial inefficiency in ageing. *Exp Gerontol, 35*, 811-820.

Burger, G., Gray, M. W., & Lang, B. F. (2003). Mitochondrial genomes: anything goes. *Trends Genet, 19*, 709-716.

Cai, Q., & Sheng, Z. H. (2009). Mitochondrial transport and docking in axons. *Exp. Neurol, 218*, 257-267.

Cai, Q., Zakaria, H. M., & Sheng, Z. H. (2012). Long time-lapse imaging reveals unique features of PARK2/Parkin-mediated mitophagy in mature cortical neurons. *Autophagy, 8*(6), 976-978.

Casadio, A., Martin, K.C., Giustetto, M., Zhu, H., Chen, M., Bartsch, D., Bailey, C. H., & Kandel, E. R. (1999). A transient, neuron-wide form of CREB-mediated long-term facilitation can be stabilized at specific synapses by local protein synthesis. *Cell, 99*, 221-237.

Chan, D. C. (2006). Mitochondrial fusion and fission in mammals. *Annu Rev Cell Dev Biol, 22*, 79-99.

Chan, S. H. H., Wu, C. A., Wu, K. L. H., Ho, Y., Chang, A. Y. W., & Chan, J. Y. H. (2009). Transcriptional Upregulation of Mitochondrial Uncoupling Protein 2 Protects Against Oxidative Stress-Associated Neurogenic Hypertension. *Circ Res, 105*, 886-896.

Chang, D. T., & Reynolds, I. J. (2006). Mitochondrial trafficking and morphology in healthy and injured neurons. *Prog Neurobiol, 80*, 241-268.

Chang, D. T., Honick, A. S., & Reynolds, I. J. (2006). Mitochondrial trafficking to synapses in cultured primary cortical neurons. *J. Neurosci, 26*, 7035-7045.

Chen, H., & Chan D. C. (2006). Critical dependence of neurons on mitochondrial dynamics. *Curr Opin Cell Biol, 18*, 453-459.

Chen, H., & Chan, D. C. (2009). Mitochondrial dynamics-fusion, fission, movement, and mitophagy-in neurodegenerative diseases. *Hum Mol Genet, 18*(2), 169-176.

Chen, S., Owens, G. C., Crossin, K. L., & Edelman, D. B. (2007). Serotonin stimulates mitochondrial transport in hippocampal neurons. *Mol Cell Neurosci, 36*(4), 472-483. doi: 10.1016/j.mcn.2007.08.004

Chen, S. D., Lin, T. K., Lin, J. W., Yang, D. I., Lee, S. Y., Shaw, F. Z., Liou, C. W., & Chuang, Y. C. (2010). Activation of calcium/calmodulin-dependent protein kinase IV and peroxisome proliferator-activated receptor γ coactivator-1α signaling pathway protects against neuronal injury and promotes mitochondrial biogenesis in the hippocampal CA1 subfield after transient global ischemia. *J. Neurosci Res, 88*, 3144-3154.

Cheng, A., Hou, Y., & Mattson, M. P. (2010). Mitochondria and neuroplasticity. *ASN Neuro, 2*(5), 243-256.

Clavel, S., Paradis, E., Ricquier, D., & Richard, D. (2003). Kainic acid upregulates uncoupling protein-2 mRNA expression in the mouse brain. *Neuroreport, 14*(16), 2015-2017.

Conrad, C. D., & Roy, E. J. (1995). Dentate gyrus destruction and spatial learning impairment after corticosteroid removal in young and middle-aged rats. *Hippocampus, 5*, 1-15.

Conti, B., Sanchez-Alavez, M., Winsky-Sommerer, R., Morale, M. C., Lucero, J., Brownell, S., Fabre, V., Huitron-Resendiz, S., Henriksen, S., Zorrilla, E. P., de Lecea, L., & Bartfai, T. (2006). Transgenic mice with a reduced core body temperature have an increased life span. *Science, 314*, 825-828.

Conti, B., Sugama, S., Lucero, J., Winsky-Sommerer, R., Wirz, S. A., Maher, P., Andrews, Z., Barr, A. M., Morale, M. C., Paneda, C., Pemberton, J., Gaidarova, S., Behrens, M. M., Beal, F., Sanna, P. P., Horvath, T., & Bartfai, T. (2005). Uncoupling protein 2 protects dopaminergic neurons from acute 1, 2, 3, 6-methyl-phenyl-tetrahydropyridine toxicity. *J. Neurochem, 93*, 493-501.

Court, F. A., & Coleman, M. P. (2012). Mitochondria as a central sensor for axonal degenerative stimuli. *Trends Neurosci, 35*, 364-372.

Creutzfeldt, O. D. (1975). Neurophysiological correlates of different functional states of the brain. In: Brain Work: The Coupling of Function, Metabolism and Blood Flow in the Brain, edited by D. H. Ingvar and N. A. Lassen. Copenhagen: Munksgaard, 22-47.

Crews, F. T., & Nixon, K. (2009). Mechanisms of neurodegeneration and regeneration in alcoholism. *Alcohol & Alcohol, 44*(2), 115-127.

de Souza-Pinto, N. C., Wilson, D. M., 3rd, Stevnsner, T. V., & Bohr, V. A. (2008). Mitochondrial DNA, base excision repair and neurodegeneration. *DNA Repair (Amst), 7*(7), 1098-1109. doi: 10.1016/j.dnarep.2008.03.011

Deng, H., Dodson, M. W., Huang, H., & Guo, M. (2008). The Parkinson's disease genes pink1 and parkin promote mitochondrial fission and/or inhibit fusion in Drosophila. *Proc Natl Acad Sci, 105*, 14503-14508.

Diano, S., Matthews, R. T., Patrylo, P., Yang, L., & Beal, M. F. (2003). Uncoupling protein 2 prevents neuronal death including that occurring during seizures: A mechanism for pre-conditioning. *Endocrinology, 144*, 5014-5021.

Diano, S., Urbanski, H. F., Horvath, B., Bechmann, I., Kagiya, A., Nemeth, G., Naftolin, F., Warden C. H., & Horvath, T. L. (2000). Mitochondrial Uncoupling Protein 2 (UCP2) in the Nonhuman Primate Brain and Pituitary. *Endocrinology, 141*(11), 4226-4238.

Dianov, G. L., Sleeth, K. M., Dianova, I. I., & Allinson, S. L. (2003). Repair of abasic sites in DNA. *Mutat. Res, 531*, 157-163.

Dikov, D., Aulbach, A., Muster, B., Dröse, S., Jendrach, M., & Bereiter-Hahn, J. (2010). Do UCP2 and mild uncoupling improve longevity? *Exp Gerontol, 45*, 586-595.

Dorr, A., Sled, J. G., & Kabani, N. (2007). Three-dimensional cerebral vasculature of the CBA mouse brain: a magnetic resonance imaging and micro computed tomography study. *Neuroimage, 35*, 1409–1423.

Druzhyna, N. M., Wilson, G. L., & Le Doux, S. P. (2008). Mitochondrial DNA repair in aging and disease. *Mech Ageing Dev, 129*(7-8), 383-90.

Dupuis, L., Di Scala, F., Rene, F., De Tapia, M., Oudart, H., Pradat, P. F., Meininger, V., & Loeffler, J. P. (2003). Up-regulation of mitochondrial uncoupling protein 3 reveals an early muscular metabolic defect in amyotrophic lateral sclerosis. *FASEB Journal, 17*(14), 2091-2093.

Echtay, K. S., Winkler, E., Frischmuth, K., & Klingenberg, M. (2001). Uncoupling proteins 2 and 3 are highly active H^+ transporters and highly nucleotide sensitive when activated by coenzyme Q (ubiquinone). *Proc Natl Acad Sci, 98*, 1416-1421.

Eriksson, P.S., Perfilieva, E., Bjork-Eriksson, T., Alborn, A. M., Nordborg, C., Peterson, D. A., & Gage, F. H. (1998). Neurogenesis in the adult human hippocampus. *Nat Med, 4*(11), 1313-1317.

Exner, N., Treske, B., Paquet, D., Holmstrom, K., Schiesling, C., Gispert, S., Carballo-Carbajal, I., Berg, D., Hoepken, H. H., & Gasser, T. (2007). Loss-of-function of human PINK1 results in mitochondrial pathology and can be rescued by parkin. *J. Neurosci, 27*, 12413-12418.

Fleury, C., Neverova, M., Collins, S., Raimbault, S., Champigny, O., Levi-Meyrueis, C., Bouillaud, F., Seldin, M. F., Surwit, R. S., Ricquier, D., & Warden, C. H. (1997). Uncoupling protein-2: a novel gene linked to obesity and hyperinsulinemia. *Nature Genet, 15*, 269-273.

Fridell, Y. W., Sanchez-Blanco, A., Silvia, B. A., & Helfand, S. L. (2005). Targeted expression of the human uncoupling protein 2 (hUCP2) to adult neurons extends life span in the fly. *Cell Metab, 1*, 145-152.

Fuster-Matanzo, A., Llorens-Martin, M., de Barreda, E. G., Avila, J., & Hernandez, F. (2011). Different Susceptibility to Neurodegeneration of Dorsal and Ventral Hippocampal Dentate Gyrus: A Study with Transgenic Mice Overexpressing GSK3β. *PLoS ONE, 6*(11), 1-9.

Galvin, J. E., Uryu, K., Lee, V. M., & Trojanowski, J. Q. (1999). Axon pathology in Parkinson's disease and Lewy body dementia hippocampus contains alpha-, beta-, and gamma-synuclein. *Proc Natl Acad Sci, 96*, 13450-5.

Gao, X., Arlotta, P., Macklis, J. D., & Chen, J. (2007). Conditional knock-out of β-catenin in postnatal-born dentate gyrus granule neurons results in dendritic malformation. *J. Neurosci, 27*(52), 14317-14325.

Gossen, M., & Bujard, H. (1992). Tight control of gene expression in mammalian cells by tetracycline-responsive promoters. *Proc Natl Acad Sci, 98*, 5547-5551.

Gossen, M., Freundlieb, S., Bender, G., Muller, G., Hillen, W., & Bujard, H., (1995). Transcriptional activation by tetracyclines in mammalian cells. *Science, 268*, 1766-1769.

Guo, X., Macleod, G. T., Wellington, A., Hu, F., Panchumarthi, S., Schoenfield, M., Marin, L., Charlton, M. P., Atwood, H. L., & Zinsmaier, K. E. (2005). The GTPase dMiro is required for axonal transport of mitochondria to Drosophila synapses. *Neuron, 47*, 379-393.

Hamanaka, R. B., & Chandel, N. S. (2010). Mitochondrial reactive oxygen species regulate cellular signaling and dictate biological outcomes. *Trends Biochem Sci, 35*(9), 505-513. doi: 10.1016/j.tibs.2010.04.002

Hammond, C. (2008). Cellular and molecular neurophysiology. *Elsevier* ISBN, 978-0-12-374127-1.

Han, M., Schottler, F., Lei, D., Dong, E. Y., Bryan, A., & Bao, J. (2006). Bcl-2 over-expression fails to prevent age-related loss of calretinin positive neurons in the mouse dentate gyrus. *Mol Neurodegener, 1*(9), 1-9.

Hanz, S., Perlson, E., Willis, D., Zheng, J. Q., Massarwa, R., Huerta, J. J., Koltzenburg, M., Kohler, M., van-Minnen, J., Twiss, J. L., & Fainzilber, M. (2003). Axoplasmic importins enable retrograde injury signaling in lesioned nerve. *Neuron, 40*, 1095-1104.

Harper, M. E., Green, K., & Brand, M. D. (2008). The efficiency of cellular energy transduction and its implications for obesity. *Annu. Rev. Nutr, 28,* 13-33.

Hashem, H. E., Elmasry, S. M., & Eladl, M. A. (2010). Dentate Gyrus in Aged Male Albino Rats (Histological and TauImmunohistochemical Study). *Egypt. J. Histol, 33*(4), 659-670.

Hirokawa, N., & Takemura, R. (2004). Kinesin superfamily proteins and their various functions and dynamics. *Exp Cell Res, 301,* 50-59.

Hoeijmakers, J. H. (2001). Genome maintenance mechanisms for preventing cancer. *Nature, 411,* 366-374.

Hollenbeck, P. J. (1996). The pattern and mechanism of mitochondrial transport in axons. *Front. Biosci, 1,* 91-102.

Horvath, T. L., Warden, C. H., Hajos, M., Lombardi, A., Goglia, F., & Diano, S. (1999). Brain Uncoupling Protein 2: Uncoupled Neuronal Mitochondria Predict Thermal Synapses in Homeostatic Centers. *J Neurosci, 19*(23), 10417-10427.

Hu, J. Y., Meng, X., & Schacher, S. (2003). Redistribution of syntaxin mRNA in neuronal cell bodies regulates protein expression and transport during synapse formation and long-term synaptic plasticity. *J. Neurosci, 23,* 1804-1815.

Ihunwo, A. O., & Schliebs, R. (2010). Cell proliferation and total granule cell number in dentate gyrus of transgenic Tg2576 mouse. *Acta Neurobiol Exp, 70,* 362-369.

Imam, S., Karahalil, B., Hogue, B., Souza-Pinto, N., & Bohr, V. (2006). Mitochondrial and nuclear DNA-repair capacity of various brain regions in mouse is altered in an age-dependent manner. *Neurobiol Aging, 27,* 1129-1136.

Kalil, R. E. (1989). Synapse formation in the developing brain. *Sci Am, 261* (6), 76-79, 82-85.

Kandel, E. R. (1979). Small systems of neurons. *Sci Am, 241*(3), 66-76.

Kang, J. S., Tian, J. H., Pan, P. Y., Zald, P., Li, C., Deng, C., & Sheng, Z. H. (2008). Docking of axonal mitochondria by syntaphilin controls their mobility and affects short-term facilitation. *Cell, 132,* 137-148.

Kann, O., & Kovacs, R. (2007). Mitochondria and neural activity. *Am J. Physiol Cell Physiol, 292,* 641-657.

Kaplan, B. B., Gioio, A. E., Hillefors, M., & Aschrafi, A. (2009). Axonal Protein Synthesis and the Regulation of Local Mitochondrial Function. *Results Probl Cell Differ, 48,* 1-25.

Karahalil, B., Hogue, A., de Souza-Pinto, N. C., & Bohr, V. A. (2002). Base excision repair capacity in mitochondria and nuclei: tissue-specific variations. *FASEB Journal, 16*(14), 1895-1902.

Kavli, B., Slupphaug, G., Mol, C. D., Arvai, A. S., Peterson, S. B., Tainer, J. A., & Krokan, H. E. (1996). Excision of cytosine and thymine from DNA by DNA by mutants of human uracil-DNA glycosylase. *EMBO J, 15*, 3442-3447.

Klingenberg, M., & Huang, S. G. (1999). Structure and function of the uncoupling protein from brown adipose tissue. Biochim. *Biophys. Acta, 1415*, 271-296.

Korshunov, S. S., Skulachev, V. P., & Starkov, A. A. (1997). High protonic potential actuates a mechanism of production of reactive oxygen species in mitochondria. *FEBS Lett, 416*, 15-18.

Kroemer, G., & Reed, J. C. (2000). Mitochondrial control of cell death. *Nat Med, 6*, 513-519.

Kubota, Y., Nash, R. A., Klungland, A., Schar, P., Barnes, D. E., & Lindahl, T. (1996). Reconstitution of DNA base excision-repair with purified human proteins: interaction between DNA polymerase beta and the XRCC1 protein. *EMBO J, 15*(23), 6662-6670.

Kwong, J. Q., Beal, M. F., & Manfredi, G. (2006). The role of mitochondria in inherited neurodegenerative diseases. *J Neurochem, 97*(6), 1659-1675. doi: 10.1111/j.1471-4159.2006.03990.x

Larsen, N. B., Rasmussen, M., & Rasmussen, L. J. (2005). Nuclear and mitochondrial DNA repair: similar pathways?. *Mitochondrion, 5*, 89-108.

Laughlin, S. B., de Ruyter van Stevenick, R. R., & Anderson, J. C. (1998). The metabolic cost of neuronal information. *Nat Neurosci, 1*, 436-441.

Lauritzen, K. H., Dalhus, B., Storm, J. F., Bjoras, M., & Klungland, A. (2011). Modeling the impact of mitochondrial DNA damage in forebrain neurons and beyond. *Mech.Ageing Dev, 132*, 424-428. doi:S0047-6374(11)00028-5

Lauritzen, K. H., Moldestad, O., Eide, L., Carlsen, H., Nesse, G., Storm, J. F., Mansuy, I. M., Bergersen, L. H., & Klungland, A. (2010). Mitochondrial DNA toxicity in forebrain neurons causes apoptosis, neurodegeneration, and impaired behavior. *Mol Cell Biol, 30*, 1357-1367.

Lebed, D. S., & Arkhipov, V. I. (2010). Expression of mitochondrial uncoupling protein UCP2 in the brain of rats after hippocampal injury inflicted by kainic acid. *Bull Exp Biol Med, 150*(2), 185-187.

Ledesma, A., de lacoba M. G., & Rial, E. (2002). The mitochondrial uncoupling proteins. *Gen Biol, 3*(12), 3015.1-3015.9.

Lee, S. K., & Hollenbeck, P. J. (2003). Organization and translation of mRNA in sympathetic neurons. *J.Cell.Sci, 116*, 4467-4478.

Lemire, J., & Appanna, V. D. (2011). Aluminum toxicity and astrocyte dysfunction: A metabolic link to neurological disorders. *J. Inorg. Biochem, 105*, 1513-1517.

Levy, M., Faas, G. C., Saggau, P., Craigen, W. J., & Sweatt, J. D. (2003). Mitochondrial regulation of synaptic plasticity in the hippocampus. *J. Biol. Chem, 278*, 17727-17734.

Li, B., Yamamori, H., Tatebayashi, Y., Shafit Zagardo, B., Tanimukai, H., Chen, S., Iqbal, K., & Grundke Iqbal, I. (2008). Failure of neuronal maturation in Alzheimer disease dentate gyrus. *J. Neuropathol. Exp. Neurol, 67*(1), 78-84.

Li, Z., Okamoto, K., Hayashi, Y., & Sheng, M. (2004). The importance of dendritic mitochondria in the morphogenesis and plasticity of spines and synapses. *Cell, 119*, 873-887.

Lindahl, T. (1993). Instability and decay of the primary structure of DNA. *Nature, 362*, 709-715.

Lindahl, T., & Wood, R. D. (1999). Quality control by DNA repair. *Science, 286*, 1897-1905.

Liu, K., Hu, J. Y., Wang, D., & Schacher, S. (2003). Protein synthesis at synapse versus cell body: enhanced but transient expression of long-term facilitation at isolated synapses. *J. Neurobiol, 56*, 275-286.

Loeb, L. A., Wallace, D. C., & Martin, G. M. (2005). The mitochondrial theory of aging and its relationship to reactive oxygen species damage and somatic mtDNA mutations. *Proc. Natl. Acad. Sci, 102*, 18769-18770.

Lu, B. (2009). Mitochondrial Dynamics and Neurodegeneration. *Curr Neurol Neurosci Rep, 9*(3), 212-219.

Mailloux, R. J., & Harper, M. E. (2012). Mitochondrial proticity and ROS signaling: lessons from the uncoupling proteins. *Trends Endocrinol Metab, 29*(9), 451-458.

Mansuy, I. M., Winder, D. G., Moallem, T. M., Osman, M., Mayford, M., Hawkinds, R. D., & Kandel, E. R. (1998). Inducible and reversible gene expression with the rtTA system for the study of memory. *Neuron, 21*, 257-265.

Martin, K.C., Casadio, A., Zhu, H., Yaping, E., Rose, J. C., Chen, M., Bailey, C. H., & Kandel, E. R. (1997). Synapse-specific, long-term facilitation of aplysia sensory to motor synapses: a function for local protein synthesis in memory storage. *Cell, 91*, 927-938.

Mattiasson, G., & Sullivan, P. G. (2006). The emerging functions of UCP2 in health, disease, and therapeutics. *Antioxid Redox Signal, 8*, 1-38.

Mattiasson, G., Shamloo, M., Gido, G., Mathi, K., Tomasevic, G., Yi, S., Warden, C. H., Castilho, R. F., Melcher, T., Gonzalez-Zulueta, M., Nikolich, K., & Wieloch, T. (2003). Uncoupling protein-2 prevents neuronal death and diminishes brain dysfunction after stroke and brain trauma. *Nat Med, 9*, 1062-1068.

Mayford, M., Bach, M. E., Huang, Y. Y., Wang, L., Hawkins, R. D., & Kandel, E. R. (1996). Control of memory formation through regulated expression of a CaMKII transgene. *Science, 247*, 1678-1683.

Miguel-Hidalgo, J. J., & Cacabelos, R. (1998). Beta-amyloid(1-40)-induced neurodegeneration in the rat hippocampal neurons of the CA1 subfield. *Acta Neuropathol, 95*(5), 455-65.

Miles, B. (2003). The electron transport chain. Retrieved January 15, 2013, from http://www.tamu.edu/faculty/bmiles/lectures/electrontrans.pdf

Miller, K. E., & Sheetz, M. P. (2004). Axonal mitochondrial transport and potential are correlated. *J Cell Sci, 117*, 2791-2804.

Misgeld, T., Kerschensteiner, M., Bareyre, F. M., Burgess, R. W., & Lichtman, J. W. (2007). Imaging axonal transport of mitochondria in vivo. *Nature Methods, 4*(7), 559-561.

Mizuno, T., Miura-Suzuki, T., Yamashita, H., & Mori, N. (2000). Distinct regulation of brain mitochondrial carrier protein-1 and uncoupling protein-2 genes in the rat brain during cold exposure and aging. *Biochem Biophys Res Commun, 278*, 691-697.

Molnar, P., & Nadler, J. V. (1999). Mossy fiber-granule cell synapses in the normal and epileptic rat dentate gyrus studied with minimal laser photostimulation. *J. Neurophysiol, 82*, 1883-1894.

Morris, R. L., & Hollenbeck, P. J. (1993). The regulation of bidirectional mitochondrial transport is coordinated with axonal outgrowth. *J. Cell Sci, 104*, 917-927.

Mortiboys, H., Thomas, K. J., Koopman, W. J., Klaffke, S., Abou-Sleiman, P., Olpin, S., Wood, N. W., Willems, P. H., Smeitink, J. A., Cookson, M. R., & Bandmann, O. (2008). Mitochondrial function and morphology are impaired in parkin-mutant fibroblasts. *Ann Neurol, 64*, 555-565.

Murphy, M. P. (2009). How mitochondria produce reactive oxygen species. *Biochem J., 417*, 1-13.

Nau, R., & Bruck, W. (2002). Neuronal injury in bacterial meningitis: mechanisms and inplications for therapy. *Trends Neurosci, 25*, 38-45.

Negre-Salvayre, A., Hirtz, C., Carrera, G., Cazenave, R., Troly, M., Salvayre, R., Pénicaud, L., & Casteilla, L. (1997). A role for uncoupling protein-2 as a regulator of mitochondrial hydrogen peroxide generation. *The FASEB Journal, 11*(10), 809-815.

Neves, G., Cooke, S. F., & Bliss T. V. (2008). Synaptic plasticity, memory and the hippocampus: a neural network approach to causality. *Nat Rev Neurosci, 9*, 65-75.

Nicholls, D. G. (2008). Oxidative stress and energy crises in neuronal dysfunction. *Ann. N. Y. Acad. Sci, 1147*, 53-60.

Nicholls, D. G., & Ward, M. W. (2000). Mitochondrial membrane potential and neuronal glutamate excitotoxicity: mortality and millivolts. *Trends Neurosci, 23*, 166-174.

Nicholson, C. (1979). Brain cell microenvironment as a communication channel. In: Schmitt FO, Worden FG, editors. The neurosciences: fourth study program. Cambridge, MA: MIT, 457-476.

Nilsen, H., Otterlei, M., Haug, T., Solum, K., Nagelhus, T. A., Skorpen, F., & Krokan, H. E. (1997). Nuclear and mitochondrial uracil-DNA glycosylases are generated by alternative splicing and transcription from different positions in the UNG gene. *Nucleic Acids Res, 25*, 750-755.

Nübel, T., & Ricquier, D. (2006). Respiration under control of uncoupling proteins: clinical perspective. *Horm. Res, 65*, 300-310.

Olichon, A., Guillou, E., Delettre, C., Landes, T., Arnauné-Pelloquin, L., Emorine, L. J., Mils, V., Daloyau, M., Hamel, C., Amati-Bonneau, P., Bonneau, D., Reynier, P., Lenaers, G., & Belenguer, P. (2006). Mitochondrial dynamics and disease, OPA1. *Biochim Biophys Acta, 1763*(5-6), 500-509.

Olsson, T. D., Wieloch, T., Diano, S., Warden, C. H., Horvath, T. L., & Mattiasson, G. (2008). Overexpression of UCP2 protects thalamic neurons following global ischemia in the mouse. *J Cereb Blood Flow Metab, 28*(6), 1186-1195.

Ottersen, O. P. (1989). Quantitative electron microscopic immunocytochemistry of neuroactive amino acids. *Anat. Embryol. (Berl), 180*(1), 1-15.

Overly, C. C., Rieff, H. I., & Hollenbeck, P. J. (1996). Organelle motility and metabolism in axons vs dendrites of cultured hippocampal neurons. *J. Cell Sci, 109*, 971-980.

Pages, V., Johnson, R. E., Prakash, L., & Prakash, S. (2008). Mutational specificity and genetic control of replicative bypass of an abasic site in yeast. *Proc natl Acad Sci, 105*, 1170-1175.

Park, J., Lee, G., & Chung, J. (2009). The PINK1-Parkin pathway is involved in the regulation of mitochondrial remodeling process. *Biochem Biophys Res Commun, 378*, 518-523.

Pebay-Peyroula, E., Dahout-Gonzalez, C., Kahn, R., Trezeguet, V., Lauquin, G. J., & Brandolin, G. (2003). Structure of mitochondrial ADP/ATP carrier in complex with carboxyatractyloside. *Nature, 426*(6962), 39-44. doi: 10.1038/nature02056

Pecqueur, C., Alves-Guerra, M. C., Gelly, C., Levi-Meyrueis, C., Couplan, E., & Collins, S., (2001). Uncoupling protein 2, in vivo distribution, induction upon oxidative stress, and evidence for translational regulation. *J. Biol Chem, 276*, 8705-8712.

Piconi, L., Quagliaro, L., & Ceriello, A. (2003). Oxidative stress in diabetes. *Clin. Chem. Lab. Med, 41*, 1144-1149.

Pinz, K. G., Shibutani, S., & Bogenhagen, D. F. (1995). Action of mitochondrial DNA polymerase gamma at sites of base loss or oxidative damage. *J. Biol Chem, 270*, 9202-9206.

Plenger, P. M., Dixon, C. E., Castillo, R. M., Frankowski, R. F., Yablon, S. A., & Levin, H. S. (1996). Subacute methylphenidate treatment for moderate to moderately severe traumatic brain injury: a preliminary double-blind placebo-controlled study, *Arch Phys Med Rehabil, 77*(6), 536-540.

Poole, A. C., Thomas, R. E., Andrews, L. A., McBride, H. M., Whitworth, A. J., & Pallanck, L. J. (2008). The PINK1/Parkin pathway regulates mitochondrial morphology. *Proc Natl Acad Sci, 105*, 1638-1643.

Ramirez-Munguia, N., Vera, G., & Tapia, R. (2003). Epilepsy, neurodegeneration, and extracellular glutamate in the hippocampus of awake and anesthetized rats treated with okadaic acid. *Neurochem Res, 10*, 1517-1524.

Reddy, P. H., & Shierndeb, U. P. (2012). Mutant huntingtin, abnormal mitochondrial dynamics, defective axonal transport of mitochondria, and selective synaptic degeneration in Huntington's disease. *Biochi Bioph Acta, 1822*, 101-110.

Reeve, A. K., Krishnan, K. J., & Turnbull, D. (2008). Mitochondrial DNA mutations in disease, aging, and neurodegeneration. *Ann. N.Y. Acad. Sci, 1147*, 21-29.

Richard, D., Clavel, S., Huang, Q., Sanchis, D., & Ricquier, D. (2001). Uncoupling protein 2 in the brain: distribution and function. *Biochem Soc Trans, 29*(6), 812-817.

Richard, D., Huang, Q., Sanchis, D., & Ricquier, D. (1999). Brain distribution of UCP2 mRNA: in situ hybridization histochemistry studies. *Int J. Obes Relat Metab Disord, 23*(6), 53-55.

Richter, C., Park, J. W., & Ames, B. N. (1988). Normal oxidative damage to mitochondrial and nuclear DNA is extensive. *Proc Natl Acad Sci, 85*(17), 6465-6467.

Ricquier, D., & Bouillaud, F. (2000). The uncoupling protein homologues: UCP1, UCP2, UCP3, StUCP and AtUCP. *Biochem J, 345,* 161-79.

Robertson, A. B., Klungland, A., Rognes, T., & Leiros, I. (2009). DNA repair in mammalian cells: Base excision repair: the long and short of it. *Cell Mol Life Sci, 66,* 981-993.

Rolfe, D. F. S., Hulbert, A. J., & Brand, M. D. (1994). Characteristics of mitochondrial proton leak and control of oxidative phophorylation in the major oxygen-consuming tissues of the rat. *Biochim. Biophys. Acta, 1118,* 405-416.

Rolseth, V., Rundén-Pran, E., Neurauter, C. G., Yndestad, A., Luna, L., Aukrust, P., Ottersen, O. P., & Bjørås, M. (2008). Base excision repair activities in organotypic hippocampal slice cultures exposed to oxygen and glucose deprivation. *DNA Repair (Amst), 7*(6), 869-878. doi: 10.1016/j.dnarep

Ropp, P. A., & Copeland, W. C. (1996). Cloning and characterization of the human mitochondrial DNA polymerase, DNA polymerase gamma. *Genomics, 36* (3), 449-458. doi: 10.1006/geno.1996.0490

Rosenzweig, E. S., & Barnes, C. A. (2003). Impact of aging on hippocampal function: plasticity, network dynamics, and cognition. *Prog Neurobiol, 69*(3), 143-79.

Rousset, S., Emre, Y., Join-Lambert, O., Hurtaud, C., Ricquier, D., & Cassard-Doulcier, A.M. (2006).The uncoupling protein 2 modulates the cytokine balance in innate immunity. *Cytokine, 35,* 135-142.

Rowland, K. C., Irby, N. K., & Spirou, G. A. (2000). Specialized synapse-associated structures within the calyx of Held. *J. Neurosci, 20,* 9135-9144.

Sarnowska, A. (2002). Application of organotypic hippocampal culture for study of selective neuronal death. *Folia Neuropathol, 40,* 101.

Saxton, W. M., & Hollenbeck, P. J. (2012). The axonal transport of mitochondria. *J cell Sci, 125,* 1-10.

Schacher, S., & Wu, F. (2002). Synapse formation in the absence of cell bodies requires protein synthesis. *J. Neurosci, 22,* 1831-1839.

Selkoe, D. J. (2002). Alzheimer's disease is a synaptic failure. *Science, 298,* 789-791.

Sheng, Z. H., & Cai, Q. (2012). Mitochondrial transport in neurons: impact on synaptic homeostasis and neurodegeneration. *Nat Rev Neurosci, 13,* 77-93.

Shepherd, G. M., & Harris, K. M. (1998). Three-dimensional structure and composition of CA3-CA1 axons in rat hippocampal slices: implications for presynaptic connectivity and compartmentalization. *J. Neurosci, 18*, 8300-8310.

Si, K., Giustetto, M., Etkin, A., Hsu, R., Janisiewicz, A. M., Miniaci, M. C., Kim, J. H., Zhu, H., & Kandel, E. R. (2003). A neuronal isoform of CPEB regulates local protein synthesis and stabilizes synapsespecific long-term facilitation in aplysia. *Cell, 115*, 893-904.

Sicotte, N., Kern, K. C., & Giesser, B. S. (2008). Regional hippocampal atrophy in multiple sclerosis. *Brain, 131*, 1134-1141.

Simon-Areces, J., Dietrich, M. O., Hermes, G., Garcia-Segura, L. M., Arevalo, M. A., & Horvath, T.L. (2012). UCP2 induced by natural birth regulates neuronal differentiation of the hippocampus and related adult behvior. *PLoS ONE, 7*(8), 1-8.

Simuni, T., & Sethi, K. (2008). Nonmotor manifestations of Parkinson's disease. *Ann. Neurol, 64*(2), 65-80.

Sofroniew, M. V. (2009). Molecular dissection of reactive astrogliosis and glial scar formation. *Trends Neurosci, 32*, 638-647.

Sofroniew, M. V., & Vinters, H. V. (2010). Astrocytes: biology and pathology. *Acta Neuropathol, 119*, 7-35.

Sola, C., Tusell, J. M., & Serratosa, J. (1999). Comparative study of the distribution of calmodulin kinase II and calcinerurin in the mouse brain. *J. Neuroscie.Res, 57*, 651-662.

Sousa, M. M., Krokan, H. E., & Slupphaug, G. (2007). DNA-uracil and human pathology. *Epub, 28*(3-4), 276-306.

Spanswick, S. C., Lehmann, H., & Sutherland, R. J. (2011). A Novel Animal Model of Hippocampal Cognitive Deficits, Slow Neurodegeneration and Neuroregeneration. *J Biomed Biotechnol, 2011*, 1-12.

Stevens, J. R. (1992). Abnormal reinnervation as a basis for schizophrenia: a hypothesis. *Arch. Gen. Psychiatry, 49*, 238-243.

Stokin, G. B., & Goldstein, L. S. (2006). Axonal transport and Alzheimer's disease. *Annu Rev Biochem, 75*, 607-627.

Stowers, R. S., Megeath, L. J., Górska-Andrzejak, J., Meinertzhagen, I. A., & Schwarz, T. L. (2002). Axonal transport of mitochondria to synapses depends on milton, a novel Drosophila protein. *Neuron, 36*, 1063-1077.

Talbot, J. D., David, G., & Barrett, E. F. (2003). Inhabitation of Mitochondrial Ca^{2+} uptake affects phasic release from motor terminals differently depending on external $[Ca^{2+}]$. *J. Neurophysiol, 90*, 491-502.

Tang, Y., & Zucker, R. S. (1997). Mitochondrial involvement in post-tetanic potentiation of synaptic transmission. *Neuron, 18,* 483-491.

The science update. (2010). Retrieved February 20, 2013, from http://thescienceupdate.blogspot.no/2010/09/now-break-it-down.html

Urlinger, S., Baron, U., Thellmann, M., Hasan, M. T., Bujard, H., & Hillen, W. (2000). Exploring the sequence space for tetracycline-dependent transcriptional activators: novel mutations yield expanded range and sensitivity. *Proc Natl Acad Sci, 97,* 7963-7968.

Valouskova, E., & Modriansky, M. (2008). Modulation of UCP2 expression by p38 - a link to cardioprotection. *Biomed Pap Med Fac Univ Palacky Olomouc Czech Repub, 152*(1), 3-7.

Verma, P., Chierzi S, Codd, A. M, Campbell, D. S, Meyer, R. L., Holt, C. E., & Fawcett, J. W. (2005). Axonal protein synthesis and degradation are necessary for efficient growth cone regeneration. *J. Neurosci, 25,* 331-342.

Verstreken, P., Ly, C. V., Venken, K. J., Koh, T. W., Zhou, Y., & Bellen, H. J. (2005). Synaptic mitochondria are critical for mobilization of reserve pool vesicles at Drosophila neuromuscular junctions. *Neuron, 47,* 365-378.

Vornov, J. J., Park, J., Thomas, A. G. (1998). Regional vulnerability to endogenous and exogenous oxidative stress in organotypic hippocampal culture. *Exp. Neurol, 149,* 109-122.

Wallace, D. C., (1994). Mitochondrial DNA sequence variation in human evolution and disease. *Proc Natl Acad Sci, 91*(19), 8739-8746.

Wang, X., & Michaelis, E. K. (2010). Selective neuronal vulnerability to oxidative stress in the brain. *Front Aging Neurosci, 2*(12). doi: 10.3389/fnagi.2010.00012

Wang, X., Pal, R., Chen, X. W., Limpeanchob, N., Kumar, K. N., & Michaelis E. K. (2005). High intrinsic oxidative stress may underlie selective vulnerability of the hippocampal CA1 region. *Brain Res, 140,* 120-126.

Wang, H., Lim, P. J., Karbowski, M., & Monteiro, M. J. (2009). Effects of overexpression of huntingtin proteins on mitochondrial integrity. *Hum Mol Genet, 18,*737-752.

Wang, X., Su, B., Lee, H. G., Li, X., Perry, G., Smith, M. A., & Zhu, X. (2009a). Impaired balance of mitochondrial fission and fusion in Alzheimer's disease. *J. Neurosci, 29,* 9090-9103.

Welberg, L. (2011). Learning and memory: CA1 triggers the trace. *Nat Rev Neurosci, 12*(12), 705. doi: 10.1038/nrn3144

Wilde, G. J., Pringle, A. K., Wright, P., & Iannotti, F. (1997). Differential vulnerability of the CA1 and CA3 subfields of the hippocampus to superoxide and hydroxyl radicals *in vitro*. *J. Neurochem, 69*, 883-886.

Yang, Y., Ouyang, Y., Yang, L., Beal, M. F., McQuibban, A., Vogel, H., & Lu, B. (2008). Pink1 regulates mitochondrial dynamics through interaction with the fission/fusion machinery. *Proc Natl Acad Sci, 105*, 7070-7075.

Youle, R J., & van der Bliek, A. M. (2012). Mitochondrial Fission, Fusion, and Stress. *Science, 337*, 1062-1065.

Zhang, H., Chatterjee, A., & Singh, K. K. (2006). Saccharomyces cerevisiae polymerase zeta functions in mitochondria. *Genetics, 172*(4), 2683-2688. doi: 10.1534/genetics.105.051029

Ziehn, M. O., Avedisian, A. A., Tiwari-Woodruff, S., & Voskuhl, R. R. (2010). Hippocampal CA1 atrophy and synaptic loss during experimental autoimmune encephalomyelitis, EAE. *Lab Invest, 90*(5), 774-786.

Appendix

Appendix 1: Determination of protein concentrations by BCA assay. The average absorbance (A 562 nm) from standard protein concentration (mg/mL) were used to build standard curve followed by determining the final concentrations of total protein in hippocampal homogenate

Standard protein concentration (mg/mL) (x)	Average absorbance (562 nm) (y)	
2	1.517	
1	0.873	
0.75	0.718	
0.50	0.560	
0.25	0.398	
0.10	0.245	
0.20	0.198	
0	0.153	
Protein samples (Hippocampus)	**Average absorbance (562 nm)**	**Concentration (mg/mL)**
Hippocampus 1	0.894	1.0405
Hippocampus 2	0.761	0.842466
Hippocampus 3	0.759	0.839488
Average	-	0.907485
Final Concentration (diluted 10x)	-	**9.07485**

y = 0,6716x + 0,1952
R² = 0,9965

Absorbance (562 nm)

Concentrations (mg/ml)
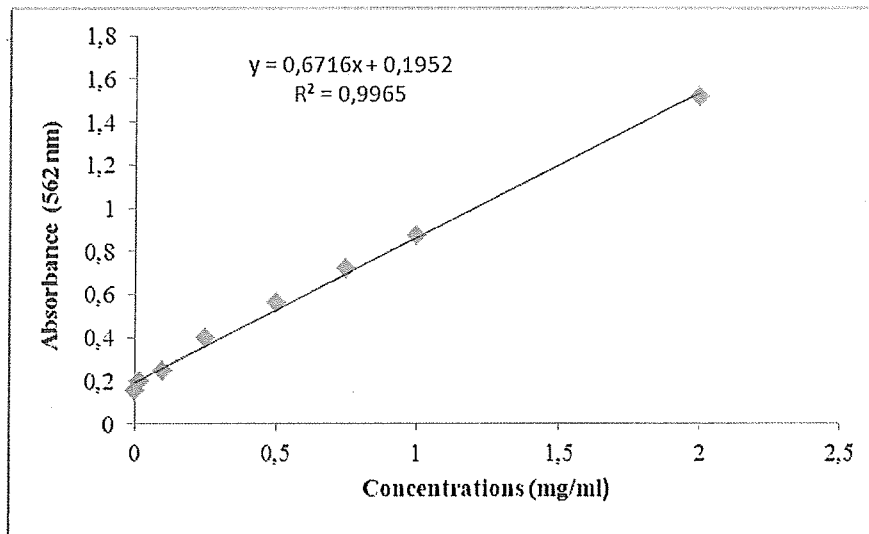
Figure: The standard curve was made in Microsoft Excel 2010, for calculating the total protein concentrations (BCA assay) in hippocampal homogenate

The concentration of protein in hippocampal extract was calculated from Y= 0.1952 + 0.6716x (Y= a+bx) equation. The equation obtained from Microsoft Excel 2010, was checked using the following formula-

where,

$$a \ (slope) = \frac{n\sum xy - (\sum x)(\sum y)}{n\sum x^2 - n(\sum x)^2} = 0.1952$$

$$b \ (y - intercept) = \frac{\sum y - a(\sum x)}{n} = 0.6716$$

Appendix 2: Calculations

Concentration (start) × Volume (start) = Concentration (final) × Volume (final)

This equation is commonly abbreviated as: $C_1 V_1 = C_2 V_2$

Using this equation-

Dilution of sample to 2 mg/mL final concentration with SDS buffer

9.07485 mg/mL × 200µL = 2 mg/mL ×V2

V2= 907.48 µL

707.48 µL SDS buffer + 200 µL original sample

Dilution of sample (1 mg/mL)

907.48 µL (2 mg/mL) sample + 907.48 µL Laemmli sample buffer

Appendix 3: The output "profile summary" shows the density (UCP2 gold particles/μm^2) of UCP2 in myelinated axons of three mutUNG1-expressing mice.

Myelinated axon (mutUNG1)-1		Myelinated axon (mutUNG1)-2		Myelinated axon (mutUNG1)-3	
Area (nm^2)	Number of UCP2 points	Area (nm^2)	Number of UCP2 points	Area (nm^2)	Number of UCP2 points
3976.58	7	19529.11	1	141625.00	6
27717.17	0	27109.34	0	17846.29	1
32691.96	1	43822.03	0	23383.69	0
39861.95	2	34743.16	0	23639.89	0
26523.28	0	27814.28	0	27206.46	1
16975.57	1	411070.72	4	23293.27	0
24726.60	1	41355.56	1	23494.21	0
49007.80	2	139778.06	4	57220.98	5
24314.68	1	29048.35	1	46320.31	1
49573.76	0	47105.62	1	35434.71	3
25244.00	1	42278.18	2	32650.10	1
35334.24	0	47092.23	1	33532.54	0
29853.76	1	98712.17	1	25937.23	0
18778.95	0	25123.44	1	32353.72	0
25393.03	0	38919.24	0	55104.48	1
24996.18	0	70775.65	1	26608.68	1
49024.54	8	234684.21	1	42507.59	0
14211.05	0	30056.37	3	28330.02	1
199482.25	2	80906.07	2	29018.22	2
36888.13	1	31174.91	4	54116.55	1
62649.54	0	271478.57	3	112707.20	1
21995.57	2	83114.67	2	111972.10	1
129230.70	2			58306.02	2
116553.44	1			52736.80	0
266821.93	6			39637.58	1
28204.43	1				
32547.95	1				
50159.82	1				
30048.00	1				
215615.57	2				
Total=1708402.58	45	Total=1875692.09	33	Total=1154983.70	29
Density =26.3403		Density =17.5935		Density =25.1085	

Appendix 4: The output "profile summary" shows the density (UCP2 gold particles/μm^2) of UCP2 in myelinated axons of three wild type mice

Myelinated axon wild type-1		Myelinated axon wild type-2		Myelinated axon wild type-3	
Area (nm^2)	Number of UCP2 points	Area (nm^2)	Number of UCP2 points	Area (nm^2)	Number of UCP2 points
15071.72	2	85353.41	2	47746.94	0
47011.86	0	83673.94	2	32924.71	0
25520.29	0	27161.25	0	41893.06	0
37100.79	0	21814.73	0	51239.84	0
37564.61	0	78315.7	2	39771.54	0
23090.67	1	30734.53	0	8248.341	0
32318.56	0	37857.64	0	34850.33	0
84052.37	0	24205.85	0	48674.59	0
238148.7	4	46645.15	0	40657.32	0
39101.76	0	275102.1	3	20739.74	0
52189.26	1	19438.69	0	32028.88	0
33267.97	0	27836.06	0	25436.57	2
42259.77	5	22169.72	0	75586.35	1
31931.76	0	211513.2	0	19872.37	1
15080.1	0	58979.15	0	35674.16	3
25615.74	1	17405.91	0	35638.99	0
42576.24	0	21792.97	0	35334.24	0
44240.64	0	47669.92	0	171835.4	1
136000.5	0	72175.49	0	100194.1	0
16160.12	0	39722.98	0	32822.57	1
42666.66	0	23318.39	0	60301.97	0
15843.65	0	29724.84	0	34935.72	0
28715.14	0			29667.91	0
29060.08	1			38776.91	5
40365.97	0			49500.09	2
56228.03	0			53346.30	1
33182.58	0				
40260.48	0				
55707.28	0				
20821.79	0				
Total=1381155.01	**15**	**Total=1302611.58**	**9**	**Total=1197698.92**	**17**
Density =10.8604		**Density =6.9091**		**Density =14.1938**	

Appendix 5: The output "profile summary" shows the density (UCP2 gold particles/μm^2) of UCP2 in dendrites of three mutUNG1-expressing mice

Dendrite (mutUNG1)-1		Dendrite (mutUNG1)-2		Dendrite (mutUNG1)-3	
Area (nm^2)	Number of UCP2 points	Area (nm^2)	Number of UCP2 points	Area (nm^2)	Number of UCP2 points
239607.10	3	284149.14	2	341998.00	3
198559.60	1	699960.28	2	763515.70	11
335352.10	3	214674.53	1	465431.80	7
253108.20	2	175844.04	2	333322.70	6
120019.60	4	341212.72	1	256418.60	3
23373.65	0	132254.75	6	145570.00	2
9319.98	0	423935.57	1	356972.60	2
192925.10	4	245837.72	0	156981.40	1
466538.60	2	466402.97	4	58054.86	1
285855.40	2	100031.64	2	284246.30	3
472724.00	4	222338.49	1	158717.80	2
520263.30	1	213165.85	2	112851.20	1
152780.20	2	168215.24	1	255591.40	4
132420.50	0	224175.36	2	323222.40	8
164786.00	1	274120.86	1	848001.80	21
205763.10	4	111876.70	3	103454.20	1
332954.30	0	291206.94	1	68906.97	3
193990.10	0	212728.82	0	321293.50	5
270854.00	3	347368.00	2	262754.70	8
586526.30	2	31714.08	1	210151.80	9
280637.80	0	66783.76	0	566767.80	4
224563.80	2	305520.14	3	683833.70	4
227437.20	2	685099.54	2	249077.80	3
142366.80	6	84995.08	1	85725.14	1
188360.60	3	366811.71	4	333771.50	2
62492.15	0	110111.83	2		
130670.70	1	193464.27	1		
21183.47	0				
459154.30	0				
90194.25	0				
183824.50	0				
Total=7168606.78	52	Total=6994000.15	48	Total=7746633.61	115
Density =7.2538		Density =6.8630		Density =14.8451	

Appendix 6: The output "profile summary" shows the density (UCP2 gold particles/μm^2) of UCP2 in dendrites of three wild type mice

Dendrite wild type-1		Dendrite wild type-2		Dendrite wild type-3	
Area (nm^2)	Number of UCP2 points	Area (nm^2)	Number of UCP2 points	Area (nm^2)	Number of UCP2 points
196942.10	1	102514.90	0	94614.80	2
275728.30	3	424533.40	2	421902.80	1
78283.89	1	330154.70	0	135439.60	2
558496.10	1	271522.10	2	72671.13	0
223847.20	3	259459.40	1	246370.20	1
45672.30	0	191126.70	0	351075.20	5
175616.30	4	163895.20	3	112755.80	0
454681.80	5	40479.83	0	238389.80	1
79444.28	0	202662.00	4	253414.60	4
79387.35	0	97640.53	0	112265.20	1
324473.20	1	81257.71	0	470728.10	4
81771.77	0	467486.30	4	211074.50	4
543908.20	2	296483.10	1	393181.00	9
157145.50	2	408624.40	0	165556.20	0
145864.70	0	394373.20	2	222380.40	0
454593.10	1	143205.70	1	145369.10	0
422858.90	2	198449.10	3	431834.00	4
173285.50	1	69918.33	0	209991.10	4
494686.10	1	76328.13	0	104137.40	1
254020.80	2	613426.40	0	238877.00	1
262969.00	2	392966.60	0	65703.74	0
386536.70	1	187426.20	1	42132.51	0
202983.50	1	445681.70	0	503741.50	4
91478.55	0	243411.40	0	92273.92	6
338027.90	3	29929.12	0	408666.3	10
641577.20	3	381287.30	1	408940.90	10
146827.50	0	487651.70	0	113335.10	4
236603.10	2	324207.00	1	227740.30	3
136062.50	6			253476.60	2
479716.50	4			379720.00	2
317355.20	0			171386.70	3
294435.30	5			598461.80	5
				442604.00	0
				752136.10	9
				256743.40	6
				491948.40	5
Total=8755280.43 Density =6.5103	57	Total=7326102.19 Density =3.5489	26	Total=9841039.02 Density =11.4825	113

Appendix 7: The output "profile summary" shows the density (UCP2 gold particles/μm^2) of UCP2 in presynaptic terminals of three mutUNG1-expressing mice

Presynaptic terminal (mutUNG1)-1		Presynaptic terminal (mutUNG1)-2		Presynaptic terminal (mutUNG1)-3	
Area (nm^2)	Number of UCP2 points	Area (nm^2)	Number of UCP2 points	Area (nm^2)	Number of UCP2 points
104083.80	1	150511.30	3	90381.79	8
44287.53	0	28723.52	1	104470.60	5
41918.18	4	39183.8	0	353823.00	3
27898.01	0	41561.52	1	34458.51	0
34821.86	0	45180.01	0	32209.72	0
58938.97	2	260591.3	2	19837.21	0
55065.96	1	188871.3	4	22228.32	0
95768.49	2	54548.56	2	104467.3	0
103132.70	1	43607.70	2	60484.48	2
38920.92	1	45046.05	0	33264.62	1
29269.39	0	45357.50	0	32437.45	1
31576.78	3	272700.9	1	48935.80	0
32465.91	0	80957.98	0	37778.94	0
130597.1	1	120488.4	1	66216.13	0
38013.36	0	54078.04	1	72316.15	2
58555.52	0	49349.39	0	27424.14	1
126315.5	1	46080.86	1	31231.84	5
33910.96	1	35210.33	0	14376.83	0
15458.52	0	29381.57	0	49193.67	1
42251.4	0	35736.11	0	112151.3	1
62899.04	0	46762.37	1	43023.32	0
119555.70	4	63228.91	1	55086.06	0
52571.03	0	64628.75	3	34346.32	0
72034.84	3	21844.87	0	47172.61	0
53729.75	1	78491.52	0	55578.34	0
69687.26	1	42762.10	0	35223.73	0
49711.07	0			78491.52	1
71110.54	1			52711.69	2
				51206.36	1
				26655.57	1
Total=1694550.09	28	Total=1984884.65	24	Total=1827183.28	35
Density =16.5235		Density =12.0913		Density =19.1551	

Appendix 8: The output "profile summary" shows the density (UCP2 gold particles/μm^2) of UCP2 in presynaptic terminals of three wild type mice

Presynaptic terminal wild type-1		Presynaptic terminal wild type-2		Presynaptic terminal wild type-3	
Area (nm^2)	Number of UCP2 points	Area (nm^2)	Number of UCP2 points	Area (nm^2)	Number of UCP2 points
33852.36	0	54875.08	0	32638.38	0
30408.01	1	58157.00	0	51261.61	0
23221.27	0	53696.26	0	72451.78	0
26200.12	1	26315.66	0	46722.18	0
80531.00	0	51708.69	0	68421.38	0
26282.17	0	39677.77	0	119306.20	4
271940.7	2	68578.77	0	44734.61	0
29450.23	1	19780.28	0	67482.01	2
25485.13	0	38241.09	0	28983.06	0
44922.14	0	43247.69	0	54520.09	0
33636.35	0	33860.73	1	95301.32	0
39048.17	0	12486.37	0	23891.05	1
24788.56	0	23184.43	0	34657.77	0
73384.45	3	69057.67	0	37864.34	0
72805.09	1	53885.48	1	41566.55	0
40449.69	0	20334.52	0	19792.00	1
57212.61	0	71411.94	0	75305.04	1
44135.15	0	18636.63	0	40084.66	0
38708.26	0	27012.23	0	21185.14	0
30295.82	0	38709.94	0	41024.03	0
83601.94	1	51392.22	1	42271.49	0
25639.18	1	59540.09	0	26203.47	0
41914.83	1	155325.3	0	90837.24	0
		14750.23	0	50215.08	0
		16791.38	0	166030.10	2
		92747.79	0		
Total=1197913.25	12	Total=1213405.26	3	Total=1392750.57	11
Density =10.0174		**Density =2.4723**		**Density =7.8980**	

Appendix 9: The output "profile summary" shows the density (UCP2 gold particles/µm^2) of UCP2 in somas of three mutUNG1-expressing mice

Soma (mutUNG1)-1		Soma (mutUNG1)-2		Soma (mutUNG1)-3	
Area (nm^2)	Number of UCP2 points	Area (nm^2)	Number of UCP2 points	Area (nm^2)	Number of UCP2 points
70180.61	1	38902.05	4	142359.6	4
63005.96	0	48776.21	1	38420.46	4
25008.11	0	175284.5	1	49777.06	0
52905.74	4	28526.64	0	174385.2	5
25753.42	1	78408.54	0	79718.98	0
53547.85	1	38603.92	0	29393.17	0
60334.3	0	18945.69	0	34580.87	0
29973.04	0	22112.04	3	19469.86	1
26710.04	0	29643.79	0	37386.85	0
23252.12	0	28672.43	0	66254.21	0
16848.98	5	37750.5	4	37054.33	4
30647.92	0	34367.93	0	54299.72	0
34818.39	0	48792.6	1	71042.23	0
25483.14	0	16583.62	1	29796.13	4
62702.92	0	40135.5	1	12898.01	0
60899.42	2	54543.79	0	30602.05	0
35879.85	0	48032.54	0	30949.32	0
40284.56	0	127171.6	3	80536.37	0
67127.29	0	49849.14	11	33047.66	0
103678.7	2	53158	0	151857.1	0
66427.84	1	49678.78	0	31075.45	0
60620.95	0	51880.32	2	269732.8	1
38736.61	0	22474.05	0	31512.81	0
163824.7	3	99401.79	3	49298.75	0
33388.37	0	41755.53	3	26421.75	0
37429.44	0	96577.79	1	46066.88	4
45659.01	1	24683.78	2	18231.5	0
45713.06	0	175969.2	4	28903.39	2
49270.91	0	39463.9	0	47662.34	1
32880.58	2	74531.28	0	84511.91	3
61467.83	0	37970	0	29925.54	1
52653.48	2	55955.79	0	45749.1	0
35355.67	0	345789.1	2	108157.2	0
37057.61	0	77899.11	0	15582.77	0
28454.57	0	59588.98	3	47500.17	0
28148.25	0	54547.07	0	17569.72	0
24862.32	0	40689.16	0	126948.9	1
48464.99	0	14639.25	4	20727.88	1
22066.17	5	14798.14	0	23779.57	0
24775.51	0	70527.88	0	323447.7	15
46232.32	1	42988.98	0	264197.8	1
64101.81	3	17795.78	0	69767.83	0
68324.7	0	15156.88	0	123024.1	0
37187.01	2	24492.12	1	80375.84	1
49170.98	0	58488.21	0	160637	4
39477.01	0	45482.1	0	86040.21	0
28323.52	0	86620.08	14	45971.87	0
69269.86	2	736311.7	0	24143.22	4
24031.83	0	44153.64	0	40117.48	0
220768.2	4	35381.88	0	22257.82	0
46042.31	0	51945.84	2	98030.74	1
187772.9	0	42246.95	0	23234.1	0
35585	0	92556.38	3	24372.55	2
44065.18	0	273541.2	1	23392.99	0
67608.88	0	108982.7	1	24703.43	0
29814.15	0	71322.34	2	21155.42	0
21543.63	3	36867.59	2	29099.96	2
32361.32	11	35768.46	2	35832.34	2
51516.67	0	27764.95	2	24182.53	0
23083.4	0	36954.41	0	5462.897	0
29345.67	0	58491.49	3	195421	4
38928.26	1	66501.55	0	73787.6	0
13428.73	0	46310.95	1	45881.78	0
299838.5	4	55982	0	68269.01	0
49338.07	0	133587.9	2	28009.02	2
143716	0	28135.15	0	25743.59	1
62193.48	0	38748.07	1	79479.82	1
23822.16	0	230735.7	0	120642.4	4
35391.71	0	83121.21	0	85802.7	2
21666.49	0	119636.6	0	41241.18	0
29638.88	0	13792.38	2	25902.48	0
40505.7	0	52923.76	1	130110.3	0
37722.65	0	100178.2	1	70498.4	0
30438.25	0	67510.59	3	45642.63	0
32698.75	2	58380.1	2	96002.83	0

Soma (mutUNG1)-1		Soma (mutUNG1)-2		Soma (mutUNG1)-3	
Area (nm²)	Number of UCP2 points	Area (nm²)	Number of UCP2 points	Area (nm²)	Number of UCP2 points
30882.16	0	21761.49	1	72636.05	1
68902.94	1	84192.49	2	114665.1	0
42242.03	1	22226.7	2	26411.92	3
66108.42	0	284976.5	7	174298.3	1
28272.74	0	26575.72	1	35468.7	0
332574.9	2	158496.1	0	71943.16	2
132313.5	1	44168.38	0	131689.4	1
158486.3	5	79727.17	3	119779.1	1
30487.39	2	124337.8	0	70385.37	9
30138.48	0	96695.73	1	27855.04	0
17304.36	2	38600.65	2	72762.18	3
6794.631	0	65315.61	0	55526.62	0
64914.28	1	148823.4	0	61145.13	1
54704.32	0	164111.3	3	26569.17	0
43955.43	0	16703.2	0	82359.52	2
21163.61	0	61145.13	0	45889.97	7
65612.09	0	74305.22	4	140018.9	1
43934.14	0	671857.7	3	77487.96	1
21366.72	0	136973.7	1	48674.66	0
30564.37	1	43771.97	0	22344.64	0
16878.47	0	43056.14	0	65166.54	0
34744.68	1	29275.23	7	100858	0
22290.58	0	23304.54	0	54719.06	0
29938.64	5	31204.85	1	35218.08	2
52031.02	2	43152.79	4	24695.24	2
81176.84	0			21137.4	0
28084.37	0			89011.64	2
23581.37	1			34454.74	0
46043.95	1			56445.56	2
36952.77	0			38217.34	1
28538.11	8			75561.61	1
15070.06	0			330792.7	3
29137.63	0			26374.24	2
20277.42	4			109405.4	2
36413.85	1			120041.2	2
24066.23	0			16523.01	2
118740.6	2			60152.47	4
28372.66	1			41267.39	2
85991.07	0			22462.58	0
31198.3	0			75058.73	2
142706.9	0			28605.27	0
50312.71	9			90996.95	3
95499.95	2			63926.54	0
32125.44	5			90988.76	1
				152993.9	2
				50609.19	2
				21818.83	1
				42405.84	2
				39909.45	4
				14601.58	0
				33920.74	1
				17935.01	0
				15458.28	4
				32064.83	1
				16454.21	0
				333754.3	0
				29879.67	0
				12929.13	0
				35840.53	1
				21392.93	1
				14621.23	1
				37760.33	1
				137660.1	2
				37380.3	4
				96966.01	0
				26176.04	1
				22251.27	0
				394596.4	9
				85584.84	6
				67422.14	9
Total=6322151.62	121	Total=8040699.31	142	Total=10327117.35	200
Density =19.1390		Density =17.6601		Density =19.3664	

Appendix 10: The output "profile summary" shows the density (UCP2 gold particles/μm^2) of UCP2 in somas of three wild type mice

Soma wild type-1		Soma wild type-2		Soma wild type-3	
Area (nm^2)	Number of UCP2 points	Area (nm^2)	Number of UCP2 points	Area (nm^2)	Number of UCP2 points
155627.85	1	88882.23	1	42176.51	0
65790.64	1	47071	0	60345.76	0
109547.86	1	44191.31	0	38605.56	0
45003.78	0	36358.16	0	52470.02	0
113384.18	0	66368.87	0	30100.81	0
54814.06	0	40469.66	0	70265.79	0
24557.64	0	27221.11	0	146592.4	1
47650.87	0	38613.75	0	43888.27	1
63828.25	2	95678.5	0	47745.88	0
112588.09	0	77052.23	0	45033.27	0
182052.87	0	54871.4	0	36882.33	0
74516.53	0	51238.2	0	56204.77	1
81738.69	0	26174.4	0	87111.5	0
74634.47	0	56999.23	0	40512.25	0
34561.21	0	45622.97	0	75107.87	1
53975.38	0	89987.91	0	49383.93	0
90417.08	0	59461.22	0	26241.56	0
28955.80	0	88761.02	0	21923.66	0
30521.78	0	35109.96	0	24518.33	0
59072.99	0	30913.28	0	33514.5	3
156971.05	0	61077.97	1	141239.2	1
14724.43	0	147886.4	3	46605.8	0
35989.59	0	39996.27	0	82526.6	0
37925.77	1	118350.8	0	66950.38	0
41057.72	0	49542.82	0	92687.42	0
40468.02	0	71812.11	0	32243.38	0
83810.82	0	72369.05	0	39935.66	0
66121.52	0	23258.67	0	36561.28	0
24490.48	0	48833.55	0	30218.75	0
145627.55	1	32020.6	0	35172.21	0
72378.87	0	30801.89	0	22456.03	0
126544.27	1	20693.49	0	67700.61	0
168286.70	4	15296.11	0	51149.75	0
81148.99	1	9477.757	0	69938.18	0
33704.51	0	16660.61	0	41789.93	0
35761.90	0	25694.45	0	22008.84	0
59749.51	1	34734.85	1	25540.48	0
65554.76	2	65122.32	1	79419.22	0
35637.41	0	55520.07	0	20423.21	0
47971.93	0	16883.38	0	63661.18	1
35021.50	0	64565.38	0	87557.05	0
17186.42	1	45503.39	0	22696.82	0
35319.63	0	28798.56	0	94122.35	0
125925.09	2	27584.76	0	54612.59	0
116453.88	0	66627.68	0	144122.2	0
34281.11	0	75984.23	0	55385.75	0
144154.95	0	191869.7	1	54933.64	0
27424.23	0	37318.06	0	46841.68	1
113708.51	0	43814.56	0	39241.13	0
149200.14	0	35316.36	0	27014.72	0
95668.67	0	14165.86	0	30284.27	0
115462.86	2	42805.52	0	48158.67	0
93044.51	0	54796.05	2	56650.32	1
31910.85	0	39758.75	0	53459.4	0
109896.77	0	29681.47	0	86213.85	1
506799.56	3	25134.24	0	53603.55	0

Soma wild type-1		Soma wild type-2		Soma wild type-3	
Area (nm^2)	Number of UCP2 points	Area (nm^2)	Number of UCP2 points	Area (nm^2)	Number of UCP2 points
57326.83	0	75887.58	0	42255.14	2
73156.95	0	30697.06	0	26195.7	0
43698.25	1	184778.6	0	34995.3	0
102545.20	0	201198.4	1	50504.36	1
33635.71	0	76988.35	1	34798.73	0
43691.707	1	36797.16	0	55929.58	0
101850.67	0	54868.12	0	59238.44	0
34019.02	0	45098.79	0	25999.13	0
125074.94	2	39843.93	0	13346.83	0
73708.97	0	53904.95	0	57836.27	0
47685.27	1	36312.29	0	111217	1
166078.61	0	31751.96	0	51539.61	0
91737.35	1	41167.47	0	42582.75	0
75782.74	0	64034.65	0	53293.96	2
27825.55	0	15417.33	0	46073.43	1
45662.28	0	29891.14	0	49082.53	0
43504.96	0	142877.3	0	67063.41	0
458210.08	1	102440.4	0	52714.09	0
52594.50	0	36487.56	0	16393.6	1
264944.75	7	74985.01	1	33003.43	0
172547.27	0	46758.14	0	80480.67	1
64999.46	0	40377.93	0	43067.61	0
		103500.2	0	47883.48	0
		34077.99	0	45564	0
		13053.62	0	64676.77	0
		73876.06	1	46848.23	0
		34061.61	0	84484.07	0
		29596.29	0	56244.08	0
		26788.67	0	24131.75	0
		32299.07	1	31168.82	0
		15828.48	0	61181.17	1
		18015.27	0	31868.26	0
		36390.92	0	31565.22	0
		46350.26	0	47903.13	1
		53813.22	0	95126.48	1
		24944.23	0	32593.92	0
		63359.77	0	19327.35	0
		24996.64	0		
Total=6828905.95	38	Total=4974320.49	15	Total=4819929.36	24
Density =5.5645		Density =3.0154		Density =4.9793	

Appendix 11: The calculated average mitochondrial area (nm^2) with standard error of the mean (SEM) in different compartments (myelinated axons, dendrites, presynaptic terminals, and somas) of three mutUNG1-expressing mice

	mutUNG1 1	mutUNG1 2	mutUNG1 3	Average	SEM
Myelinated axon	1708402.58	1875692.09	1154983.70	1579692.79	217776.39
Dendrite	7168606.78	6994000.15	7746633.61	7457620.18	235978.53
Presynaptic terminal	1694550.09	1984884.65	1827183.28	1835539.34	83916.57
Soma	6322151.62	8040699.31	10327117.35	8229989.42	1160001.60

Appendix 12: The calculated average mitochondrial area (nm^2) with standard error of the mean (SEM) in different compartments (myelinated axons, dendrites, presynaptic terminals, and somas) of three wild type mice

	Wild type-1	Wild type-2	Wild type-3	Average	SEM
Myelinated axon	1381155.01	1302611.58	1197698.92	1293821.83	53141.25
Dendrite	8755280.43	7326102.19	9841039.02	8640807.21	728252.45
Presynaptic terminal	1197913.25	1213405.26	1392750.57	1268023.02	62524.91
Soma	6828905.95	4974320.49	4819929.36	5541051.93	645467.38

Appendix 13: The significant differences of average mitochondrial area (nm^2) between wild type and mutUNG1-expressing mice were calculated. Superscript with asterisk (*) in a vertical column are significantly different (Student's *t*-test, * $p < 0.05$ and ** p-value < 0.01)

	t-test (p < 0.05)
Myelinated axon	0.135
Dendrite	0.07
Presynaptic terminal	0.002**
Soma	0.05*

Appendix 14: The calculated average individual mitochondrial size (nm^2) with standard error of the mean (SEM) in different compartments (myelinated axons, dendrites, presynaptic terminals, and somas) of three mutUNG1-expressing mice

	mutUNG1 1	mutUNG1 2	mutUNG1 3	Average	SEM
Myelinated axon	56946.75	85258.73	108706.49	83637.32	14963.72
Dendrite	231245.38	259037.04	309865.34	266715.92	23018.09
Presynaptic terminal	60519.64	76341.71	60906.10	65922.49	5210.80
Soma	63860.11	80406.99	108706.49	84324.53	13093.38

Appendix 15: The calculated average individual mitochondrial size (nm^2) with standard error of the mean (SEM) in different compartments (myelinated axons, dendrites, presynaptic terminals, and somas) of three wild type mice

	Wild type-1	Wild type-2	Wild type-3	Average	SEM
Myelinated axon	46038.50	59209.61	46065.34	50437.82	4385.90
Dendrite	273602.51	261646.50	273362.19	269537.07	3945.89
Presynaptic terminal	52083.18	46669.43	55710.02	51487.54	2626.73
Soma	87550.07	52918.30	51827.19	64098.52	11730.00

Appendix 16: The significant differences of average individual mitochondrial size (nm^2) between wild type and mutUNG1-expressing mice were calculated. Superscript with asterisk (*) in a vertical column are significantly different (Student's t-test, * $p<0.05$)

	t-test ($p < 0.05$)
Myelinated axon	0.05*
Dendrite	0.45
Presynaptic terminal	0.03*
Soma	0.15

Appendix 17: The calculated average UCP2 density (UCP2 GP/μm^2) with standard error of the mean (SEM) in different compartments (myelinated axons, dendrites, presynaptic terminals, and somas) of three mutUNG1-expressing mice

	mutUNG1 1	mutUNG1 2	mutUNG1 3	Average	STDEV	SQRT	SEM
Myelinated axon	26.3404	17.5935	25.10858	23.01416	4.7346	1.7320	2.7335
Dendrite	7.2538	6.8630	14.8451	9.6540	4.499	1.7320	2.5980
Presynaptic terminal	16.5235	12.0913	19.1551	15.9233	3.5699	1.7320	2.0611
Soma	19.1390	17.6601	19.3664	18.7218	0.9264	1.7320	0.5348

Appendix 18: The calculated average UCP2 density (UCP2 GP/μm^2) with standard error of the mean (SEM) in different compartments (myelinated axons. dendrites, presynaptic terminals, and somas) of three wild type mice

	Wild type-1	Wild type-2	Wild type-3	Average	STDEV	SQRT	SEM
Myelinated axon	10.8604	6.9091	14.1938	10.6545	3.6467	1.7320	2.1054
Dendrite	6.5103	3.5489	11.4825	7.1806	4.0090	1.7320	2.3146
Presynaptic terminal	10.0174	2.4723	7.8980	6.7959	3.8913	1.7320	2.2466
Soma	5.5645	3.0154	4.9793	4.5197	1.3352	1.7320	0.7708

Appendix 19: The calculated significant differences of UCP2 density (UCP2 GP/μm^2) between wild type and mutUNG1-expressing mice were calculated. Superscript with asterisk (*) in a vertical column are significantly different (Student's t-test, * p-value ≤ 0.05 and *** p-value ≤ 0.001)

	t-test (p < 0.05)
Myelinated axon	0.02*
Dendrite	0.516
Presynaptic terminal	0.04*
Soma	0.0001***

Appendix 20: The following average numbers of mitochondria were calculated for UCP2 density (UCP2 GP/μm^2) in three mutUNG-1 expressing mice

	mutUNG1-1	mutUNG1-2	mutUNG1-3	Average
Myelinated axon	30	22	25	25
Dendrite	31	27	25	28
Presynaptic terminal	28	26	30	28
Soma	99	100	95	98

Appendix 21: The following average numbers of mitochondria were calculated for UCP2 density (UCP2 GP/μm^2) in three wild type mice

	Wild type-1	Wild type-2	Wild type-3	Average
Myelinated axon	30	22	26	26
Dendrite	32	28	36	32
Presynaptic terminal	23	26	25	24
Soma	78	94	93	88

Appendix 22: The calculated average UCP2 density (UCP2 GP/μm^2) with standard error of the mean (SEM) in different neuronal compartments in stratum pyramidal and hilus. Superscript with asterisk (*) in a vertical column are significantly different (Student's t-test, ** p-value $\leq$ 0.01 and *** p-value $\leq$ 0.001)

	WT	SEM	mutUNG1-expressing	SEM	t-test
Stratum radiatum					
Myelinated axon	12.7958	2.5591	33.2893	6.4774	0.006**
Dendrite	6.5490	0.9355	15.6794	3.9198	0.1391
Presynaptic terminal	6.6321	1.3264	25.9547	3.7078	0.0008***
Pyramidal cell soma	6.1006	1.2201	29.1074	7.2768	0.01**
Hilus					
Myelinated axon	7.6229	0.9528	23.5516	5.8879	0.006**
Dendrite	9.8933	1.2366	17.8521	4.46303	0.1975
Presynaptic terminal	7.2773	1.8193	26.6386	3.3298	0.008**
Granular cell soma	7.0790	1.4158	36.5125	9.1281	0.002**